Chapter 8
Thickening

Abstract The chapter analyzes thickening in-depth. In an extensive introduction, the history of thickening is laid out from the Stone Age to the present, emphasizing people and institutions that have been important actors. The chapter then reviews the thickeners used in the mining-mineral industry. During sedimentation, particles settle individually except for collision among them, exerting interaction between them solely through the fluid. At a certain concentration, particles begin to touch each other permanently transforming the suspension into a network of solid particles called sediment. At that point forces among particles are transmitted directly from particle to particle. If settling particles that reach the bottom of the vessel and lie one on top of the other are incompressible, such as glass beads, the whole process ends, but if they are compressible, as in the case of flocculated copper flotation tailings, the weight of the sediment compresses the flocs lying underneath expelling the water from the pores. This phenomenon of extracting water by compression is called consolidation. The theory of sedimentation-consolidation is deduced from the equations for a particulate system and constitutive equations for the solid-fluid interaction force and sediment compressibility are postulated. Batch and continuous sedimentation are analyzed and simulations are compared to data from the literature. Experimental determination of thickening parameters and instruments for their determination are presented. Old and new methods for thickening design are reviewed and software for the design and simulation of batch and continuous thickening are presented. Finally, strategies for the operation and control of industrial thickening are discussed.

8.1 Introduction

8.1.1 From the Stone Age to the Middle Ages

Thickening is not a modern technique and was certainly not invented in the Americas. Whenever people have tried to obtain concentrates from ore, two processes have been used inseparably, *crushing and washing*. There is evidence

F. Concha A, *Solid–Liquid Separation in the Mining Industry*,
Fluid Mechanics and Its Applications 105, DOI: 10.1007/978-3-319-02484-4_8,
© Springer International Publishing Switzerland 2014

that in the 4th Egyptian dynasty, around 2,500 BC, the ancient Egyptians dug for and washed gold. There is also evidence of washing gold in Sudan in the 12th dynasty. Nevertheless, the earliest written reference to crushing and washing in Egypt is Agatharchides, a Greek geographer who lived 200 years before Christ. Ardillon in his book "Les mines du Laurion dans l'antiquité" described the process used in the extensive installation for crushing and washing ores in Greece between the 5th and 3rd centuries BC. In his book "The living rock", Wilson (1994) described mining gold and copper in the Mediterranean from the fall of the Egyptian Dynasties to the Middle Ages and the Renaissance (Concha and Bürger 2002a).

The development of mineral processing from unskilled labor to craftsmanship and eventually to an industry governed by scientific discipline is largely due to the Saxons in Germany and Cornishmen in England, beginning in the 16th century. An international exchange of technology began between these two countries and continued for an extended period. But it was in Saxony where Agricola (1950) wrote his book "De Re Metallica 1950", the first major contribution to the development and understanding of the mining industry, published in Latin in 1556, and shortly after translated to German and Italian. Agricola's book had a tremendous impact, not only on the mineral industry but also on society in general, and continued to be the leading textbook for miners and metallurgists outside the English-speaking world for at least another 300 years. Apart from its immense practical value as a manual, the greatest influence of *De Re Metallica* was in preparing the ground for the introduction of a system of mining education, which, with various modifications to suit local conditions, was later to be adopted internationally.

Agricola's book describes several methods for washing gold, silver, tin and other metallic ores. He described settling tanks used as classifiers, jigs and thickeners, and settling ponds used as thickeners or clarifiers. These devices operated in batches or semi-continuously. A typical description is as follows; see Figs. 8.1 and 8.2:

> To concentrate copper at the Neusohol in the Carpathians, the ore is crushed and washed and passed through three consecutive washer-sifters. The fine particles are washed through a sieve in a tub full of water, where the undersize settle to the bottom of the tub. At a certain stage of filling tub with sediment the plug is drawn to let the water run out. Then, the mud is removed with a shovel and taken to a second tub and then to a third tub where the whole process is repeated. The copper concentrate that has settled in the last tub is taken out and smelted.

It is evident from these references that by using washing and sifting processes, from the ancient Egyptians and Greeks to the mediaeval Germans and Cornishmen knew the practical effect specific gravity of the various components of an ore and used sedimentation in operations that can now be identified as classification, clarification and thickening. There is also evidence that in the early years no distinction was made among these three operations.

Fig. 8.1 Settling tanks described by Agricola

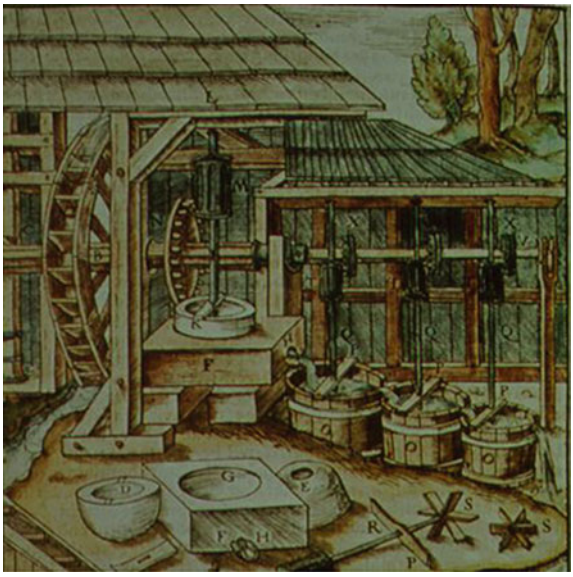

Fig. 8.2 Washing and settling according to Agricola

8.1.2 The Invention of the Dorr Thickener

Clarification and thickening involve the settling of one substance in solid particulate form on a second substance in liquid form. While clarification deals with very dilute suspensions, thickening produces more concentrated pulps. Perhaps

this is why clarification was the first of these operations to be described mathematically. The work of Hazen in 1904 was the first to analyze factors affecting particle settling from dilute suspensions in water. He showed that the detention time is not a factor of the design of settling tanks, but rather that the solid removed is proportional to the surface area of the tank, to the settling properties of the solid matter, and inversely proportional to the flow rate through the tank.

The invention of the Dorr thickener in 1905 can be considered a starting point of modern thickening. It made continuous dewatering of dilute pulp possible, whereby a regular discharge of a thick pulp of uniform density takes place concurrently with the overflow of a clarified solution. Scraper blades or rakes driven by a suitable mechanism and rotating slowly over the bottom of the tank, which usually sloped gently toward the center, moved the material as fast as it settled without enough agitation to interfere with the settling (Dorr 1915).

The first reference to variables affecting sedimentation was in 1908. Authors such as Ashley (1909), Nichols (1908a, b), Forbes (1912), Clark (1915), Free (1912) and Ralston (1916) studied the effect of solid and electrolyte concentrations, the degree of flocculation and temperature on the process.

Mishler (1912, 1916), an engineer and superintendent at the Tigre Mining Company concentrator in the Sonora desert in Mexico, was the first to show by experiment that the rate of settling slimes is different for diluted and concentrated suspensions. While the settling speed of diluted slimes is usually independent of the depth of the settling column, thick slime sedimentation rates increase with the depth of the settling column. He devised a formula by which laboratory results could be used in continuous thickeners.

Based on Clark's results (Clark 1915) and their own experiments, Coe and Clevenger (1916) recognized that the settling of an initially homogenous flocculent suspension gives rise to four settling zones. From top to bottom, they distinguished (see Fig. 8.3) a clear water zone A, a zone of constant initial concentration B, a transition zone of variable concentration C and a compression zone D.

Coe and Clevenger (1916) argued that the *solid handling capacity*, today called *solid flux*, has a maximum value in the thickener at a certain dilution, between the

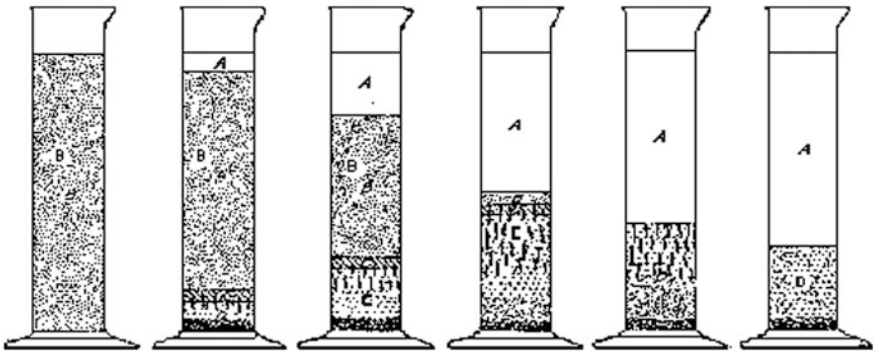

Fig. 8.3 Batch settling of a compressible pulp according to Coe and Clevenger (1916)

feed and the discharge concentration. Independently from Mishler (1912) they developed a similar equation, which with certain corrections, continues to be the most reliable method of thickener design to date.

Several authors described the settling of suspensions by extending Stokes' equation, or by empirical modeling (Egolf and McCabe 1937; Ward and Kammermeyer 1949; Work and Kohler 1940; Kammermeyer 1941), but no further important contributions were made on thickening technology until the 1940s. Stewart and Roberts (1933), reviewing the state-of-the-art of thickening, wrote:

> The basic theory is old but limitations and modifications are still but partially developed. Especially in the realm of flocculent suspensions is the underlying theory incomplete. Practical testing methods for determining the size of machines to be used are available, but the invention and development of new machines will no doubt be greatly stimulated by further investigation of the many interesting phenomena observed in practice and as fresh problems are uncovered.

8.1.3 Operating Variables in a Continuous Thickener

In the decade after Comings published his paper "Thickening of calcium carbonate slurries" (Comings 1940) at least nine engineering theses under his guidance at the University of Illinois considered the effect of operating variables in continuous thickening. Comings and his co-workers described these findings in an important paper (Comings et al. 1954). They show four zones in a continuous thickener: the clarification zone at the top, the settling zone underneath, the upper compression zone further down and the rake action zone at the bottom. Two of the most important features in the operation of a thickener were expressed for the first time, firstly that the concentration in the settling zone is nearly constant for a thickener at a steady state, with the concentration depending on the rate at which the solid is fed to the thickener and not on the concentration of the feed. It was verified that in most cases the feed was diluted to an unknown concentration on entering the thickener. The second finding was that for the same feed rate, increasing or decreasing the sediment depth could adjust the underflow concentration.

Roberts (1949) advanced the empirical hypothesis that the rate at which water is eliminated from a pulp in compression is always proportional to the amount of water left in the sediment.

8.1.4 Kinematical Theory of Sedimentation

Coe and Clevenger's design procedure (1916), which was the only quantitative work on sedimentation during the first half of the 20th century, was based on a macroscopic balance of the solid and fluid in a sedimentation vessel and on the observation of the different concentrations established in the thickener. No underlying sedimentation theory existed.

In his celebrated paper "A theory of sedimentation" in 1952 G. J. Kynch, a mathematician at the University of Birmingham in Great Britain, presented a kinematical theory of sedimentation based on the propagation of concentration waves in the suspension (Kynch 1952). The suspension was considered a continuum and the sedimentation process was represented by the continuity equation of the solid phase (See Chap. 5 of his book).

The basic assumption of Kynch's theory is that at any point in the flow field the settling velocity is a function solely of the concentration of local solids. Kynch showed that if the form of the flux-density function and the initial concentration of a suspension are known, the solution of the continuity equation can be constructed by the method of characteristics, and that this procedure describes the complete sedimentation process.

This chapter had a major influence on the development of thickening thereafter. When Comings moved from Illinois to Purdue University, research on thickening continued there for another 10 years. Three theses by Tory (1961), Stroupe (1962) and De Haas (1963) analyzed Kynch's theory and proved its validity by experiments with glass beads. Their results were published in a series of joint papers (Shannon et al. 1963; Shannon and Tory 1965, 1966). Batch sedimentation was regarded as the process of propagating concentration waves upwards from the bottom of the settling vessel. The concept of an *ideal suspension* and *ideal thickener* was presented for the first time by Shannon and Tory (1966) and complemented by Bustos et al. (1990a, 1999) and by Concha and Bustos (1992).

Kynch's theory was so successful that there was a tendency to extend its validity. Several authors, among them Fitch (1983) and Font (1988), tried to modify Kynch's theory to account for the compressive effects. This approach encountered several problems that could not be solved within the theory and a different theory was needed.

At the beginning of the 1980s, mathematicians from the University of Concepción in Chile and the Darmstadt Technical University in Germany and later the University of Stuttgart in Germany, in collaboration with the Department of Metallurgical Engineering at the University of Concepción, worked on conservation laws. They started a comprehensive study of the mathematical aspects of sedimentation. Their results were published in the doctoral theses by Bustos (1984), Kunik (1990) and in several papers by Bustos, Bürger, Concha, Wendland and other collaborators and in the book by Bustos et al. (1999). The first step in their work was to establish a rigorous framework for the theory of *batch* sedimentation of ideal suspensions (Kynch's theory). Using the method of characteristics, Bustos and Concha (1988a, b) and Concha and Bustos (1991) constructed entropy weak solutions of Kynch's problem, in which zones of constant concentrations are separated by shocks, rarefaction waves or combinations of these. For flux density functions with two inflexion points, they presented five modes of sedimentation. These finding were complemented with two other *Modes of Sedimentation* in Bustos et al. (1999) and Bürger and Tory (2000).

Similar solutions can be constructed by the method of characteristics for *continuous* sedimentation of ideal suspensions (Bustos et al. 1990a; Bustos and

Concha 1996; Concha and Bustos 1992; Concha and Bürger 1998). The solution of this equation leads to three *Modes of Continuous Sedimentation*. For a detailed or a concise overview of the construction of weak solutions, see Bustos et al. (1999) or Concha and Bürger (1998) respectively. See also Chap. 5.

On the basis of the construction of weak solutions, Bustos et al. (1990b) formulated a simple control model for continuous sedimentation of ideal suspensions in an ideal continuous thickener. It shows that certain steady states can always be recovered after perturbation of the feed flux density by solving two initial and boundary value problems at known times.

Diehl (1997, 1999) and Bürger et al. (2001, 2002) studied the effect of vessels with varying cross section and boundary conditions. Diehl showed that basically the suspension concentration increases because of its conical shape. Bürger et al. (2002) indicated that because of the varying cross sections, characteristics and isoconcentration lines do not coincide; numerical methods must be used to obtain results. Chancelier et al. (1994), Diehl (1997) and Bürger et al. (2002) treated the feed, discharge and overflow mechanisms as discontinuities of the flux density function adding a source term at the feed level, thus making boundary conditions unnecessary.

8.1.5 Phenomenological Theory of Sedimentation-Consolidation

The experience of several authors, among them Yoshioka et al. (1957), Hassett (1958, 1964a, b, 1968), Shannon et al. (1963), and Scott (1968a, b), demonstrate that, while Kynch's theory accurately predicts sedimentation for suspension of equally sized rigid particles, this is not the case for suspensions of compressible materials.

Behn (1957) was the first writer to attempt to apply consolidation theory to the settling of compressible slurries, but it was Mompei Shirato et al. (1970) who first solved the combined settling-consolidation problem. Using material coordinates, they obtained settling curves and excess pore pressure profiles. It took another five years for Adorján (1975, 1976) to present an ad-hoc theory of sediment compression, giving the first satisfactory method of thickener design.

At about the same time, a group of researchers in Brazil gave the phenomenological sedimentation theory a proper framework. Important research was going on in Brazil in the 1970s on thickening and flows through porous media in general. At COPPE, the Graduate School of the Federal University of Rio de Janeiro, several researchers and graduate students were applying a newly developed mathematical tool, the *Theory of Mixtures* of continuum mechanics to particulate systems. The findings of Giulio Massarani, Affonso Silva Telles, Rubens Sampaio, I-Shih Liu, José Teixeira Freire and João D'Avila (D'Avila 1976, 1978; D'Avila and Sampaio 1977; D'Avila et al. 1978), to mention only a few, were presented at

the Porous Media Symposia organized uninterruptedly every year since 1973 by Massarani and his group. This series was renamed the Brazilian Congress on Particulate Systems in 1996. Contributions presented at these meetings are well documented in yearly-published annals.

With strong ties to the Brazilian researchers, the author of this book worked in the same direction at the University of Concepción in Chile. Initial findings were presented by Bascur and Concha at the 1975 IMPC in Sao Paulo Brazil, by Bascur (1976) and Barrientos (1978) in their Engineering Theses, and Concha and Barrientos (1980) at the Engineering Foundation Conference on Particle Technology in New Hampshire, USA. Independently, Kos (1977) used the Theory of Mixtures to set up a boundary value problem for batch and continuous sedimentation. Thacker and Lavelle (1977) used the same theory for incompressible suspensions.

During the 1980s several papers, among them Buscall and White (1987), Auzerais et al. (1988), Landmann et al. (1988), Bascur (1989) and Davis and Russel (1989) showed that the phenomenological model based on the Theory of Mixtures was well accepted by the international scientific community.

The *phenomenological theory of sedimentation-consolidation* assumes that a particulate system composed of two superimposed continuous media with some restrictions obeys local mass and momentum balances and constitutive equations for stresses and forces. The result is a non-linear degenerate parabolic differential equation (Bürger and Concha 1998; Bürger et al. 1999; Bustos et al. 1999) describing the sedimentation and consolidation of flocculated suspensions.

Bürger et al. (2000b) and Bürger and Karlsen (2001) devised numerical methods for solving this equation. These numerical methods have built-in properties to appropriately reproduce discontinuities of the entropy solutions, especially the *suspension-sediment interface,* where the equation changes from parabolic to hyperbolic. This property makes it unnecessary to track the interface explicitly, that is, the scheme has the so-called *shock-capturing property* Bürger et al. (2000d). Garrido et al. (2000) showed the application of this method to several batch sedimentation processes published in the literature.

Concha and coworkers (Garrido et al. 2004, 2003) developed a thickener design and simulation procedure based on the numerical method of Bürger and Karlsen (2001). This procedure was the most comprehensive design method yet presented in the literature. Garrido (2005) and Concha et al. (2006a, b) presented methods and new instrumentation to determine thickening parameters and Segovia and Concha (2012) designed and constructed on-line instruments to determine these parameters. Using these instruments Segovia et al. (2011) and Betancourt et al. (2013) presented algorithms for the automatic control of thickeners.

A research group in Melbourne Australia developed steady state thickener models based on the same theory but with slightly different variables and parameters. Their results are equivalent to those of Concha and co-workers (Green 1997; Green et al. 1998; De Kretser et al. 2001; Usher et al. 2001; Usher 2002; Shane et al. 2005).

8.2 Equipment

The continuous thickener is a typical device that has not changed much since Dorr invented it in 1905. They have become larger and are built of different materials, such as wood, steel or cement and their raking system has been improved and modernized, but their elements continue to be the same. Figure 8.4 shows the original *Dorr thickener*. The cylindrical tank is the body of the equipment, with the feedwell, overflow launder, rakes and underflow discharge, all common elements in any modern thickener.

In small units of less than 30 m in diameter, the cylindrical tank is steel or wood, while tanks up to 150 m in diameter are made of concrete. The bottom of the thickener is made of the same material as the tank and has a cone in the center to improve sediment evacuation.

The feedwell is a small concentric cylinder designed to thoroughly mix incoming pulp with the flocculant and in some cases to dilute the feed and deliver it evenly into the thickener. Many thickeners have baffles to accomplish these tasks. See Figs. 8.5 and 8.6. We will discuss this subject further in Sect. 8.7.

Rakes transport the sediment from the bottom of the tank to the underflow discharge orifice. The rakes, which can have several supporting structures, rotate at a rate on the order of one revolution per hour. A secondary effect of the rakes is to produce channels in the sediment through which water can escape to the surface, thus increasing the pulp density of the underflow. The rakes can have a central motor as shown in Fig. 8.6 or a peripheral tracking system, Fig. 8.7.

All thickener models have mechanism to lift the rakes whenever the torque to move the sediment becomes excessive. See Figs. 8.8 and 8.9.

Supernatant water overflows at the top of the thickener through overflow launders as shown in Fig. 8.10. The overflow launder at the tank periphery receives water recovered from the pulp and evacuates it slowly to avoid dragging fine particles. A flow of about 0.1 (m^3/min/m of perimeter) is common.

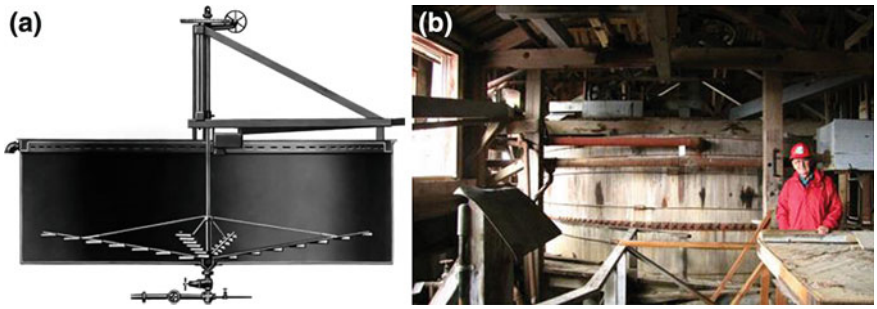

Fig. 8.4 Original Dorr thickener. **a** Schematic Dorr thickener invented in 1905 (Dorr 1936). **b** 6 m diameter Dorr thickener, Kennicott Alaska 1938 (conventional thickener)

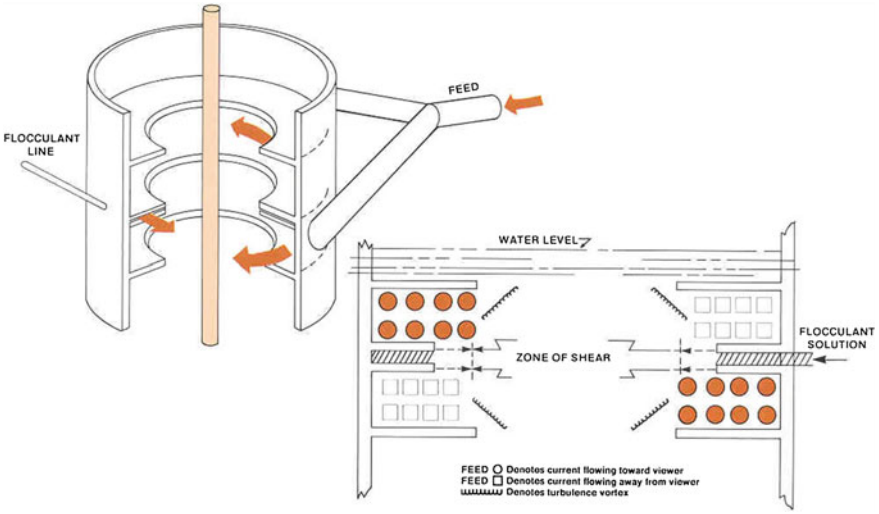

Fig. 8.5 Feedwell with two tangential entries and internal baffles (courtesy Dorr-Oliver)

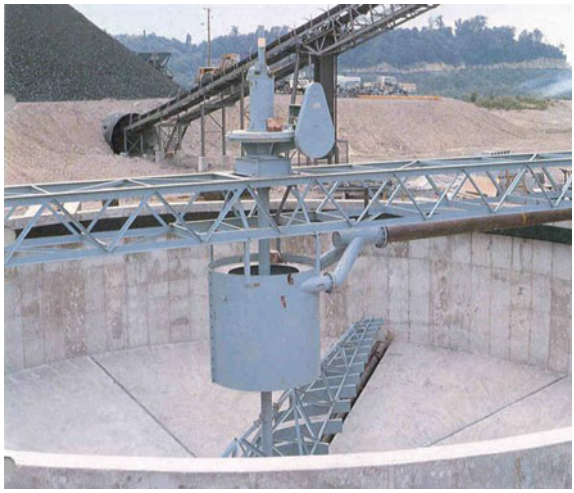

Fig. 8.6 Small thickener with two tangential entries showing centrally driven rakes (courtesy Dorr-Oliver)

8.2.1 Conventional, High Rate, High Density and Paste Thickeners

Thickeners are usually classified into four types: conventional thickeners, high-rate thickeners, high-density thickeners and paste thickeners. See Fig. 8.11.

In a *Conventional Thickener* the feedwell is located in the upper part of the tank. When the feed enters it, it is diluted to the so-called *conjugate concentration*

Fig. 8.7 Thickener with peripheral tracking system (courtesy of Eimco process equipment)

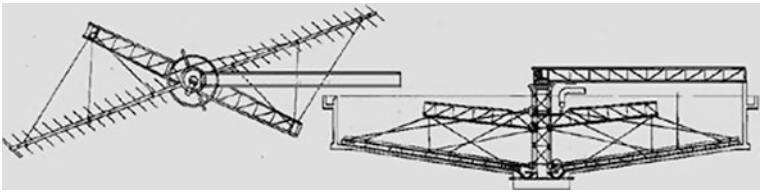

Fig. 8.8 Rakes with lifting system (courtesy of Dorr-Oliver)

Fig. 8.9 Rakes with lifting system (courtesy of Eimco process equipment)

by an upcoming flow of water. The diluted suspension settles at a constant velocity to form sediment at the bottom of the tank. Figure 8.12 shows a scheme of a conventional thickener.

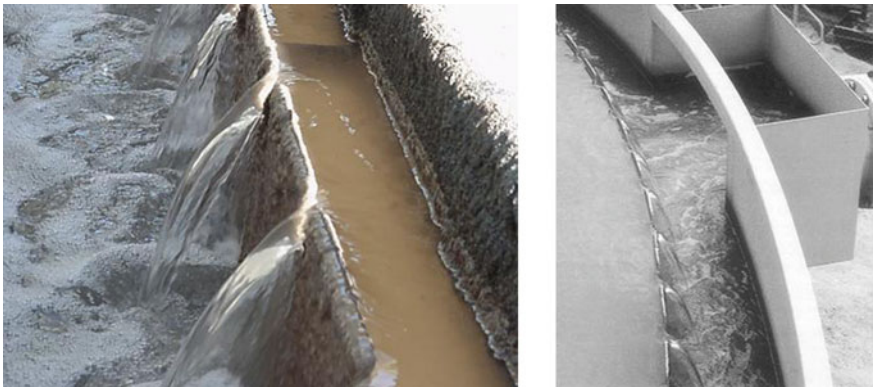

Fig. 8.10 Overflow launders (courtesy of Outokumpu Supaflo technologies)

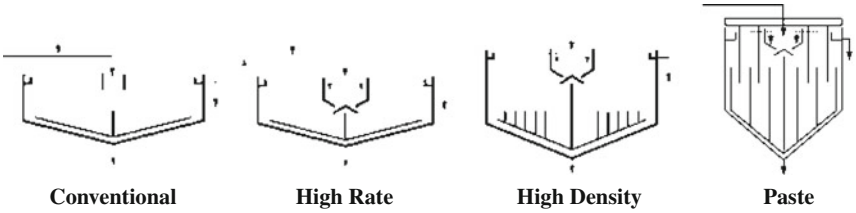

Fig. 8.11 Schematic drawings of the different types of thickeners (Fl Smith)

Fig. 8.12 Schematic drawings of a conventional thickener

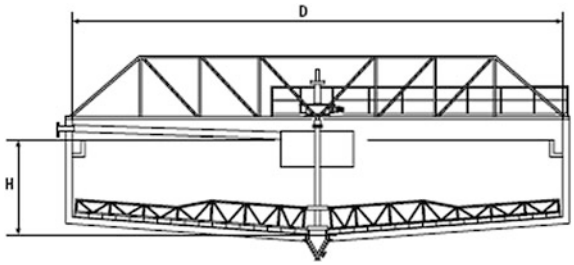

In the early 1960s machines known as *high capacity* or *high rate thickeners* were introduced into the mining industry by various manufacturers (Eimco HI-CAP, Enviroclear High Capacity CT). See Fig. 8.13.

These thickeners have longer feedwells that deliver the feed directly into the sediment. When the feed is mixed with the high-density sediment, it increases in concentration forming a suspension with a concentration equal to or higher than the critical concentration. Therefore there is no settling zone in this type of thickener. Often the underflow of high capacity thickeners is recycled to the feed,

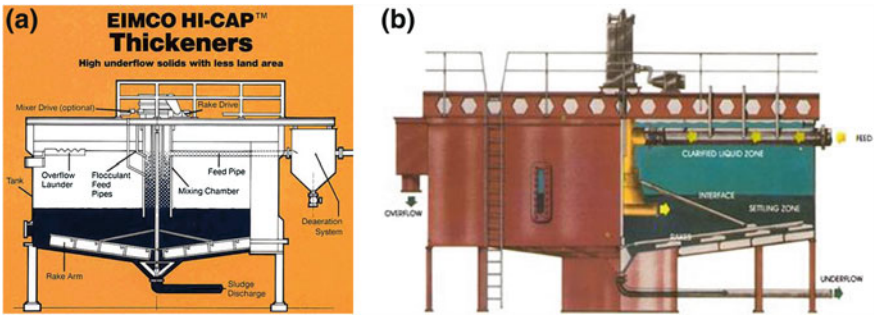

Fig. 8.13 Schematic view of high capacity thickeners. **a** EIMCO HI-CAP thickener (Eimco 2011). **b** EVIRO-CLEAR CT (Enviro Clear 2011)

producing a mixture of higher concentration that supposedly increases the equipment capacity.

Later in this chapter we will show that it is more appropriate to talk of conventional and high capacity *operations* than of conventional and high capacity *thickeners*, and furthermore, that if one chooses to operate a thickener in a high capacity mode, there is always a conventional operation that has equal or higher capacity. It is the flocculant dose, the feed dilution and the optimum shear rate that eventually defines the capacity of a thickener.

The term *high capacity* or *high rate thickeners* is used for small to medium sized thickener but also for large conventional thickeners processing very high tonnage due to the optimization of flocculation by careful choice of the flocculant dose and feed slurry concentration. See Fig. 8.14.

High-density and paste thickeners are similar to conventional or high rate thickeners, but with steeper cones and much higher cylindrical tanks. The additional height produces more pressure on the sediment at the bottom of the tank and therefore denser underflow. Picket fences are used in both types of thickeners to help consolidate the sediment. The only difference between them is that paste thickeners are much taller and slimmer than High Density thickeners. Figure 8.15 shows a schematic view and Figs. 8.16 and 8.17 show high-density thickeners.

Fig. 8.14 125 m high-rate thickener (Smith 2013)

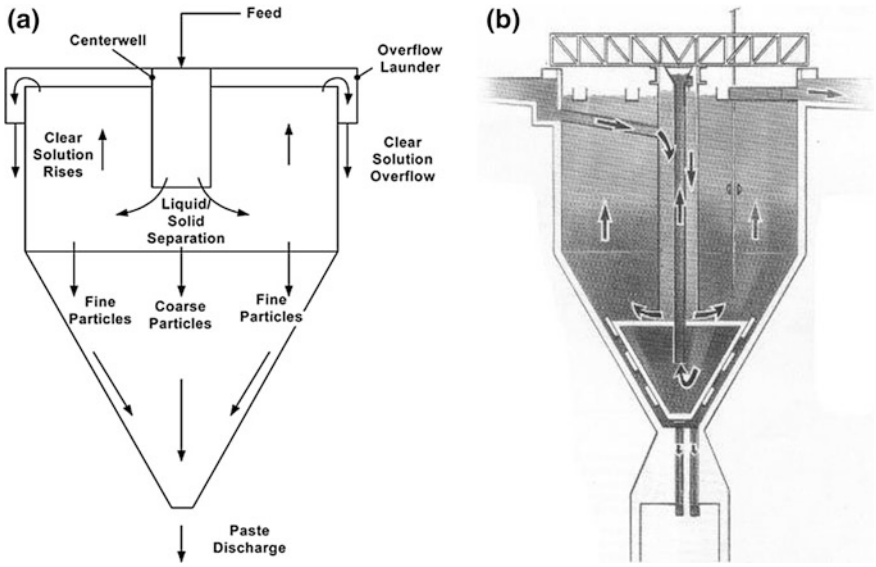

Fig. 8.15 Schematic views of paste thickeners. **a** Conventional mode of operation Innovat (2013). **b** High capacity mode of operation Delkor (2013)

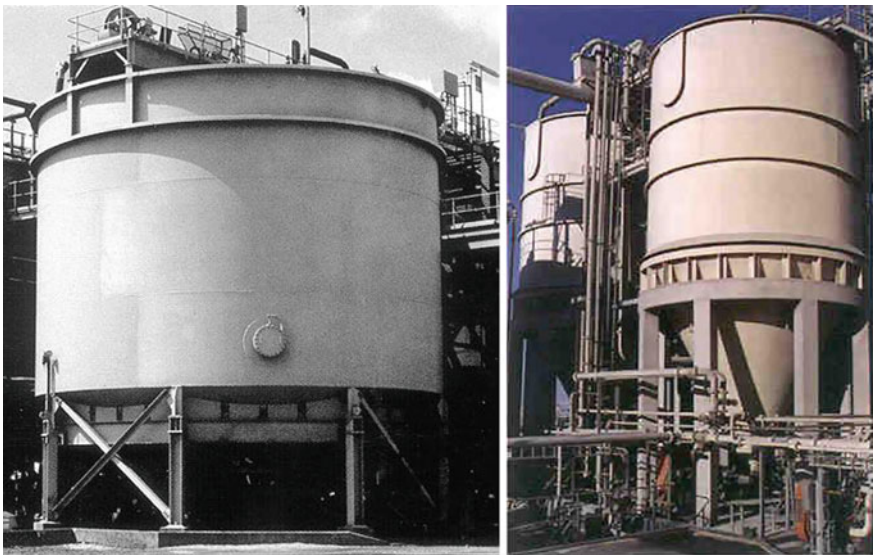

Fig. 8.16 View of high density and paste thickeners (courtesy of Eimco process equipment)

Fig. 8.17 View of paste thickeners. (courtesy of Eimco process equipment)

8.3 Thickening Theory

Thickening consists of the superposition of two phenomena, sedimentation and consolidation, which behave differently.

During sedimentation, particles settle individually by collision among them and through the fluid by pressure and friction. See Fig. 8.18a. Sedimentation of individual particles and suspensions, which was analyzed in Chaps. 4 and 5, consist of gravity settling particles or flocs in a fluid, in our case, water. At a certain

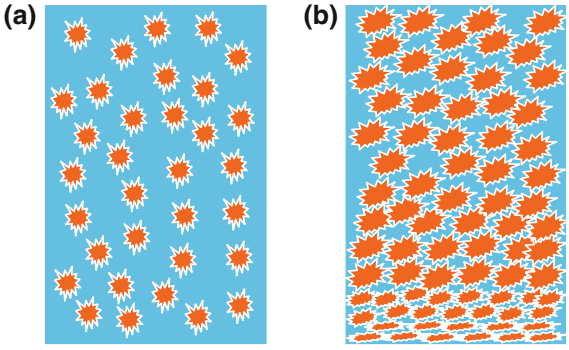

Fig. 8.18 Physical model of sedimentation and consolidation.
a Sedimentation.
b Consolidation

concentration, particles begin to touch each other transforming the suspension into a network of solid particles called *sediment*. Now, forces among particles are transmitted directly from particle to particle. If settling particles that reach the bottom of the vessel and lay one on top of the other are incompressible, such as glass beads, the whole process ends, but if they are compressible, as is the case with flocculated copper flotation tailings, the weight of the sediment compresses the flocs lying underneath expelling the water from the pores. This phenomenon of extracting water by compression is called *consolidation*. See Fig. 8.18b.

Consolidation is an important discipline in several fields besides thickening, for example in Geotechnique, which studies the behavior of the ground when buildings are constructed. In this case, the applied force on the consolidating material is the external weight of buildings. In thickening, the force compressing the sediment is its own weight, which makes a major difference in the theory of consolidation given the scale of the forces.

Sedimentation and consolidation are usually separated by an interface having a characteristic concentration. The concentration of this interface, where the sedimenting particles or flocs begin to touch each other, is called a *critical concentration*, also known as *compressive yield point* by authors from the field of colloidal science.

8.3.1 Dynamic Thickening Process

Field Equations

The phenomenological theory of sedimentation ignores the individuality and physical structure of particles and fluids, and considers the solid and the fluid as continuous media. The properties of the solid and fluid involved in thickening are those describing sedimentation and consolidation: (1) the concentration of the suspension; (2) the solid phase velocity, (3) the fluid phase velocity, (4) the solid–fluid interaction force, (5) the excess pore pressure and (6) the compressibility of the sediment. Properties (1) to (6) have the following associated *field variables*. See Chap. 3.

$$\text{Solid concentration, as volume fraction} \quad \varphi(z,t) \tag{8.1}$$

$$\text{Solid flux density} \quad f(z,t) \tag{8.2}$$

$$\text{Convective pulp velocity} \quad q(z,t) \tag{8.3}$$

$$\text{Solid--fluid interaction force} \quad m_d(z,t) \tag{8.4}$$

$$\text{Excess pore pressure} \quad p_e(z,t) \tag{8.5}$$

$$\text{Solid stress effective} \quad \sigma_e(z,t) \tag{8.6}$$

These variables constitute a *dynamic thickening process* in regions where the variables are continuous when they obey the following four *field equations*. See Chap. 3.

$$\frac{\partial \varphi}{\partial t} + \frac{\partial f}{\partial z} = 0 \tag{8.7}$$

$$\frac{\partial q}{\partial z} = 0\,, \quad \text{with} \quad q = v_s - (1-\varphi)v_r \tag{8.8}$$

$$\frac{\partial \sigma_e}{\partial z} = -\Delta\rho\varphi g + \frac{m_d}{1-\varphi} \tag{8.9}$$

$$\frac{\partial p_e}{\partial z} = -\frac{m_d}{1-\varphi} \tag{8.10}$$

where $f = \varphi v_s$ is the solid flux density function, $v_r = v_s - v_f$ is the relative solid–fluid velocity and m_d is the solid–fluid dynamic interaction force. To understand the conditions for these equations to be valid, see Chap. 3.

At discontinuities, the field equations are not valid and the following *jump conditions* should be used:

$$[f] = \sigma[\varphi]; \quad [q] = 0 \tag{8.11}$$

where σ is the displacement velocity of the discontinuity. For conditions that σ must obey, see Eqs. (5.12, 5.13).

Constitutive Equations

Since we have six field variables and only four field equations, two constitutive equations should be established to describe the relationship between the dynamic variables m_d and σ_e and the kinematic variables φ and v_r:

$$m_d = m_d(\varphi, \varphi_c v_r) \tag{8.12}$$

$$\sigma_e = \sigma_e(\varphi, \varphi_c, v_r) \tag{8.13}$$

Compressibility of the Sediment

Experience has demonstrated that the solid effective stress can be expressed solely as a function of the concentration. As we noted at the beginning of this chapter, the only way momentum is transferred directly from particle to particle during sedimentation is by particle collision. Therefore, for solid concentrations below the critical level where particles are suspended in the fluid, the effective stress is a constant. At concentration greater than the critical concentration, the network of particles formed transmits forces directly among particles in the sediment. The self-weight of the particles is transmitted through the network

producing compression and increasing the solid concentration of the sediment. This phenomenon can be characterized by the following restriction for solid effective solid stress $\sigma_e(\varphi)$:

$$\sigma'_e = \frac{d\sigma_e}{d\varphi} = \begin{cases} 0 & \text{for } \varphi < \varphi_c \\ \geq 0 & \text{for } \varphi \geq \varphi_c \end{cases} \tag{8.14}$$

Two common expressions have been used for the solid effective stress:

$$\sigma_e(\varphi) = \begin{cases} \text{constant for} & \varphi < \varphi_c \\ \alpha \exp(\beta\varphi) \text{for} & \varphi \geq \varphi_c \end{cases} \tag{8.15}$$

$$\sigma_e(\varphi) = \begin{cases} \text{constant} & \text{for} \quad \varphi < \varphi_c \\ \sigma_0 \left(\left(\frac{\varphi}{\varphi_c} \right)^n - 1 \right) & \text{for} \quad \varphi \geq \varphi_c \end{cases} \tag{8.16}$$

Solid–Fluid Interaction Force During Sedimentation ($\varphi < \varphi_c$)

During settling, for $\varphi < \varphi_c$, the flocs move slowly through the fluid and the hydro-dynamical force can be represented as a linear function of relative solid–fluid velocity:

$$m_d = -\mu K(\varphi) v_r \tag{8.17}$$

where $K(\varphi)$ is the *translational solid–fluid resistance coefficient*. Replacing $K(\varphi)$ in Eq. (8.9), with $\sigma'_e(\varphi) = 0$, yields:

$$0 = -\Delta\rho\varphi g - \frac{\mu K(\varphi) v_r}{1 - \varphi}; \quad \varphi < \varphi_c$$

from which the relative solid–fluid velocity v_r is:

$$v_r = -\frac{\Delta\rho\varphi(1-\varphi)g}{\mu K(\varphi)} \tag{8.18}$$

Replacing v_r from (8.18) in (8.8); from the result calculate v_s and, multiplying by φ, obtain:

$$f = q\varphi - \frac{\Delta\rho\varphi^2(1-\varphi)^2 g}{\mu K(\varphi)} \tag{8.19}$$

Defining a parameter $f_{bk}(\varphi)$ in the form:

$$f_{bk}(\varphi) = -\frac{\Delta\rho\varphi^2(1-\varphi)^2 g}{\mu K(\varphi)}, \tag{8.20}$$

Eq. (8.19) can be written in the form:

$$f = q\varphi + f_{bk}(\varphi), \quad \text{for } \varphi < \varphi_c \tag{8.21}$$

Finally, replacing (8.21) in (8.7) yields:

$$\frac{\partial \varphi}{\partial t} + \frac{\partial}{\partial z}(q\varphi + f_{bk}(\varphi)) = 0, \quad \text{for } \varphi < \varphi_c \tag{8.22}$$

Equation (8.22) describes the *sedimentation of particles, compressible or not, in a suspension of less than the critical concentration* ($\varphi < \varphi_c$). It can be identified as Kynch's equation for continuous sedimentation of ideal suspensions. See Eqs. 5.8 and 5.10. The function $f_{bk}(\varphi)$, defined by (8.20), is the *Kynch solid flux density function* and can be considered the constitutive equation for the sedimentation process. The Kynch sedimentation process is completely determined once the constitutive equation and the initial conditions are established.

Adding Eqs. (8.9) and (8.10) gives:

$$\frac{\partial (p_e + \sigma_e)}{\partial z} = -\Delta\rho\varphi g$$

from which the excess pore pressure can be obtained once (8.22) is solved for $\varphi(z)$:

$$p_e(z) = -\left(\sigma_e + \Delta\rho g \int_z^L \varphi(\xi) d\xi\right) \tag{8.23}$$

Solid–Fluid Interaction Force During Consolidation ($\boldsymbol{\varphi \geq \varphi_c}$)

During consolidation, the fluid moves slowly though the porous bed constituting the sediment and can be quantified by the permeability of the bed and the viscosity of the fluid. For the slow motion of a Newtonian fluid through a compressible porous bed, Darcy's equation is valid (see Chap. 6):

$$m_d = -\frac{\mu}{k(\varphi)}(1-\varphi)^2 v_r \tag{8.24}$$

where $k(\varphi)$ and μ are the permeability of the sediment and the fluid viscosity respectively. Replacing m_d from (8.24) in (8.9) and from this result calculate v_r:

$$v_r = -\frac{k(\varphi)}{\mu} \times \frac{\Delta\rho\varphi g}{(1-\varphi)}\left(1 + \frac{\sigma_e'(\varphi)}{\Delta\rho\varphi g}\frac{\partial\varphi}{\partial z}\right) \quad \text{for } \varphi \geq \varphi_c \tag{8.25}$$

Replacing (8.25) in (8.8) and multiplying by φ, gives us:

$$f = q\varphi - \frac{k(\varphi)}{\mu} \times \frac{\Delta\rho\varphi^2 g}{(1-\varphi)}\left(1 + \frac{\sigma_e'(\varphi)}{\Delta\rho\varphi g}\right)\frac{\partial\varphi}{\partial z} \quad \text{for } \varphi \geq \varphi_c \tag{8.26}$$

Parameter $f_{bk}(\varphi)$, for $\varphi \geq \varphi_c$, is defined in the form:

$$f_{bk}(\varphi) = -\frac{k(\varphi)}{\mu} \times \frac{\Delta\rho\varphi^2 g}{(1-\varphi)} \quad \text{for } \varphi \geq \varphi_c, \tag{8.27}$$

and note that Eq. (8.27) has the same role as Eq. (8.20) but now permeability $k(\varphi)$ is the parameter instead of the translational resistance coefficient $K(\varphi)$.

Equations (8.20) and (8.27) can be combined to define an extended Kynch solid flux density function for all values of φ:

$$f_{bk}(\varphi) = \begin{cases} -\dfrac{\Delta\rho\varphi^2(1-\varphi)^2 g}{\mu K(\varphi)} & \text{for } \varphi < \varphi_c \\ -\dfrac{k(\varphi)}{\mu}\Delta\rho\varphi^2 g & \text{for } \varphi \geq \varphi_c \end{cases}, \tag{8.28}$$

Substituting (8.28) on Eq. (8.8), we can write the solid flux density function for the whole range of concentration in the form:

$$f = q\varphi + f_{bk}(\varphi)\left(1 + \frac{\sigma_e'(\varphi)}{\Delta\rho\varphi g}\right)\frac{\partial\varphi}{\partial z} \quad \text{for } 0 < \varphi < 1 \tag{8.29}$$

Thickening Equation

Replacing (8.29) in (8.7) yields:

$$\frac{\partial\varphi}{\partial t} + \frac{\partial}{\partial z}\left(q\varphi + f_{bk}(\varphi)\left(1 + \frac{\sigma_e'(\varphi)}{\Delta\rho\varphi g}\frac{\partial\varphi}{\partial z}\right)\right) = 0, \quad \text{for } 0 < \varphi < 1 \tag{8.30}$$

which can be written in the form

$$\frac{\partial\varphi}{\partial t} + \frac{\partial}{\partial z}(q\varphi + f_{bk}(\varphi)) = \frac{\partial}{\partial z}\left(-\frac{f_{bk}(\varphi)\sigma_e'(\varphi)}{\Delta\rho\varphi g}\frac{\partial\varphi}{\partial z}\right), \quad \text{for } 0 < \varphi < 1 \tag{8.31}$$

Equation (8.31) is a *degenerate parabolic partial differential equation*. The name comes from the fact that for values of $\varphi < \varphi_c$; $\sigma_e(\varphi) = 0$ the equation becomes *hyperbolic*:

$$\frac{\partial\varphi}{\partial t} + \frac{\partial}{\partial z}(q\varphi + f_{bk}(\varphi)) = 0, \quad \text{for } \varphi < \varphi_c \tag{8.32}$$

This result shows that for *compressible flocculated suspensions Kynch's equation is still valid in those regions where the concentration is less than critical.*

Still another form of expressing Eq. (8.31) is obtained by defining the *diffusion coefficient* $\mathfrak{D}$ in the form:

$$\mathfrak{D} = \begin{cases} 0 & \text{for } \varphi < \varphi_c \\ -\dfrac{f_{bk}(\varphi)\sigma_e'(\varphi)}{\Delta\rho\varphi g} & \text{for } \varphi \geq \varphi_c \end{cases} \tag{8.33}$$

then replacing (8.33) in (8.31) the following alternative of the thickening equation is obtained as a *convective-diffusion equation*:

$$\frac{\partial \varphi}{\partial t} + \frac{\partial}{\partial z}(q\varphi + f_{bk}(\varphi)) = \frac{\partial}{\partial z}\left(\mathfrak{D}(\varphi)\frac{\partial \varphi}{\partial \mathfrak{z}}\right), \quad \text{for } 0 \leq \varphi < 1 \tag{8.34}$$

8.3.2 Batch Thickening

To obtain a description of batch thickening, we will repeat and complete the stages in the sedimentation process described in Chap. 5.

(a) Before sedimentation starts, the suspension is flocculated and homogenized by agitation so that its concentration is constant.
(b) At the beginning of sedimentation, all flocs settle at the same speed forming a well-defined water-suspension interface in the upper part of the column. This interface descends at the same speed as the flocs. This stage is called *hindered settling*. A diffuse interface indicates incomplete flocculation, especially of the fine particles.
(c) When the flocs reach the bottom of the column, they rapidly occupy the entire available area forming a *sediment*. From then on, the flocs accumulate one on top of another, compressing those lying underneath. We say the sediment is under *compression* or *consolidation*.
(d) The interface between the sediment and the settling suspension has no flocs lying on top of it and therefore suffers no compression. The concentration at which this occurs is called *critical concentration*.
(e) Following a given constant concentration φ over a period of time, for example, setting an X Ray instrument such as that described by Been and Sills (1981) at a given concentration, it will move upwards during sedimentation from the bottom of the column at a constant characteristic speed as time passes. This upward motion is termed the *wave of constant concentration* φ.
(f) At a certain instant, the water-suspension and the suspension-sediment interfaces meet. The coordinates at this time are called *critical height* and *critical time* and they define the *critical point* where hindered sedimentation ends and flow in the porous media and consolidation prevails. In time, consolidation ends and a characteristic concentration profile is established in the column. Water in the upper part is followed by a concentration gradient from the critical concentration at the top to the sediment to a maximum concentration at the bottom of the column. Figure 8.19 is a typical sedimentation curve showing the interfaces and constant concentration lines.

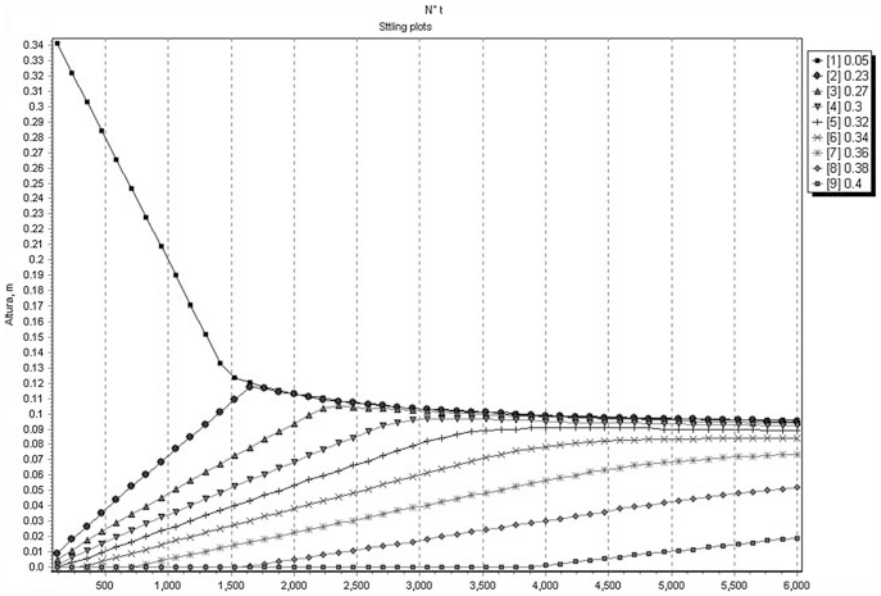

Fig. 8.19 Sedimentation *curve* for a copper flotation tailing, showing the water-suspension interface ($\varphi = 0.05$) and the suspension-sediment interfaces ($\varphi = 0.23$) and several *lines* of constant concentration. Data from Becker (1982)

(a) Initial and boundary value problem

In batch sedimentation there is no convective flow, therefore $q = 0$ and (8.31) reduce to:

$$\frac{\partial \varphi}{\partial t} + \frac{\partial}{\partial z}\left(f_{bk}(\varphi)\left(1 + \frac{1}{\Delta\rho\varphi g}\frac{\partial \sigma_e(\varphi)}{\partial z}\right)\right) = 0, \quad 0 \le z \le L; \text{ for } 0 < \varphi < 1 \tag{8.35}$$

From stage (a) of batch sedimentation, the initial condition is known and is set at $\varphi(z,t) = \varphi_0$ for $0 \le z \le L$, and the boundary condition at $z = L$ is $\varphi(L,t) = 0$.

At the bottom of the column, where $z = 0$, the velocity of the solid is zero and therefore the solid flux $f_{bk}(0,t) = 0$. From (8.29), for $t \ge 0$, the boundary condition is $\partial\varphi/\partial z|_{z=0} = \Delta\rho\varphi g/\sigma_e'(\varphi)$. Then the initial-boundary condition can be expresses as:

$$\varphi(z,0) = \varphi_0, \quad \text{for } 0 \le z \le L \tag{8.36}$$

$$\varphi(L,t) = 0, \quad \text{for } t > 0 \tag{8.37}$$

$$\left.\frac{\partial \varphi}{\partial z}\right|_{z=0} = \frac{\Delta\rho\varphi g}{\sigma_e'(\varphi)}, \quad \text{for t} \ge 0 \tag{8.38}$$

where L and φ_0 are the initial height and initial concentration of the suspension.

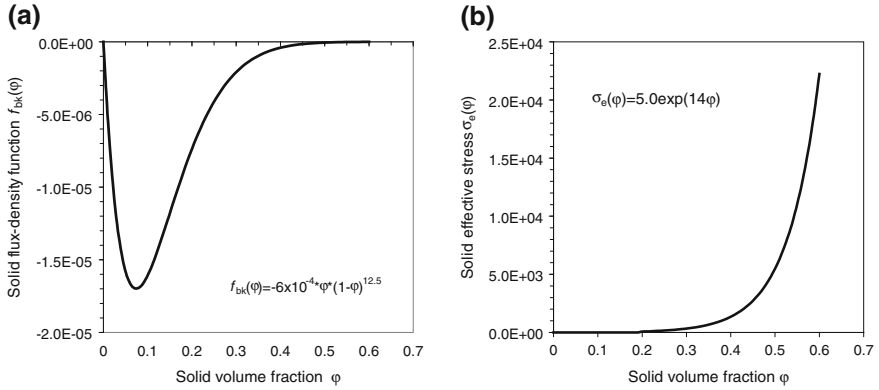

Fig. 8.20 Thickening parameters for a flocculated copper flotation tailing. Data from Becker (1982). **a** Solid flux density function. **b** Solid effective stress

Figure 8.20 shows the typical form of parameters $f_{bk}(\varphi)$ and $\sigma_e(\varphi)$.

$$f_{bk}(\varphi) = u_\infty \varphi(1-\varphi)^c \quad \text{and} \quad \sigma_e(\varphi) = \begin{cases} 0 & \text{for} \quad \varphi \le \varphi_c \\ \alpha \exp(\beta\varphi) & \text{for} \quad \varphi > \varphi_c \end{cases} \tag{8.39}$$

where u_∞, c, α and β are empirical parameters.

Mathematical analysis by Bürger et al. (2000b) imply that the initial-boundary value problem, given by Eqs. (8.35) to (8.39), has a unique solution depending on φ_0 and is therefore well posed, even in cases where $\sigma_e'(\varphi)$ is discontinuous at $\varphi = \varphi_c$.

(b) **Numerical solution**

The initial-boundary value problem is solved numerically using a finite-difference operator splitting method described by Bürger and Concha (1998). The equation is split into a second order diffusion equation, a linear convective equation and a non-linear first order hyperbolic equation, which are solved numerically for each time step by an implicit finite difference method, a second order upwind method and a second order total-variation diminishing method, respectively. For details see Bürger and Concha (1997, 1998), Bustos et al. (1999) and Bürger et al. (2000c). The algorithm for the solution of the equation is given in Fig. 8.21.

The solution to this problem, with parameters shown in Fig. 8.20, is given by the settling curve in Fig. 8.19 and the concentration profile in Fig. 8.22.

(c) **Simulation and comparison with published experimental results**

Several cases published in the literature were simulated with Eq. (8.35) and compared with the experimental results (Bürger et al. 1999, 2000a; Garrido et al. 1999). All simulations of batch sedimentation with the phenomenological model

Fig. 8.21 Algorithm for the simulation of batch sedimentation according to Garrido et al. (2001)

$$L, t, \varphi_0, \varphi_c, \rho_s, \rho_f, u_\infty, c, \alpha, \beta \text{ or } \sigma_0, n$$

$$\Downarrow$$

Determine Δt romthe CFL condition

Solve the mdel functions

$$\frac{\partial \varphi}{\partial t} + \frac{\partial f_{bk}(\varphi)}{\partial z} = -\frac{\partial}{\partial z}\left(\frac{f_{bk}(\varphi) \times \sigma_e^{'}(\varphi)}{\Delta \rho \varphi g} \frac{d\varphi}{dz} \right)$$

Using the model functions

$$f_{bk}(\varphi) = u_\infty \varphi (1-\varphi)^c$$

$$\sigma_e(\varphi) = \alpha \exp(\beta \varphi)$$

by the generalized upwind method with extrapolation.

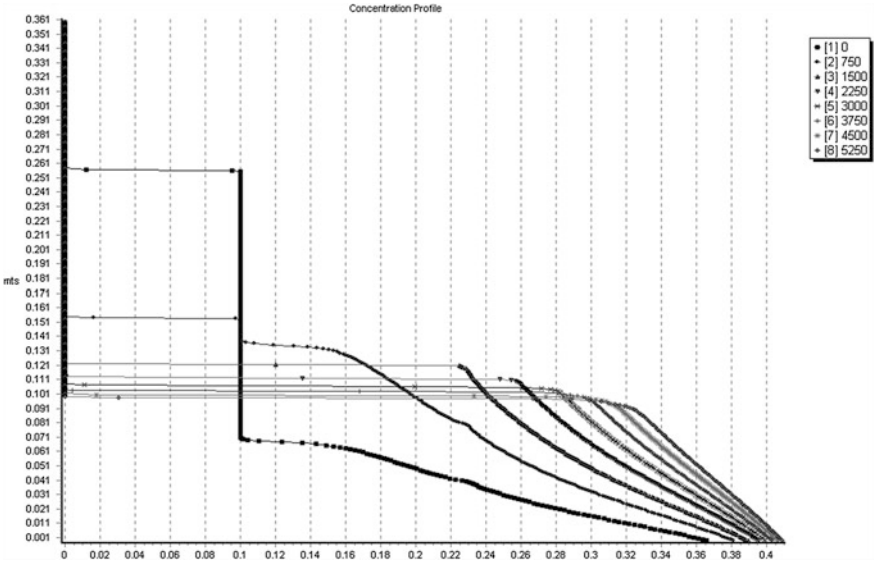

Fig. 8.22 Concentration profile for batch sedimentation with parameters given in Fig. 8.20

closely approximate the experimental results for the settling curve, concentration profile and excess pressure profile. These results affirm the value of the model presented in this work. See Figs. 8.22, 8.23, 8.24, 8.25, 8.26, 8.27.

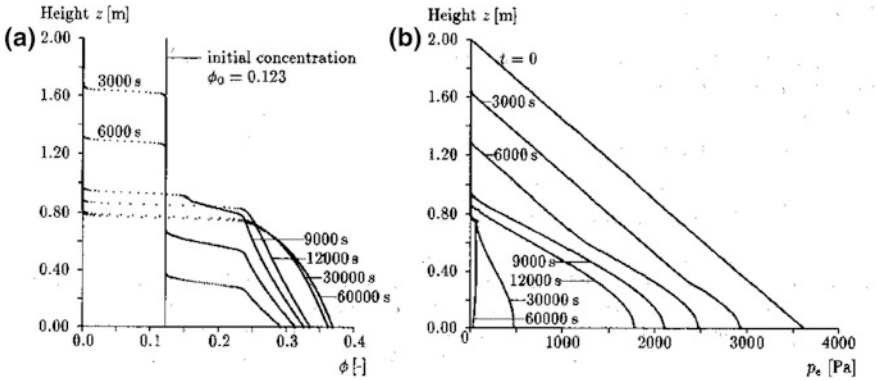

Fig. 8.23 Simulation of the sedimentation of a flotation copper tailing (Bürger and Concha 1998). **a** Concentration profiles. **b** Excess pore pressure profiles

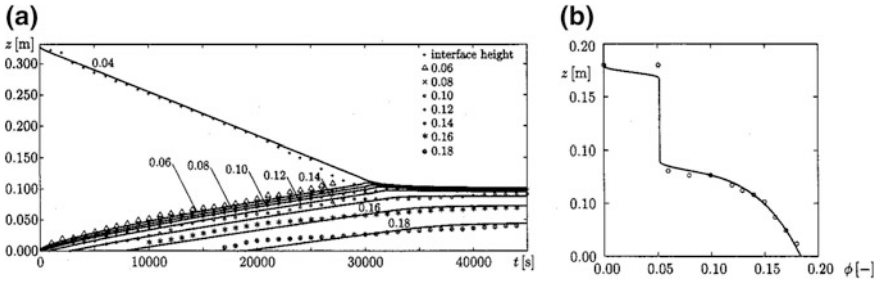

Fig. 8.24 Simulation and experimental sedimentation data of Holdich and Butt (1997) (Garrido et al. 2000). **a** Settling curve. **b** Concentration profile for 22.000 s

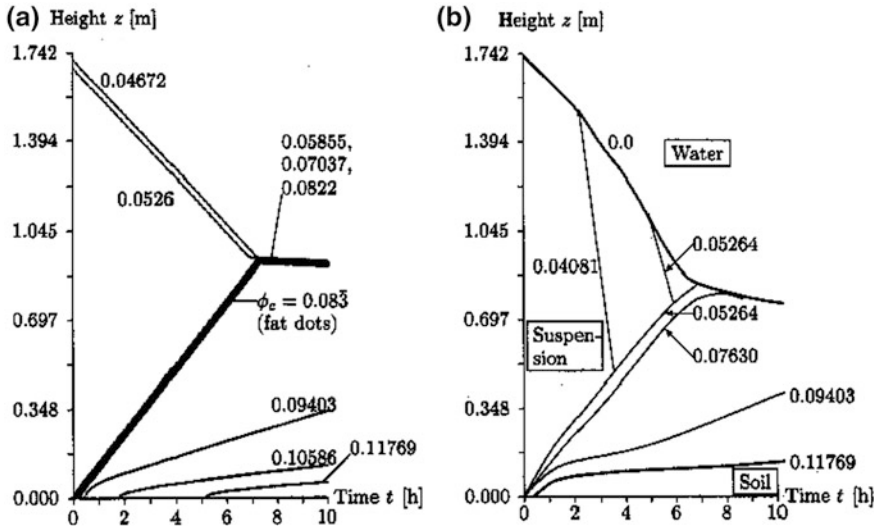

Fig. 8.25 Comparison of simulated and experimental results of Been and Sills (1981) for the settling and consolidation of a soil. **a** Simulation. **b** Experimental

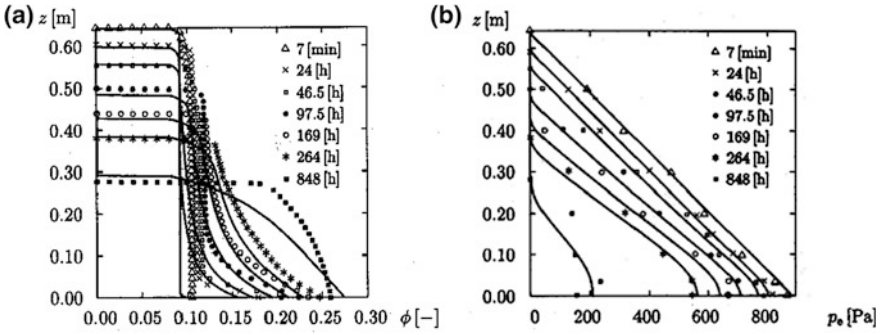

Fig. 8.26 Simulation and experimental data from Been y Sills (1981) experiment N° 11, (Bürger et al. 2000a). **a** Concentration profile. **b** Excess pore pressure profile

8.3.3 Model of Conventional Thickening

To analyze continuous conventional thickening it is useful to study separately steady state and transient behavior. For steady state, the field equations are significantly simplified with $\partial\varphi/\partial t = 0$ and there is no need to solve the entire degenerate parabolic equation numerically.

(a) **Field equations at steady state**

Equations (8.35) to (8.39) represent the transient evolution of the field variables in a continuous thickener. Eliminating the time dependence of these equations, the steady state in a continuous thickener is obtained for regions where the variables are continuous:

$$\frac{\partial f}{\partial z} = 0 \tag{8.40}$$

$$\frac{\partial q}{\partial z} = 0, \quad \text{with } q = v_s - (1-\varphi)v_r \tag{8.41}$$

$$\frac{\partial \sigma_e}{\partial z} = -\Delta\rho\varphi g + \frac{m_d}{1-\varphi} \tag{8.42}$$

$$\frac{\partial p_e}{\partial z} + \frac{\partial \sigma_e}{\partial z} = -\Delta\rho\varphi g \tag{8.43}$$

Equations (8.40) and (8.41) indicate that the solid flux density f and the volume average velocity q are constant in the thickener and are determined by boundary conditions. At discontinuities, fluxes are continuous and $\sigma[\varphi^+, \varphi^-] = 0$ and $[q] = 0$.

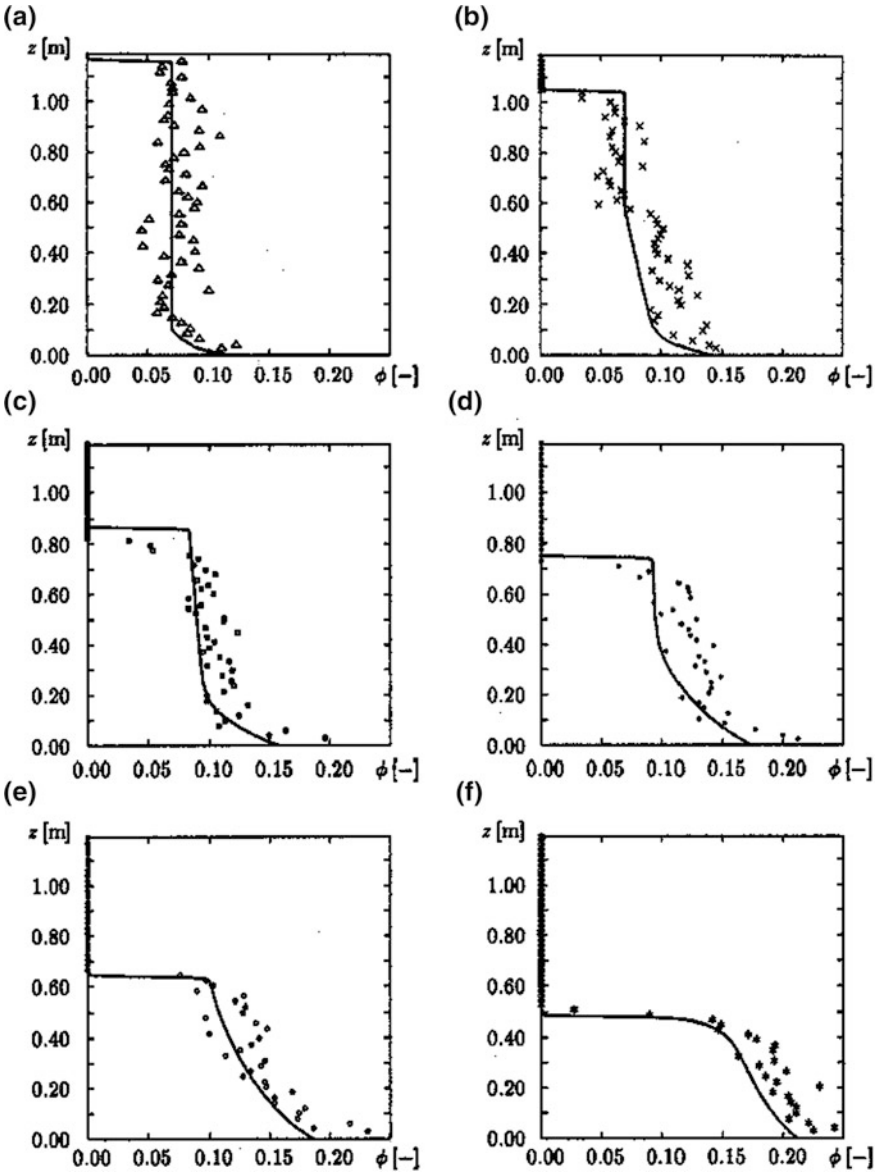

Fig. 8.27 Comparison of simulated results with experimental results of kaolin suspensions. Dreher (1997): **a** t = 0.052 days, **b** t = 0.312 days, **c** t = 0.87 days, **d** t = 2.13 days, **e** 3.91 days and f = 13.27 days (Bürger et al. 2000)

(b) **Solution of the boundary value problem**

Feed

The feed to the thickener is assumed totally flocculated in the feedwell and is mixed with the upcoming water as it enters the thickener body at $z = L$. It dilutes rapidly and spreads evenly throughout the thickener's cross-section. The only source of solids in the thickener is the feed and, since no solid passes to the overflow, the solid flux density is continuous at the feed level. This phenomenon is modeled by assuming a *surface source* of strength f_F at the feed level L. Ideal Continuous Thickener (ICT), (see Sect. 5.3.1 for the definition). If we choose $Q_F > 0$, the volume flow of the feed pulp of solid concentration φ_F, the solid feed flux density f_F is defined by:

$$f_F = \frac{-Q_F \varphi_F}{S} < 0$$

where S is the thickener's cross-sectional area. Then, by (8.40):

$$f(z) = f_F$$

Due to the dilution of the feed, the concentration at the feed level φ_L, known as *conjugate concentration* can be obtained by solving the implicit equation:

$$f(L) = f_F = q\varphi_L + f_{bk}(\varphi_L)$$

The thickener will show a zone I with water (see Fig. 8.28), a zone II with the constant conjugate concentration φ_L, a zone III with varying concentration from φ_c to φ_L, depending on the *Mode of Continuous Sedimentation* (see Chap. 5, Sect. 5.2.2) and a zone IV of sediment.

Underflow

At the underflow, $z = 0$, the pulp of concentration φ_D is evacuated by gravity or by pumping through an orifice at the bottom of the thickener at a volume flow rate of Q_D without mixing with any other source of solid or water. We model this as a surface sink f_D defined by:

$$f_D = \frac{-Q_D \varphi_D}{S}$$

The volume average velocity at the underflow is:

$$q = -\frac{Q_D}{S} = \frac{f_D}{\varphi_D}$$

The solid flux density at the underflow is then:

$$f_D = f_F = q\varphi_D \tag{8.44}$$

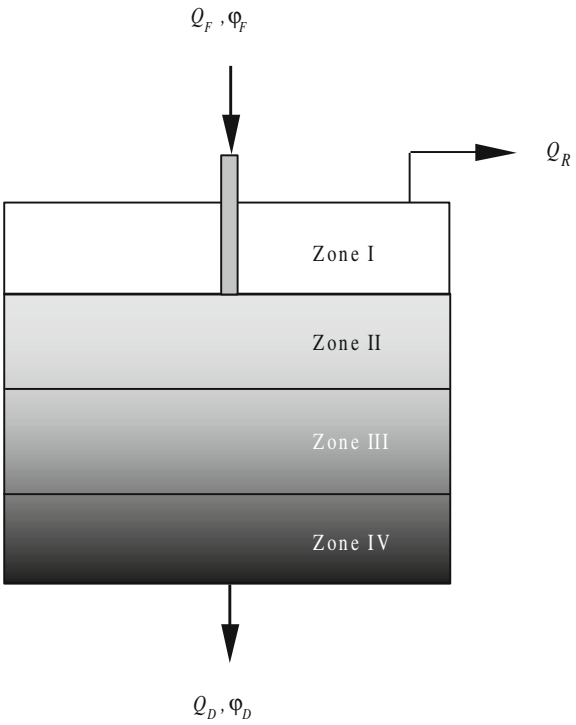

Fig. 8.28 Ideal conventional thickener (*ICT*). Zone I water, Zone II suspension of constant concentration, Zone III suspension of variable concentration and Zone IV sediment

Eq. (8.41) shows that q is independent of z, therefore:

$$q(z) = q = \frac{f_F}{\varphi_D} \tag{8.45}$$

A zone IV of increasing concentration will form below zone III, from the critical concentration φ_c to the underflow concentration φ_D. Figure 8.28 shows the four zones in a thickener at a steady state. The concentration profile $z = z(\varphi)$ in zone IV at steady state can be obtained from Eq. (8.42) $\partial z/\partial\varphi$:

$$\frac{\partial z(\varphi)}{\partial \varphi} = \frac{f_{bk}(\varphi)\sigma'_e(\varphi)}{\Delta\rho\varphi g} \frac{1}{(f_F - f_{bk}(\varphi) - q\varphi)} \tag{8.46}$$

Integrating this expression with $q = f_F/\varphi_D$ and boundary condition $z = 0$ and $\varphi = \varphi_D$ results in:

$$z(\varphi) = \int_{\varphi_D}^{\varphi} \frac{f_{bk}(\xi)\sigma'_e(\xi)}{\Delta\rho\xi g(f_F(1 - \xi/\varphi_D) - f_{bk}(\xi))} d\xi \tag{8.47}$$

Figure 8.29 shows a typical concentration profile of the sediment in a continuous thickener.

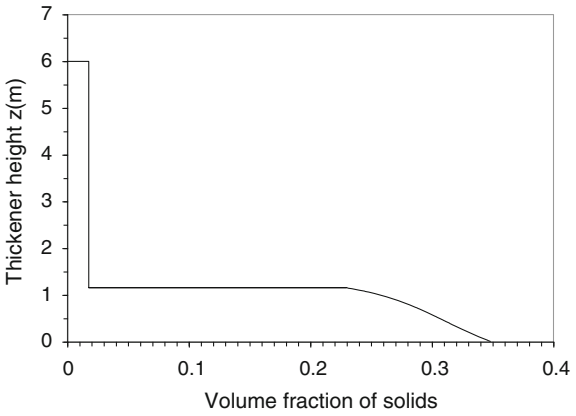

Fig. 8.29 Typical concentration profile in a continuous thickener at steady state

Overflow

In a conventional thickener at steady state no solid particle passes to the overflow and therefore solids are restricted to $0 \leq z \leq L$. If the overflow of water is designated by $Q_R > 0$, the macroscopic balance of pulp, solid and water in the thickener is:

$$\text{Solid}: \quad Q_F \varphi_F = Q_D \varphi_D$$

$$\text{Pulp}: \quad Q_R = Q_F - Q_D \tag{8.48}$$

$$\text{Water}: \quad Q_R = Q_F \left(1 - \frac{\varphi_F}{\varphi_D}\right) \equiv Q_D \left(\frac{\varphi_D}{\varphi_F} - 1\right) \tag{8.49}$$

(c) **Existence of a steady state**

The concentration in a thickener is either constant or increases downwards, that is, the concentration gradient is zero or negative, $\partial\varphi/\partial z \leq 0$. From Eq. (8.46):

$$\frac{\partial \varphi}{\partial z} = \underbrace{-\frac{\Delta \rho \varphi g}{\sigma_e'(\varphi) f_{bk}(\varphi)}}_{>0} \underbrace{\left(q\varphi + f_{bk}(\varphi) - f_F\right)}_{\leq 0} \leq 0 \tag{8.50}$$

Since $f_{bk} < 0$, the first term of (8.50) is positive and the term in round braked must be less than or equal to zero, that is:

$$f_k = q\varphi + f_{bk}(\varphi) \leq f_F \tag{8.51}$$

The Inequality (8.51) indicates that *at steady state in a flux-density function versus concentration plot, in the range* $\varphi_L \leq \varphi \leq \varphi_D$, *the term* $q\varphi + f_{bk}(\varphi)$ *should always be below the straight horizontal line representing the feed flux density* f_F.

Figure 8.30a shows a valid steady state where f_F lies above the continuous flux density curve and an invalid steady state, where the feed flux density is under the continuous flux density curve. Figure 8.30b shows the corresponding concentration profiles. For an invalid steady state the thickener overflows.

Problem 8.1 Consider a flotation tailing 35[%] solid in concentration with the following thickening parameters: $f_{bk}(\varphi) = -6.05 \times 10^{-4}\varphi(1-\varphi)^{12.09}$ m/s and $\sigma_e(\varphi) = 5.35\exp(17.9\varphi)$. The solid and fluid densities are $\rho_s = 2.65$ t/m^3 and $\rho_f = 1.0$ t/m^3 respectively. Plot the solid flux density function versus concentration and the concentration profiles for the following three solid feed fluxes $F = 178$ tph, $F = 200$ tph and $F = 260$ tph in a thickener of $D = 53$ m in diameter and an underflow of $w_D = 57.3$ % solid by weight.

Data			
F (tph)	178.0	200.0	260.0
D (m)	43.0	43.0	43.0
S (m^2)	1,452.2	1,452.2	1,452.2
ρ_s (ton/m^3)	2.65	2.65	2.65
ρ_f (ton/m^3)	1.0	1.0	1.0
w_F (%weight)	35.0	35.0	35.0
w_D (%weight)	57.3	57.3	57.3
Results			
φ_F	0.169	0.169	0.169
φ_D	0.336	0.336	0.336
ρ Pulp (ton/m^3)	1.28	1.28	1.28
Q_F (m^3/h)	139.2	156.4	203.3
Q_D (m^3/h)	199.82	224.51	291.87
q (m/s)	−3.82E−05	−4.29E−05	−5.58E−05
f_F (m/s)	−1.28E−05	−1.44E−05	−1.88E−05

Figure 8.31 shows two valid and one invalid steady state. Figure 8.32 gives the corresponding concentration profiles. The profile corresponding to the invalid steady state tends to infinite and the thickener could not handle that feed rate without overflowing.

8.3.4 Model of Conventional Thickening in Vessels with Varying Cross-Section

Conventional thickeners have two sections with different areas, a cylinder at the top and conical at the bottom to aid to the underflow discharge. The ideal conventional thickener used for modeling a real thickener ignores these facts and assumes a constant cross section for the equipment. In the following section, we will introduce a model for an ideal varying cross-section thickener.

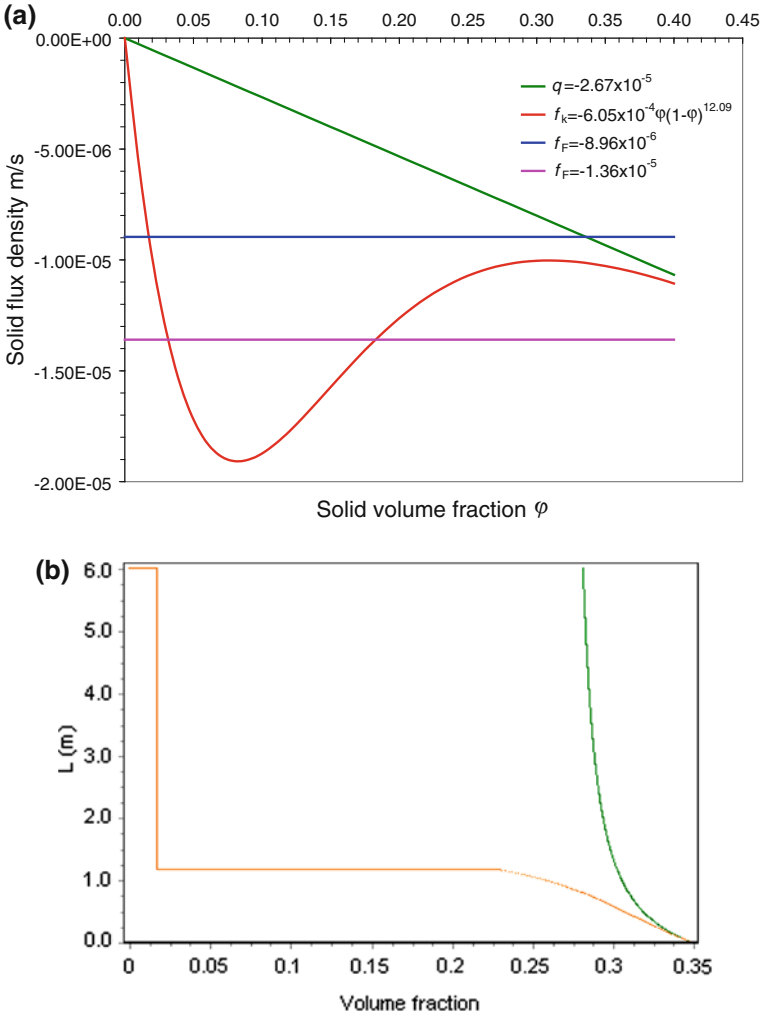

Fig. 8.30 **a** Valid solid flux density ($f = -8.96 \times 10^{-6}$ m/s) and invalid solid flux density ($f = -1.36 \times 10^{-5}$ m/s) versus concentration at steady state. **b** Concentration profiles for examples in Fig. 8.31a

Consider the settling of a flocculated suspension with constant concentration $\varphi(z,t)$ on each horizontal cross-section in a vessel with varying cross-sections sections $S(z)$, where $0 \leq z \leq L$ is the vertical coordinate. The solid and fluid particles are subjected to the effect of stresses, gravity, buoyancy and drag force.

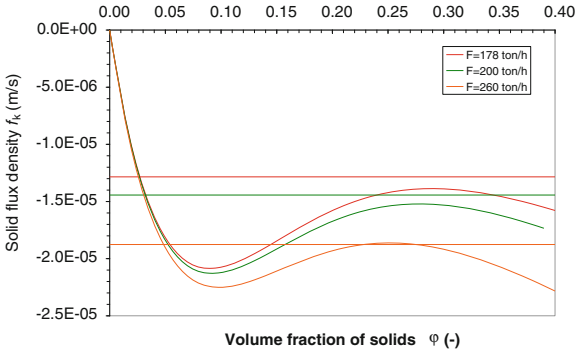

Fig. 8.31 Solid flux density function versus concentration for Problem 8.1. Two valid steady states for $F_1 = 178$ (tph) and $F_2 = 200$ (tph) and one invalid steady state for $F_3 = 260$ (tph), with the same feed and underflow concentration

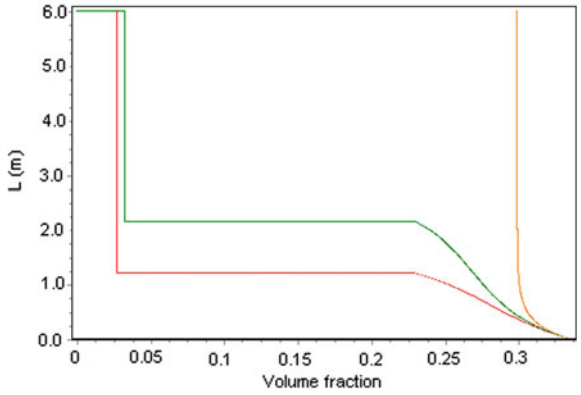

Fig. 8.32 Concentration profile for problem 8.1

Continuity Equation

If the suspension is considered a continuous superimposed two-component medium, the conservation of mass for the solid and fluid components are:

$$\frac{\partial \varphi}{\partial t} + \frac{1}{S(z)} \frac{\partial}{\partial z} (S(z) \varphi v_s) = 0, \quad 0 \leq z \leq L, \, t > 0 \tag{8.52}$$

$$-\frac{\partial \varphi}{\partial t} + \frac{1}{S(z)} \frac{\partial}{\partial z} \left(S(z)(1 - \varphi) v_f \right) = 0, \quad 0 \leq z \leq L, \, t > 0 \tag{8.53}$$

where t is time and v_s and v_f are the solid and fluid velocity components respectively and $S(z)$ is the varying cross-sectional area.

Adding these two equations, the mass balance of the suspension is obtained:

$$\frac{\partial}{\partial z} (S(z) q(z, t)) = 0 \tag{8.54}$$

where $q = v_s - (1-\varphi)v_r$ is the volume average velocity and v_r is the relative solid–fluid velocity. Note that:

$$-S(z)q(t) = Q(z,t) > 0 \tag{8.55}$$

$Q(z,t)$ is the volume flowrate of suspension through the thickener, which according to (8.55) is independent of z:

$$Q(z,t) = Q(0,t) = Q_D(t), \quad 0 \le z \le L,\ t > 0 \tag{8.56}$$

where $Q_D > 0$ is the prescribed suspension volume underflow rate. From $q = v_s - (1-\varphi)v_r$,

$$\varphi v_s = q\varphi + \varphi(1-\varphi)v_r = -\frac{Q_D(t)}{S(z)}\varphi + \varphi(1-\varphi)v_r \tag{8.57}$$

Substituting equation into (8.52) yields:

$$\frac{\partial \varphi}{\partial t} + \frac{1}{S(z)}\frac{\partial}{\partial z}(-Q_D(t)\varphi + S(z)\varphi(1-\varphi)v_r) = 0, \quad 0 \le z \le L,\ t > 0 \tag{8.58}$$

We saw that the relative solid–fluid velocity v_r can be written in terms of the Kynch flux density function $f_{bk}(\varphi)$ and the solid effective stress $\sigma_e(\varphi)$ in the form:

$$v_r = \frac{f_{bk}(\varphi)}{\varphi(1-\varphi)}\left(1 + \frac{\sigma_e'(\varphi)}{\Delta\rho\varphi g}\frac{\partial \varphi}{\partial z}\right) \quad \text{for } 0 \le z \le L \tag{8.59}$$

Therefore replacing in Eq. (8.58) gives:

$$\frac{\partial \varphi}{\partial t} + \frac{1}{S(z)}\frac{\partial}{\partial z}\left(-Q_D(t)\varphi + S(z)f_{bk}(\varphi)\left(1 + \frac{\sigma_e'(\varphi)}{\Delta\rho\varphi g}\frac{\partial \varphi}{\partial z}\right)\right) = 0$$

which can be written for $0 \le z \le L;\ t > 0$ in the form:

$$\frac{\partial \varphi}{\partial t} + \frac{1}{S(z)}\frac{\partial}{\partial z}(-Q_D(t)\varphi + S(z)f_{bk}(\varphi)) = \frac{1}{S(z)}\frac{\partial}{\partial z}\left(S(z)\frac{-f_{bk}(\varphi)\sigma_e'(\varphi)}{\Delta\rho\varphi g}\frac{\partial \varphi}{\partial z}\right) \tag{8.60}$$

Equation (8.60) is a degenerate parabolic partial differential equation representing the sedimentation of a flocculated suspension in a thickener with varying cross-sections. This equation reduces to a hyperbolic equation representing the sedimentation of an ideal suspension when the concentration is less than or equal to the critical, $\varphi < \varphi_c$:

$$\frac{\partial \varphi}{\partial t} + \frac{1}{S(z)}\frac{\partial}{\partial z}(-Q_D(t)\varphi + S(z)f_{bk}(\varphi)) = 0, \quad \text{for } 0 \le z \le L,\ t > 0 \tag{8.61}$$

Initial and Boundary Conditions

Consider Eq. (8.61). At $t = 0$, the initial concentration distribution is known:

$$\varphi(z,t) = \varphi_0(z), \quad for\ 0 \le z \le L \tag{8.62}$$

At $z = z_F$, the thickener is fed with a suspension of concentration $\varphi_F(t)$ at a volume flow rate of $Q_F(t) \ge 0$. Therefore, the solid flux at the feed is $Q_F(t)\varphi_F(t) \ge 0$:

$$Q_F(t)\varphi_F(t) = Q_D(t)\varphi_D - S(L)f_{bk}(\varphi_L), \quad \text{for } t \ge 0 \tag{8.63}$$

where $\varphi_L = \varphi(L,t)$. At $z = 0$, the solid flux density f_D reduces to its convective part, therefore:

$$f(0,t) = q\varphi_D$$

and the boundary condition is:

$$\left.\frac{\partial\varphi}{\partial z}\right|_{z=0,t} = -\left.\frac{\Delta\rho\varphi g}{\sigma_e'(\varphi)}\right|_{z=0,t}, \quad \text{for } t \ge 0 \tag{8.64}$$

The difficulty in solving Eq. (8.60) is the degeneracy into a non-linear hyperbolic equation for $\varphi < \varphi_c$. Since this equation is discontinuous for $\varphi < \varphi_c$, it has weak solutions that need an additional entropy condition to single out the physically relevant solution. Such a solution for (8.60) was proven by Bürger and Karlsen (2001).

Steady State

At steady state, Eq. (8.60) becomes:

$$S(z)f(z) = S_F f_F = -Q_F\varphi_F, \quad \text{for } 0 \le z \le L \tag{8.65}$$

Since at $z = 0$ the *solid flux* is $Q_D\varphi_D$,

$$Q_F\varphi_F = Q_D\varphi_D \tag{8.66}$$

On the other hand, for a constant underflow rate of Q_D, the steady state solution of Eq. (8.60) is:

$$-Q_D\varphi(z) + S(z)f_{bk}(\varphi) = -S(z)\frac{f_{bk}(\varphi)\sigma_e'(\varphi)}{\Delta\rho\varphi g}\frac{d\varphi}{dz} + C \tag{8.67}$$

where C is an integration constant. Using the boundary condition (8.64) for a desired underflow concentration φ_D yields $C = -Q_D\varphi_D$. Replacing this value in (8.67) we have:

$$-Q_D(\varphi(z) - \varphi_D) + S(z)f_{bk}(\varphi) = -S(z)\frac{f_{bk}(\varphi)\sigma_e'(\varphi)}{\Delta\rho\varphi g}\frac{d\varphi}{dz}, \quad \text{for } 0 \le z \le L \tag{8.68}$$

Existence of a Steady State

We have a steady state if the concentration increases downwards in the thickener, that is, if:

$$\frac{d\varphi}{dz} \leq 0 \quad for\ 0 \leq z \leq z_c \tag{8.69}$$

where z_c is the top of the sediment layer at $\varphi = \varphi_c$. Since the right side of (8.68) is negative, we have:

$$-Q_D(\varphi(z) - \varphi_D) + S(z) f_{bk}(\varphi) \leq 0, \quad \text{for } 0 \leq z \leq z_c \tag{8.70}$$

Concentration Profile

(a) In the hindered settling region, where $\varphi \leq \varphi_c$, Eq. (8.70) becomes:

$$-Q_D(\varphi(z) - \varphi_D) + S(z) f_{bk}(\varphi) = 0$$

and, since $Q_D \varphi_D = Q_F \varphi_F$, the concentration in Kynch's region can be obtained by solving $\varphi(z)$ for values $z_c \leq z \leq L$, from the implicit algebraic equation:

$$-Q_D \varphi(z) + S(z) f_{bk}(\varphi(z)) = -Q_F \varphi_F \tag{8.71}$$

(b) In the sediment, where $0 \leq z \leq z_c$, we can write from (8.60):

$$\frac{d\varphi}{dz} = \frac{\Delta\rho\varphi g}{f_{bk}(\varphi)\sigma'_e(\varphi)} \left(-\frac{Q_D}{S(z)}(\varphi(z) - \varphi_D) + f_{bk}(\varphi(z)) \right), \quad 0 \leq z \leq z_c \tag{8.72}$$

This equation can be solved with the boundary condition $\varphi(0) = \varphi_D$.

8.3.5 Clarifier-Thickener Model

In the 1970s and 1980s, equipment called *High Capacity Thickeners* were introduced to the mining industry by various manufacturers such as Eimco and Enviroclear, among others. See Fig. 8.13a and b.

These devices were promoted as having smaller unit area requirements than conventional installations. The distinct feature of this device was that the feed was introduced via a deep feedwell below the top of the sediment. The claim was that by eliminating the settling zone it was possible to reduce space requirements.

Although the conventional thickener model, as described above, is the best tool available today to design, simulate and control industrial thickeners, it has theoretical and practical drawbacks. From a theoretical point of view, there is deficient interpretation of the global conservation principle because it does not consider the overflow stream in the solid balance equation. From a practical point of view, the model does not permit the suspension to rise over the feeding level, which is

sometimes the case in high capacity thickeners. This is not very relevant in conventional thickeners, but is especially important in thickener fed under the sediment level. These problems led to the development of the clarifier-thickener model (Diehl 1995, 1996, 1997, 2000 2001; Bürger et al. 2001, 2003).

In spite of the fact that the Conventional Thickener model, as shown in the previous section, is the best tool available today to design, simulate and control industrial thickeners, it has theoretical and practical draw backs. From a theoretical point of view, there is a deficient interpretation of the global conservation principle by not consider the overflow stream in the solid balance equation. From a practical point of view, the model does not permit the suspension to rise over the feeding level, which is sometimes the case in High Capacity Thickeners. This fact has little relevance in conventional thickeners, but is especially important in thickener fed under the sediment level. These problems lead to the development of the Clarifier-Thickener Model (Diehl 1995, 1996, 1997, 2000, 2001; Bürger et al. 2001, 2003).

Consider a thickener and divide the vessel into two zones: (1) $z \geq z_F$, where the solids can flows upwards and $z \leq z_F$, where the solid flows downwards. $z = z_F$ represents the feeding level, $z = 0$ represents the underflow level, $z = z_c$, is the surface of the sediment level and $z = z_O$ is the overflow level. See Fig. 8.33.

The feed volume flowrate of pulp and solid are introduced as a singular surface sources of strength $Q_F(t)$ and $Q_F(t)\varphi_F(t)$ at $z = z_F$. The underflow volume flux of pulp and solid, $Q_D(t)$ and $Q_D(t)\varphi_D(t)$ respectively, leave as a singular surface sinks at $z = 0$. $Q_O(t)$ and $Q_O(t)\varphi_O(t)$ are the overflow volume flux and solid overflow volume flux at $z = z_O$, with $Q_i > 0$; with $i = F, D, O$.

Macroscopic mass balances yields:

$$Q_F(t) = Q_D(t) + Q_O(t) \tag{8.73}$$

$$Q_F(t)\varphi_F(t) = Q_D(t)\varphi_D(t) + Q_O(t)\varphi_O(t) \tag{8.74}$$

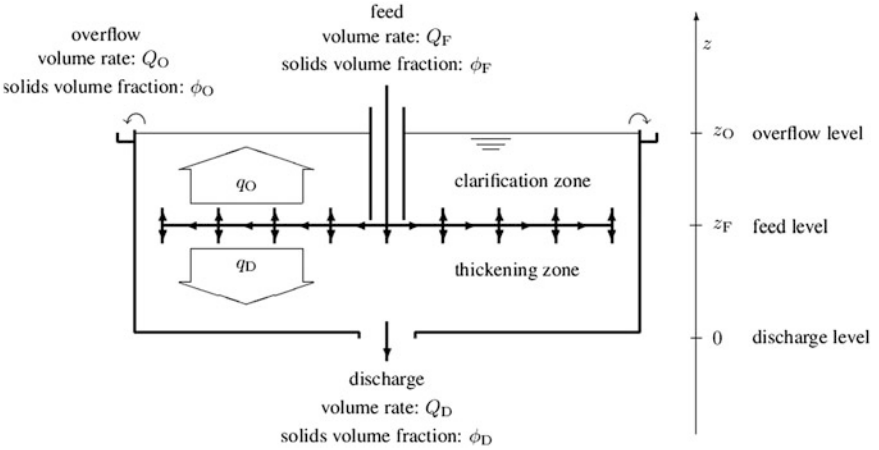

Fig. 8.33 Schematic view of a clarifier-thickener

Defining:

$$q_F = -\frac{Q_F}{S}, \quad q_D = -\frac{Q_D}{S}, \quad q_O = \frac{Q_O}{S}$$

which can be written as

$$q_F(t) = q_D(t) - q_O(t) \tag{8.75}$$

$$q_F(t)\varphi_F(t) = q_D(t)\varphi_D(t) - q_O(t)\varphi_O(t) \tag{8.76}$$

The spacial velocities for both zones are

$$q(t) = \begin{cases} q_O(t) & \text{for} \quad z_F < z < z_O \\ q_D(t) & \text{for} \quad 0 < z < z_F \end{cases} \tag{8.77}$$

and the solid flux density $\tilde{f}_k(z,t,\varphi)$ for both zones including the singular surface $q_F(t)\varphi_F(t)$ is

$$\tilde{f}_k(z,t,\varphi) = \begin{cases} q_O(t)(\varphi - \varphi_F) & \text{for} \quad z \geq z_O \\ q_O(t)(\varphi - \varphi_F) + f_{bk}(\varphi) & \text{for} \quad z_O > z > z_F \\ q_D(t)(\varphi - \varphi_F) + f_{bk}(\varphi) & \text{for} \quad z_F \geq z > 0 \\ q_D(t)(\varphi - \varphi_F) & \text{for} \quad z \leq 0 \end{cases} \tag{8.78}$$

Figure 8.34 shows the flux density functions for $z_O > z > z_F$ and $z_F \geq z > 0$.

With these variables, the phenomenological sedimentation-consolidation equation reads:

$$\frac{\partial \varphi}{\partial t} + \frac{\partial}{\partial z}\tilde{f}_k(z,t,\varphi) = -\frac{\partial}{\partial z}\left(\frac{f_{bk}(\varphi)\sigma_e'(\varphi)}{\Delta\rho\varphi g}\frac{\partial \varphi}{\partial z}\right) \tag{8.79}$$

The numerical solution to this problem was presented by Bürger et al. (2003). This numerical scheme ensures that the solution generate converges to physically relevant one.

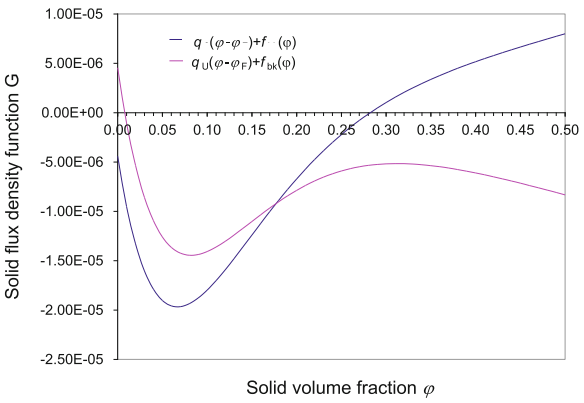

Fig. 8.34 Solid flux density functions in the clarification and thickening zones

Steady States

At steady state yields

$$\tilde{f}_k(z,\varphi) = -\left(\frac{f_{bk}(\varphi)\sigma'_e(\varphi)}{\Delta\rho\varphi g}\frac{\partial\varphi}{\partial z}\right) \tag{8.80}$$

The conditions to obtain a steady state are:

- That $d\varphi/dz<0$ for $0\le z\le z_c$, where $z=z_c$ is the location of the critical concentration φ_c.
- That at discontinuities the jump condition $\sigma(+.-)=\left(f_k^+-f_k^-\right)/(\varphi^+-\varphi^-)$ is valid and that the concentration should satisfy the jump stability (entropy of the jump).
- The term in bracket at the right side of (8.80) is continuous function of z.

Modes of Operation

Betancourt and Concha (2011) argue that it is better to talk about a high capacity mode of operation instead of high capacity thickener. It is possible to establish two modes of operation for the clarifier-thickener depending on the location of the critical concentration φ_c: if φ_c occurs in the thickening zone $0<z<z_F$, we have the *Conventional Mode* of operation, and if φ_c occurs in the clarification zone $z_F<z<z_O$ we say that the unit is operated in *high capacity* mode.

Conventional Mode of Operation

This mode of operation is characterized by a continuous concentration profile from $z=0$ to $z=z_c<z_F$.

$$\begin{aligned}\frac{d\varphi}{dz} &= \frac{(q_D(\xi-\varphi_D)+f_{bk}(\xi))\Delta\rho\xi g}{f_{bk}(\xi)\sigma'_e(\xi)} \quad \text{for} \quad 0\le z\le z_c \\ \varphi(0) &= \varphi_D\end{aligned} \tag{8.81}$$

In the region $z_c<z<z_F$ the concentration takes the constant value φ_L, called *conjugated concentration*. The profile is calculated by integrating with boundary condition $\varphi(0)=\varphi_D$, provided $q_D(\xi-\varphi_D)+f_{bk}(\xi)<0$. The conjugate concentration φ_L is calculated from

$$q_D\varphi_D = q_D\varphi_L + f_{bk}(\varphi_L) \tag{8.82}$$

considering the entropy stability conditions (see Bürger and Narváez 2007):

$$\begin{aligned} q_O\varphi + f_{bk}(\varphi) &\le 0 \quad \text{for} \quad \varphi\in(0,\varphi_L) \\ q_D(\varphi_L-\varphi)+f_{bk}(\varphi_L)-f_{bk}(\varphi) &\ge 0 \quad \text{for} \quad \varphi\in(\varphi_L,\varphi_c)\end{aligned} \tag{8.83}$$

High Capacity Mode of Operation

The High capacity mode of operation is characterized by a continuous concentration profile from $z = 0$ to $z_c > z_F$, followed by a concentration $\varphi = 0$ for $z_c < z \leq z_O$. The concentration profile for this mode of operation is calculated from:

$$\frac{d\varphi}{dz} = \begin{cases} \dfrac{(q_D(\varphi - \varphi_D) + f_{bk}(\varphi))\Delta\rho\varphi g}{f_{bk}(\varphi)\sigma_e'(\varphi)} & \text{for} \quad z_D \leq z < z_F \\ \dfrac{(q_O\varphi + f_{bk}(\varphi))\Delta\rho\varphi g}{f_{bk}(\varphi)\sigma_e'(\varphi)} & \text{for} \quad z_F < z \leq z_c \end{cases} \tag{8.84}$$

$$\varphi(0) = \varphi_D$$

provided the following entropy conditions holds

$$\begin{array}{ll} q_D(\varphi - \varphi_D) + f_{bk}(\varphi) \leq 0; & \text{for } \varphi(z_F) \leq \varphi \leq \varphi_D \\ q_O\varphi + f_{bk}(\varphi) \leq 0; & \text{for } 0 < \varphi \leq \varphi(z_F) \end{array} \tag{8.85}$$

Problem 8.2 Consider a flotation tailing with the following thickening parameters: $f_{bk}(\varphi) = -6.05 \times 10^{-4}\varphi(1-\varphi)^{12.09}$ and $\sigma_e = 5.35\exp(17.9\varphi)$. The material, with solid a density 2.65 t m^3 and a fluid density of 1.0 t/m^3, will be treated in a Clarifier-Thickener with $D = 53$ m in diameter and 5 m in height. The feedwell delivers the feed al $z_F = 1.2$ m and the sediment should not rise above 2 m. If the feed and underflow concentrations are $w_F = 35.0$ % and $w_D = 57.3$ % solid by weight respectively. (1) What is the capacity of the thickener, the volume average velocity and de volume overflow velocity? (2) Draw the solid flux density functions and (3) draw the concentration profile.

Solution

$F = 179.337$ tph solid; $q_D = 2.5859\text{E}{-5}$; $q_\text{O} = 2.5108\text{E}{-5}$

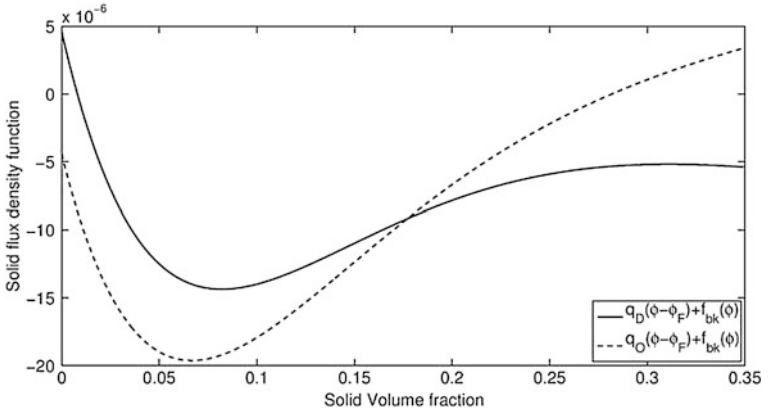

Flux density function fro problem 8.2.

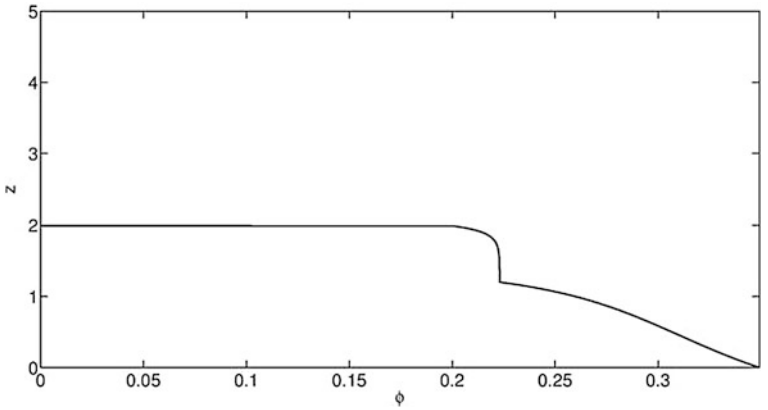

Concentration profile for problem 8.2.

8.4 Thickening Parameters and Their Determination

There is agreement today that conventional thickeners can be designed based on laboratory experiments. Nevertheless, one of the difficulties in thickening is laboratory determination of parameters. Although the thickening process is described by both sedimentation and consolidation, to ignore consolidation leads to errors. Most experimental work to determine parameter today is solely related to sedimentation.

8.4.1 Relevant Parameters

Parameters describing the thickening process are the solid flux-density function $f_{bk}(\varphi)$ and the solid effective stress $\sigma_e(\varphi)$. The solid flux density function is related to the resistance coefficient $K(\varphi)$ for concentrations below the critical level, and to the sediment permeability $k(\varphi)$ for concentrations equal to or greater than the critical. The solid effective stress $\sigma_e(\varphi)$ is related to the compressibility of the sediment.

Initial Settling Velocity

Two simple models are often used to describe the initial settling velocity as a function of concentration, one with two parameters u_∞ and c, presented by Richardson and Zaki in 1954, and the other with three parameters u_∞, φ_m, n, presented by Michels and Bolger in (1962):

$$u(\varphi) = \begin{cases} u_\infty (1-\varphi)^c & \text{Richardson and Zaki or} \\ u_\infty \left(1 - \frac{\varphi}{\varphi_m}\right)^n & \text{Michels and Bolger} \end{cases} \tag{8.86}$$

Solid Flux Density Function

The solid flux density function is given for values less and greater than the critical concentration by:

$$f_{bk}(\varphi) = \begin{cases} \varphi \times u(\varphi) & \text{for} \quad \varphi < \varphi_c \\ k_0 \left(\frac{\varphi_c}{\varphi}\right)^m & \text{for} \quad \varphi \geq \varphi_c \end{cases} \tag{8.87}$$

where the *coefficient of resistance* $K(\varphi)$ is given by

$$K(\varphi) = -\left(\frac{\Delta\rho\varphi^2(1-\varphi)^2 g}{\mu \times f_{bk}(\varphi)}\right) \text{for } \varphi < \varphi_c \tag{8.88}$$

and the permeability of the sediment $k(\varphi)$ by:

$$k(\varphi) = \frac{\mu}{\Delta\rho\varphi^2 g} f_{bk}(\varphi) \tag{8.89}$$

Initial Settling Velocity

Settling experiments are usually performed with different solid concentrations in one or two-liter capacity graduate cylinders, with an initial suspension height of around 35 cm. For each concentration, the height of the water suspension interface is recorded as a function of time.

Problem 8.3 Calculate the initial settling velocities for a suspension of calcium carbonate with solid and fluid densities of $\rho_s = 2{,}710\,(\mathrm{kg/m^3})$ and $\rho_f = 1{,}000\,(\mathrm{kg/m^3})$ respectively.

Table 8.1 gives the experimental height of the water-suspension interface. Settling plots are drawn with these data, see Fig. 8.35. The initial settling velocities are obtained from the linear sections of the settling plots for short times. A straight line is drawn for each concentration, see Fig. 8.36. The slopes of these lines yield the settling velocities shown at the bottom of Table 8.1.

From Fig. 8.36 the initial settling velocities as a function of φ are:

$$u(0.017) = -2.91 \times 10^{-4}\,\mathrm{m/s}, \quad v_s(0.044) = -7.97 \times 10^{-5}\,\mathrm{m/s}$$

$$u(0.103) = -3.07 \times 10^{-5}\,\mathrm{m/s}, \quad v_s(0.265) = -1.16 \times 10^{-6}\,\mathrm{m/s}$$

Table 8.1 Settling velocity data for a calcium carbonate suspension

$\varphi = 0.265$		$\varphi = 0.103$		$\varphi = 0.044$		$\varphi = 0.017$	
Time (s)	Height (m)	Time (s)	Height (m)	Time (s)	Height (m)	Time (s)	Height (m)
0	0.338	0	0.338	0	0.338	0	0.338
1,692	0.336	1080	0.292	1,080	0.210	468	0.128
2,304	0.335	1,368	0.284	1,332	0.186	720	0.076
3,204	0.331	1,692	0.274	1,620	0.162	1,008	0.051
6,804	0.329	1,980	0.265	1,908	0.144	1,908	0.044
10,404	0.326	2,556	0.247	2,520	0.112	2,520	0.041
15,804	0.319	3,132	0.230	3,096	0.096	5,508	0.037
23,004	0.312	6,120	0.172	6,120	0.079	9,108	0.030
37,404	0.301	9,720	0.162	9,720	0.073	14,508	0.029
51,804	0.291	15,120	0.150	15,120	0.064	21,708	0.029
66,204	0.277	22,320	0.139	22,320	0.061	36,108	0.028
80,604	0.274	36,720	0.127	36,720	0.057	50,508	0.028
95,004	0.264	51,120	0.122	51,120	0.056	64,908	0.027
109,404	0.257	65,520	0.118	65,520	0.056	79,308	0.027
123,804	0.252	79,920	0.117	79,920	0.054	93,708	0.027
138,204	0.247	94,320	0.115	94,320	0.054	108,108	0.026
152,604	0.243	108,720	0.115	108,720	0.054	122,508	0.026
167,004	0.238	123,120	0.115	123,120	0.054	136,908	0.025
181,404	0.235	137,520	0.113	137,520	0.054	151,308	0.025
195,804	0.232	151,920	0.113	151,920	0.054	165,708	0.025
210,204	0.230	166,320	0.113	166,320	0.054	180,108	0.025
v_s (m/s) =	−1.160E−06	−3.070E−05		−7.970E−05		−2.910E−04	

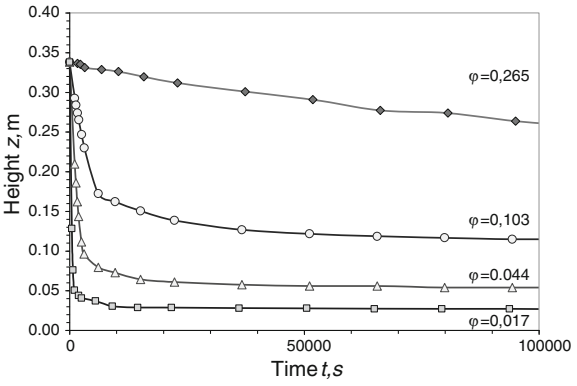

Fig. 8.35 Settling curve for calcium carbonate suspensions at four different concentrations. Data in Table 8.1

The initial settling velocities are correlated with concentration using Richardson and Zaki's equation $u(\varphi) = u_\infty(1-\varphi)^c$. The result is shown in Fig. 8.37, obtaining the following parameters: $u_\infty = -1.72 \times 10^{-4}$ and $c = 15.6$.

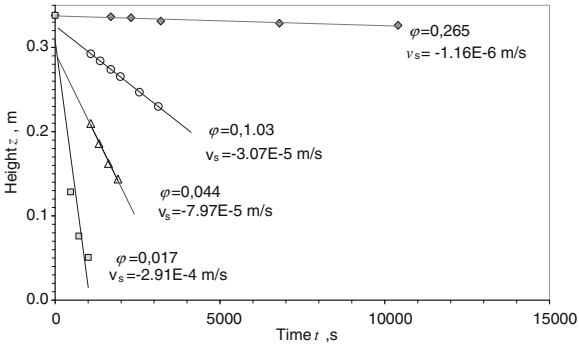

Fig. 8.36 Initial settling velocities for cases of Table 8.1 and Fig. 8.35

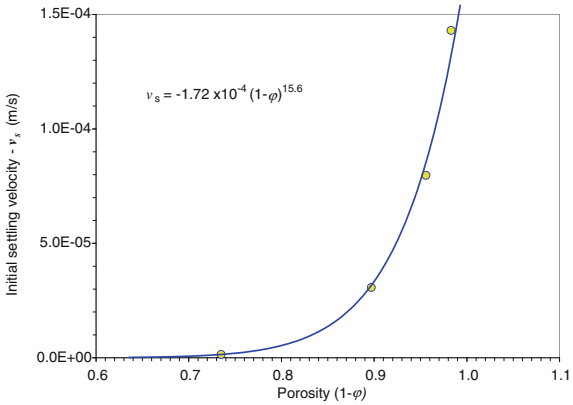

Fig. 8.37 Initial settling velocity function according to Richardson and Zaki for the cases in Table 8.1 and Fig. 8.35

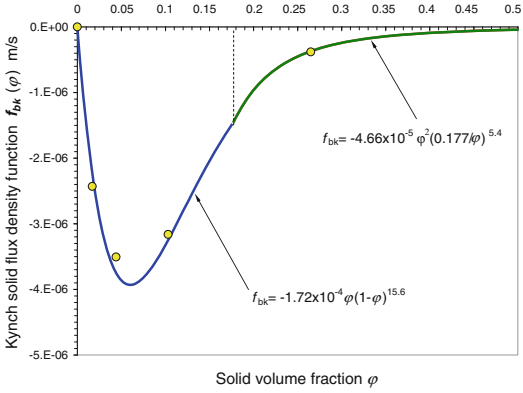

Fig. 8.38 Kynch solid flux density function for the cases in Table 8.1 and Richardson and Zaki's equation

Flux Density Function

The solid flux density function is given in Eq. (8.90) and Fig. 8.38, where the critical concentration was $\varphi_c = 0.177$ and Eq. (8.87) was used to obtain $k_0(\varphi_c)$ and m:

$$f_{bk}\varphi = \begin{cases} -1.72 \times 10^{-4}\varphi(1-\varphi)^{15.6} & \text{for} \quad \varphi < \varphi_c \\ -4.66 \times 10^{-5}\varphi^2(0.177/\varphi)^{5.4} & \text{for} \quad \varphi \geq \varphi_c \end{cases} \tag{8.90}$$

The effect of the parameters c and u_∞ on the flux density function are shown in Figs. 8.39 and 8.40.

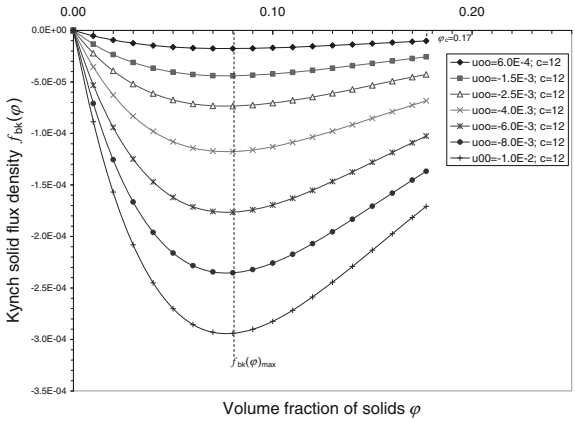

Fig. 8.39 Effect of the u_{oo} parameter on the solid flux density function. The *dotted line* joins the points of maximum solid flux densities

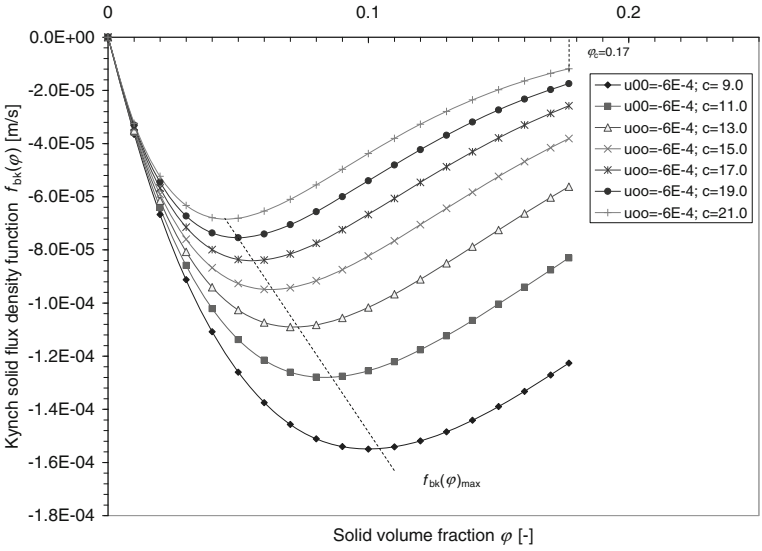

Fig. 8.40 Effect of the c parameter on the solid flux density function. The *dotted line* joins the points of maximum solid flux densities

Resistance Coefficient and Permeability

The solid–liquid resistance coefficient $K(\varphi)$ and the permeability $k(\varphi)$ can be obtained from Eqs. (8.88) and (8.89) and from the solid flux density function $f_{bk}(\varphi)$ on (8.90) (Fig. 8.41, 8.42):

$$K(\varphi) = -9.75 \times 10^{-5} \varphi / (1 - \varphi)^{15.6} \tag{8.91}$$

$$k(\varphi) = -4.66 \times 10^{-5} \varphi^2 (0.177/\varphi)^{5.4} \tag{8.92}$$

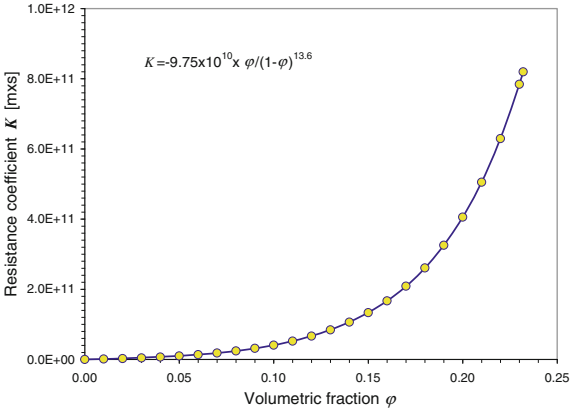

Fig. 8.41 Resistance coefficient for the cases in Table 8.1

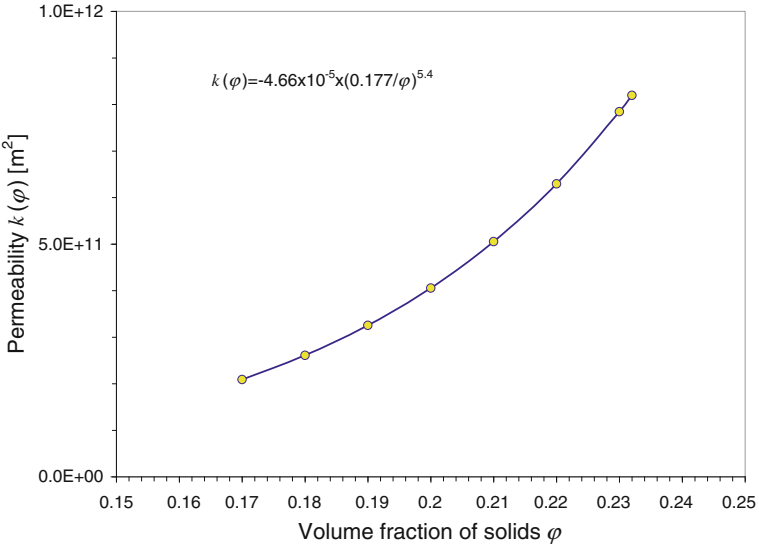

Fig. 8.42 Permeability

Critical Concentration

Roberts (1949) proposed the following equation for consolidation of compressible suspensions:

$$\frac{d\mathfrak{D}}{dt} = -\mathfrak{K}(\mathfrak{D} - \mathfrak{D}_\infty), \text{ for } \quad \mathfrak{D}_c \geq \mathfrak{D} \geq \mathfrak{D}_\infty \tag{8.93}$$

where $\mathfrak{D}$ is the dilution, that is, the ratio of mass of water to mass of solid in the suspension, $\mathfrak{K}$ is a rate constant and t is time. The subscript c and ∞ refer to the critical and the equilibrium dilution. He considered $\mathfrak{D} - \mathfrak{D}_\infty$ proportional to $z - z_\infty$, where z_∞ is the final sediment height (Tory and Shannon 1965) then, $\mathfrak{D}$ can be substituted by z in equation and Robert's equation may can be written in the integrated form:

$$\frac{z - z_\infty}{L - z_\infty} = \exp(-\mathfrak{K}t), \quad \text{for} \quad \mathrm{L} \geq \mathrm{z} \geq \mathrm{z}_\infty \tag{8.94}$$

Obviously, Eq. (8.94) is not valid for the whole sedimentation range, but only for consolidation. Robert showed that, in plotting Eq. (8.94) for the whole sedimentation range, three straight lines can be drawn with the solution of this equation, one for hindered settling, one for the intermediate range and the last for consolidation. See Fig. 8.43. The critical point in this figure is the intersection of the second and the third lines. With the value of the critical time t_c, the critical height z_c can be obtained from the settling plot.

Problem 8.4 Calculate the critical concentration for data for Problem 8.3. Figure 8.43 shows the plot of $(z - z_\infty)/(L - z_\infty)$ versus t for a concentration $\varphi = 0.044$.

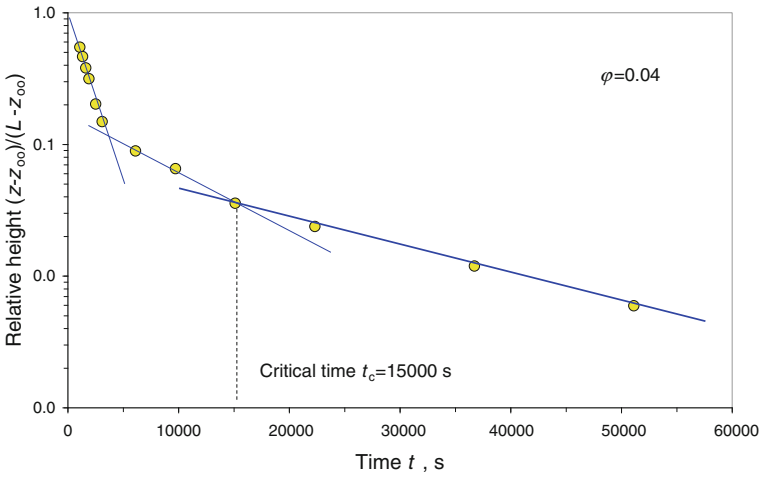

Fig. 8.43 Settling data plotted according to Robert's equation for a suspension with an initial concentration of $\varphi_0 = 0.044$

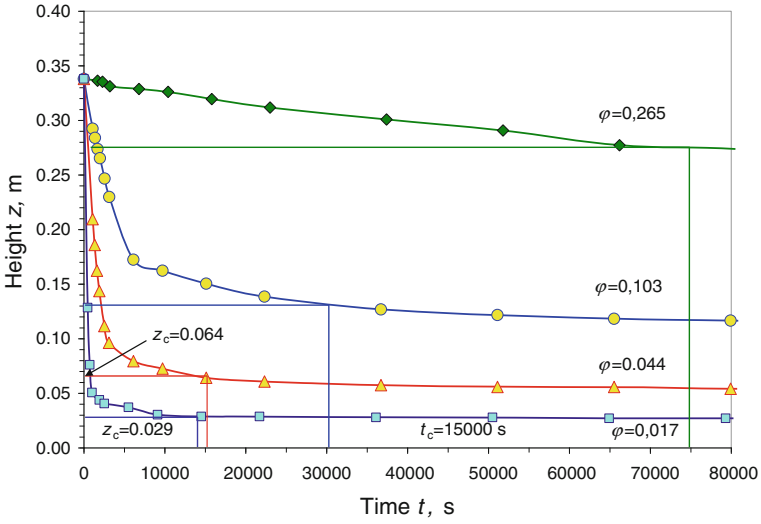

Fig. 8.44 Calculation of the critical height and critical time for the concentration $\boldsymbol{\varphi} = 0.044$ are $z_c = 0.064$ m, $t_c = 15{,}000$ s

From Fig. 8.43, the critical time for the concentration $\varphi = 0.044$ is $t_c = 15{,}000$ s. The critical height $z_c = 0.064$ m is obtained from the settling plot for $t_c = 15{,}000$ s, see Fig. 8.44.

In Kynch's theory, φ_c is the final concentration, therefore φ_c can be obtained from the volume balance at $t = 0$ and $t = t_c$:

$$L\varphi_o = z_c\varphi_c \tag{8.95}$$

For the case of Fig. 8.44:

$$\varphi_c = 0.338 \times 0.044/0.064 = 0.232 \tag{8.96}$$

The critical concentration obtained in this way depends on the initial suspension concentration φ_0, because Eq. (8.95) is valid only for Kynch's regime at the end of sedimentation. It converges to a constant value as the initial concentration tends to zero (Mode of sedimentation I, see Chap. 5). Therefore, for every test with a different initial concentration, a critical concentration is calculated and plotted against the initial concentration, as shown in Table 8.2 and Fig. 8.45. Extrapolation to $\varphi_0 = 0$ gives the critical concentration $\varphi_c = 0.177$.

A simpler and more accurate method for calculating the critical concentration is based on the conservation of the total solid mass before and after sedimentation, similar to (8.95), but now with compression. Before settling, the pulp is homogenized with a solid mass $\rho_s LS\varphi_0$, where S is the cross sectional area of the column, L is the initial height of the suspension and ρ_s and φ_0 are respectively its density

Table 8.2 Initial versus critical concentrations

φ	L	t_c	z_c	φ_c
0.017	0.338	14,500	0.029	0.198
0.044	0.338	15,000	0.064	0.232
0.103	0.338	30,000	0.130	0.268
0.265	0.338	75,000	0.275	0.326

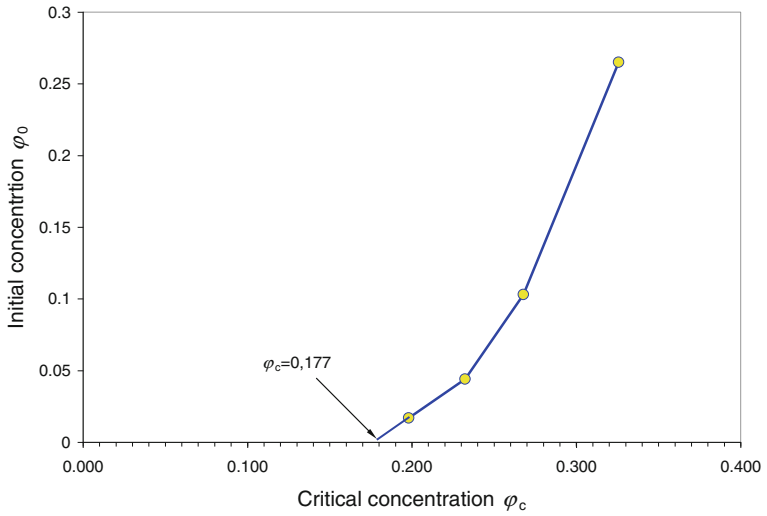

Fig. 8.45 Critical versus initial concentration. The final value of the critical concentration is $\boldsymbol{\varphi_c} = 0.177$

and concentration. After sedimentation all the solid material is contained in the sediment, so the following equation is valid:

$$L\varphi_0 = \int_{\varphi_D}^{\varphi_c} \varphi d\varphi \tag{8.97}$$

Solid Effective Stress

Consolidation occurs due to the self-weight supported by the sediment layers and its effect is seen in the concentration profile. Therefore, the constitutive equation for *effective solid stress* can be calculated by using the measured values of the concentration profile at the end of a batch sedimentation-consolidation process.

Consider equation:

$$\frac{\partial \sigma_e}{\partial z} = -\Delta\rho\varphi g - \frac{\mu}{k(\varphi)}(1-\varphi)v_r, \quad \text{for } \varphi \geq \varphi_c \tag{8.98}$$

At the end of the consolidation process, all velocities are zero. Therefore $v_r = 0$ in the previous equation. Writing $\partial\sigma_e/\partial z = \partial\sigma_e/\partial\varphi \times d\varphi/dz$, Eq. (8.98) can be written in the form:

$$\frac{\partial \sigma_e}{\partial \varphi} = -\frac{\Delta\rho\varphi g}{d\varphi/dz}\bigg|_{t\to\infty}, \quad \text{for} \quad 0 \leq z \leq z_c \tag{8.99}$$

Measuring the concentration profile at the end of the consolidation process, the functional form of the solid effective stress can be obtained by integrating this equation in the range $\varphi_D \leq \varphi \leq \varphi_c$:

$$\sigma_e(\varphi) = -\int_{\varphi_D}^{\varphi} \frac{\Delta\rho\xi g}{(d\xi/dz)} \mathrm{d}\xi \tag{8.100}$$

As we have already seen, there are two models in common use for the solid effective stress $\sigma_e(\varphi)$, an exponential function and a potential function:

$$\sigma_e(\varphi) = \begin{cases} \alpha \exp(\beta\varphi) & \text{or} \\ \sigma_0\left(\left(\frac{\varphi}{\varphi_c}\right)^m - 1\right) & \text{for } \varphi \geq \varphi_c \end{cases} \tag{8.101}$$

Determination of the Critical Concentration

Since at the top of the sediment, $z = z_c$, and the concentration is $\varphi = \varphi_c$, to find the critical concentration, the concentration profile of the sediment should be integrated until Eq. (8.100) is satisfied. Using the exponential equation of (8.101) for the solid effective stress, from (8.99) we have:

$$d\varphi/dz = -\frac{\Delta\rho\varphi g}{\alpha\beta \exp(\beta\varphi)}; \quad \text{for } 0 \leq z \leq z_c \tag{8.102}$$

Problem 8.5 Defining $A_1 = -\frac{\alpha\beta}{\Delta\rho g}$ and $A_2 = \alpha$, the values of α, β and φ_c can be simultaneously determined by means of the following numerical integration of the mass balance (Fig. 8.46):

$$\varphi_0 L = \int_{\varphi_D}^{\varphi_c} z(\varphi) d\varphi \tag{8.103}$$

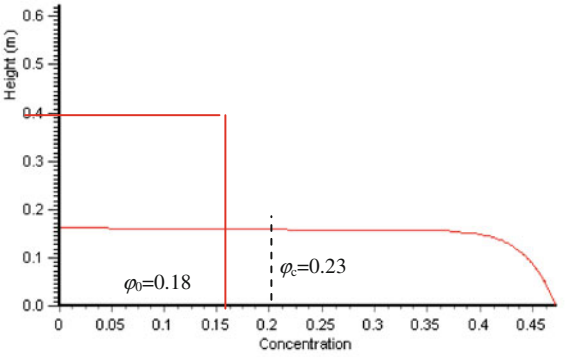

Fig. 8.46 Calculation of the consolidation parameters and the critical concentration

$$\varphi_0 L = \varphi_c \left(A_1 \ln(\varphi_c) + A_2 \varphi_c + \frac{(A_2 \varphi_c)^2}{2 \times 2!} + \cdots + \frac{(A_2 \varphi_c)^n}{n \times n!} \right) + A_3$$
$$+ \left(A_1 \left(\varphi \ln(\varphi) - \varphi + \frac{A_2 \varphi}{2} + \frac{(A_2 \varphi)^2 \varphi}{2 \times 3!} + \cdots + \frac{(A_2 \varphi)^n \varphi}{n \times (n+1)!} \right) + A_3 \varphi \right) \Bigg|_{\varphi_c}^{\varphi_D} \tag{8.104}$$

where φ_D and φ_c are respectively the underflow and critical concentration. For example, for $L = 0.4\,(\mathrm{m})$ and $\varphi_0 = 0.18$, the application of (8.104) yields the values $\alpha = 2.35$, $\beta = 17.9$ and $\varphi_c = 0.23$.

Permeability

The determination of the permeability for the region $\varphi \geq \varphi_c$ can be done once the critical concentration has been determined.

For values greater than the critical concentration, the following empirical equation can be used:

$$f_{bk}(\varphi) = k_0 \left(\frac{\varphi_c}{\varphi} \right)^m \tag{8.105}$$

For example, in Fig. 8.47, for $\varphi = \varphi_c = 0.23$, $f_{bk}(\varphi_c) = k_0 = 6.67 \times 10^{-12}$ and the best value for the parameter $m = 0.8$ is obtained by non-linear regression.

8.5 Instrumentation for the Automatic Determination of Thickening Parameters

It is surprising that until recently the Marcy balance and one-liter graduate cylinders were the off-line instruments to routinely measure pulp concentrations and thickening parameters in the laboratory and in plants. These artifacts have been

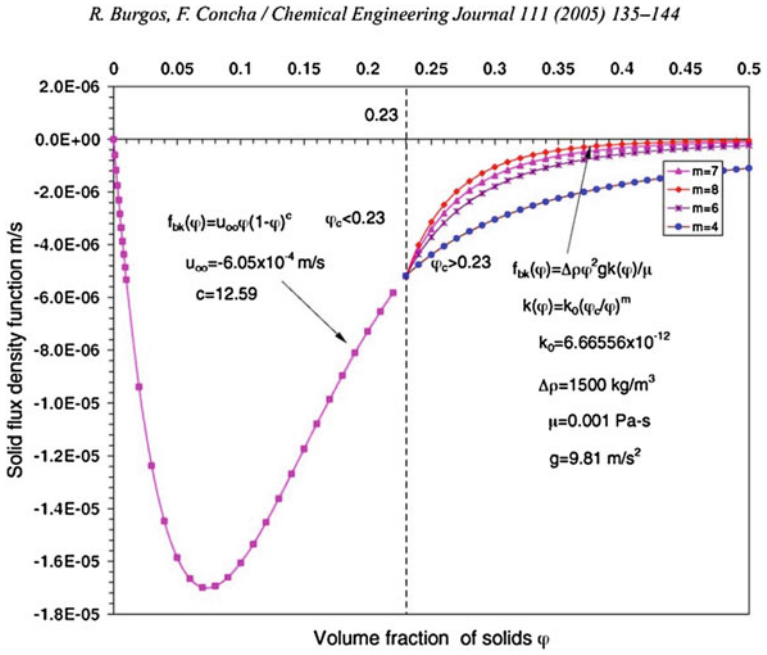

Fig. 8.47 Solid flux-density function. From Burgos and Concha (2005)

used for most of the 20th century. They are obsolete but are still used by many laboratories in mineral processing. One of the aims of my academic and professional work has been to update theory and instrumentation in this area.

8.5.1 Measuring Suspension Concentrations

Controlling pulp density in a concentrator is a daily task. Knowledge of this parameter is essential in processes as diverse as grinding, flotation, solid–liquid separation, and concentrate and trailing transport. The Marcy balance is used in laboratories and plants despite its limitations and imprecise readings. Two new instruments have been developed by Concha et al. (2011) called the *DensiTest* and *Industrial Picnometer*, which use the same principles as the Marcy balance, but with a digital strain gauge and a robust picnometer for larger samples.

The advantage of the DensiTest, beside its precision, is that the vessel can have any volume since it can be introduced to the instrument as input data. The results can be obtained in all the units used in mineral processing, such as pulp density, % solid by weight, volume fraction and dilution (Fig. 8.48).

The *Industrial Picnometer* can be used to determine solid, liquid and suspension densities. The instrument consists of a balance and a touch screen notebook

Fig. 8.48 Suspension concentration measurement

Fig. 8.49 Industrial picnometer (Cettem instruments)

concealed in a robust valise. A simple software program directs the operator during measurement (Fig. 8.49).

8.5.2 Solids Flux Density Function

Traditionally thickener *unit areas* were obtained by settling tests with suspensions of several concentrations in one or two-liter graduate cylinders, measuring the water-suspension interface at regular intervals. In a plot of the water-suspensions

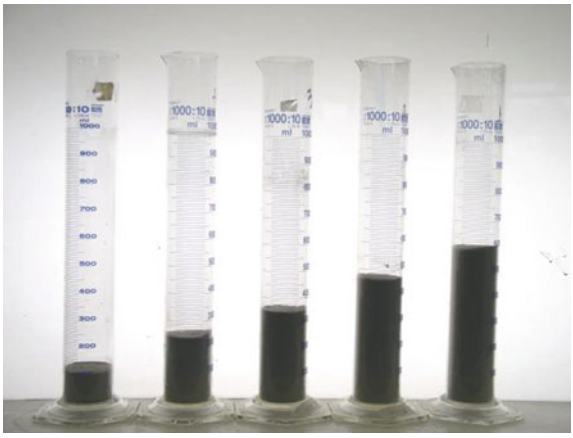

Fig. 8.50 Batch sedimentation experiment with different suspension concentrations

interfaces versus time, the initial straight line was chosen to indicate the suspension hindered settling velocities (Fig. 8.50).

The principal problem with this experimental procedure is that it is difficult to make simultaneous measurements in several graduate cylinders and, therefore, there is no certainty that all measurements are made under the same conditions. On the other hand, measurements in diluted suspensions at the beginning of the test, which are of primordial importance, are difficult to read by the naked eye.

To solve this problem an instrument called *SediRack* was developed at the University of Concepción (Concha et al. 2005, 2011). SediRack can perform five simultaneous settling tests. The instrument consists of a frame, with five transparent one-liter tubes with rubber stoppers that contain the suspension. There is a central axis for the rotation of the tubes to homogenize all five suspensions simultaneously. Once homogenous suspensions are attained, an appropriate dose of a flocculant is injected and further agitation as necessary. Alternatively a rocking motion can complement rotation.

Once homogenization is completed, the water-suspension interface in the tubes is recorded by the video camera of a notebook. The data are processed automatically to produce the settling velocities for the suspension concentrations. Using an optimization procedure, the software calculates the solid flux density function and Coe and Clevenger thickener unit area. See Figs. 8.51 and 8.52.

Figures 8.53 and 8.54 show the settling curves and the calculated solid flux density function and thickener unit area obtained by Coe and Clevenger's method. (See the next section).

SediRack On-line (PSE)

Although it is important for a mineral processing plant to perform periodic laboratory batch tests to determine thickening parameters and in this way adjust operations, it is even more important to be able to make on-line determinations of these parameters. For this purpose, the University of Concepción developed an on-

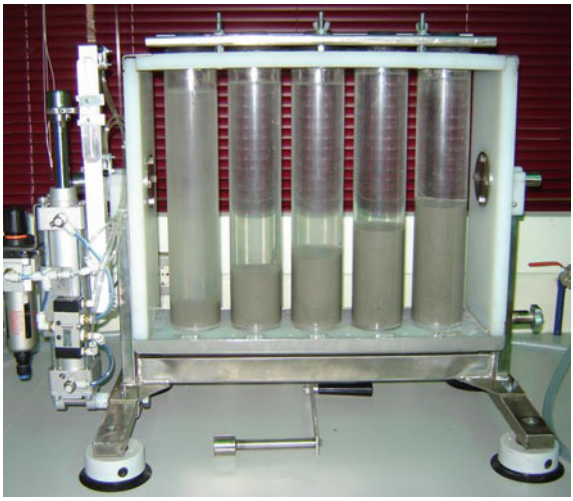

Fig. 8.51 SediRack instrument to measure the solid flux density function

Fig. 8.52 *SediRack* complete with notebook with webcam

line version of the SediRack, called (PSE). See Fig. 8.55 (Segovia and Concha 2012 patent pending).

PSE is an instrument to determine the settling velocity of suspensions in an industrial thickener. The instrument is based on the laboratory instrument SediRack that was developed and patented by the University of Concepción and used successfully in laboratories and concentrators in Chile. After its validation in Chilean copper concentrators, it was able to:

1. Determine the settling velocities of flocs coming out of the feedwell, which is an important parameter to design control strategies.
2. Determine the dilution in the feedwell.
3. Determine the dilution of the feed entering the thickener.
4. Determine the optimal flocculation dose for a pulp entering the thickener.

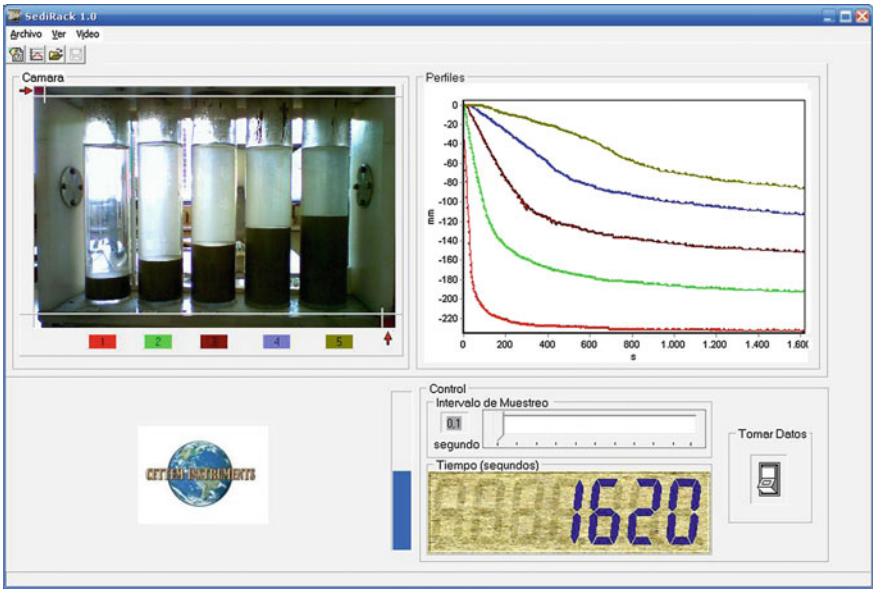

Fig. 8.53 Settling plots obtained for five different concentrations

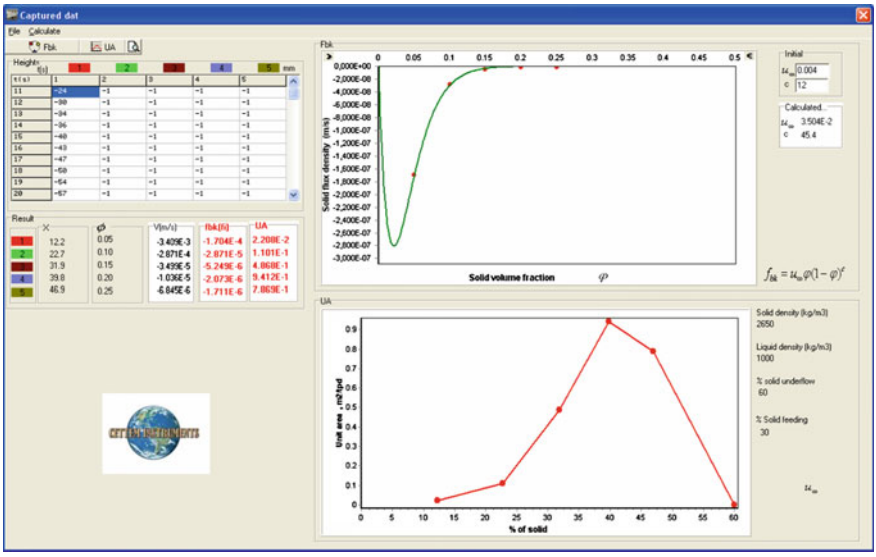

Fig. 8.54 Solid flux density and thickening unit area obtained

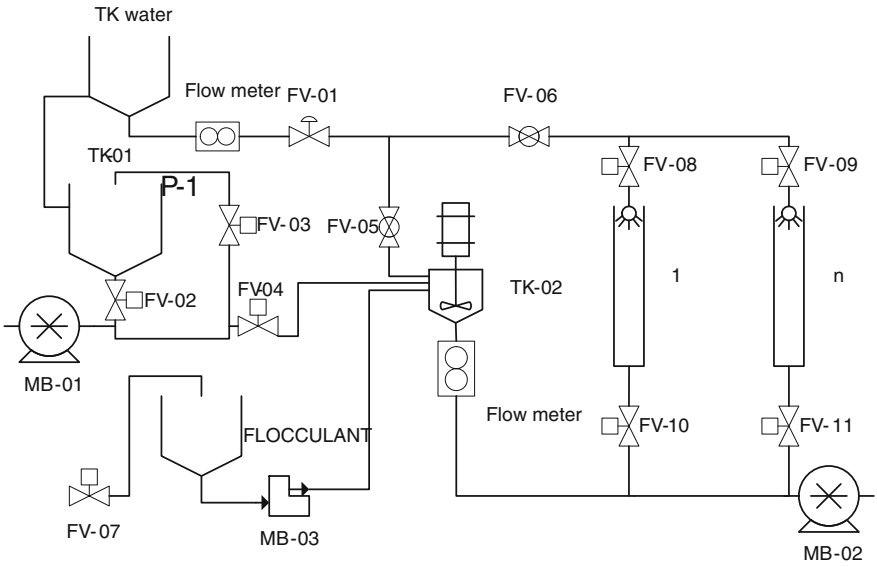

Fig. 8.55 Scheme of the PSE instrument (SediRack on-line)

The instrument has six main components:

- Tank for storing and homogenizing the pulp.
- Tank for storing and preparing the flocculant.
- Set of settling tubes to measure the settling velocity.
- An ultra-flocculation reactor (See Chap. 7).
- Flow meters, pumps, and valves.
- Video camera to record the water-suspension interface.

Figure 8.56 shows the complete PSE system.

A complete test takes about 10 min. The settling curves and the numerical results of the initial settling velocities for different suspension concentrations are given in Fig. 8.57.

8.5.3 Solids Effective Solid Stress

An instrument called *SediTest* was developed by Concha et al. (2008) The instrument consists of a settling column with 16 conductivity sensors. It measures the conductivity profile when consolidation is complete. Figure 8.58 shows the

Fig. 8.56 PSE instrument. **a** General view. **b** Sedimentation tubes. **c** Flocculant tank and dose pumps. **d** Pulp mixing tank

first prototype of the instrument. Figure 8.59 shows the evolution of conductivity during the settling experiment.

The conversion between conductivity and concentration is done with an empirical equation based on Maxwell's work (Garrido 2005):

$$\varphi = \frac{(k_s + 2k_f)(1 - K)}{(k_f - k_s)(K + 2)} \tag{8.106}$$

where k_f and k_s are the concentration and the conductivity of the suspension, k_f is the conductivity of the fluid, k_s is the conductivity of the solid and $K = k_s/k_f$. The

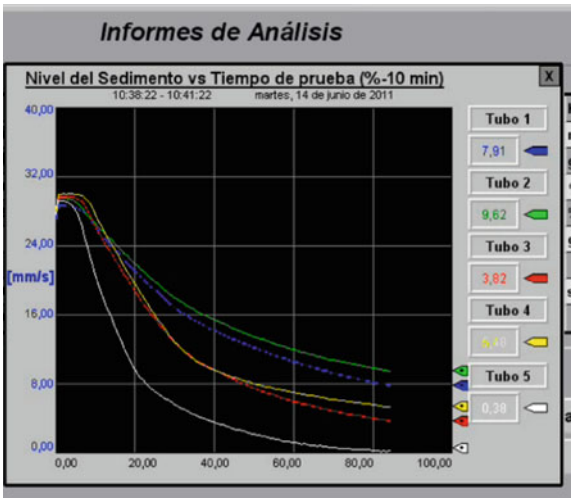

Fig. 8.57 Initial settling velocities from PSE

Fig. 8.58 Prototype of seditest instrument to measure sediment compressibility

computer software chooses long-term conductivities and converts them into concentrations and plots them, as shown in Fig. 8.60.

Equation (8.106) reference goes here converts into concentration profile into the solid effective stress $\sigma_e(\varphi)$ (Fig. 8.61).

SediTest On-line (SMC)

For the compressibility of the sediment, represented by the solid effective stress $\sigma_e(\varphi)$, an on-line instrument was also developed at the University of Concepción by (Segovia and Concha 2012; patent pending). See Figs. 8.62 and 8.63.

The SMC On-line determines the compressibility of sediment by measuring the concentration profile in a thickener. It consists of the following components:

- Airflow controller to maintain constant flow in the instrument.
- Level detection of the detector.

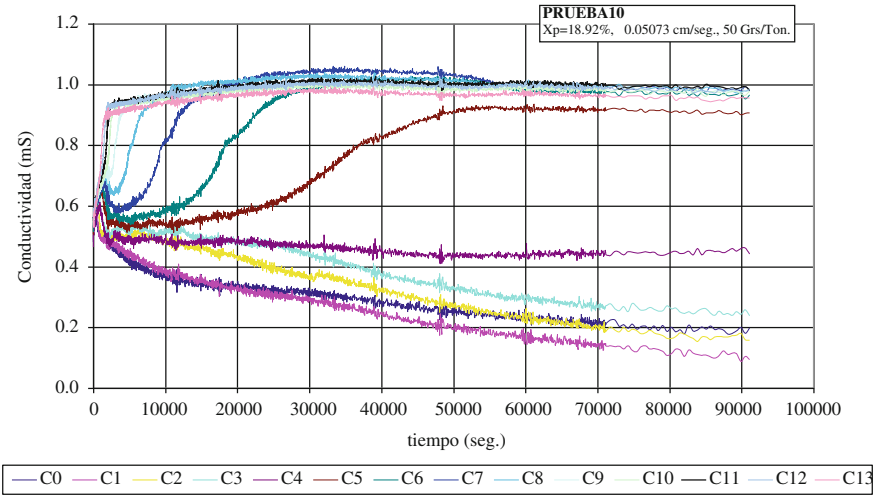

Fig. 8.59 Conductivity values at different heights in the settling column as a function of time

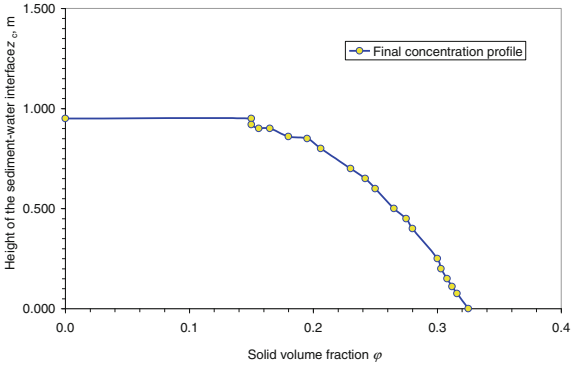

Fig. 8.60 Concentration profile at the end of sedimentation

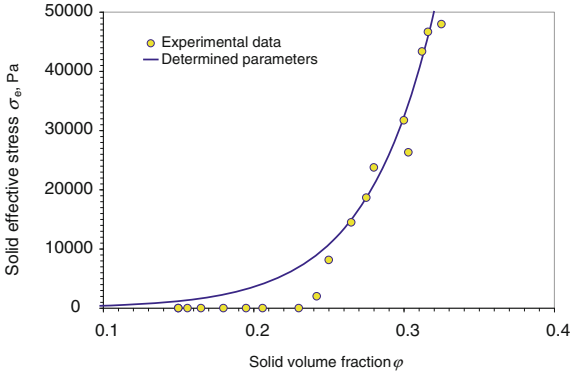

Fig. 8.61 Solid effective stress $\sigma_e(\varphi)$ versus φ

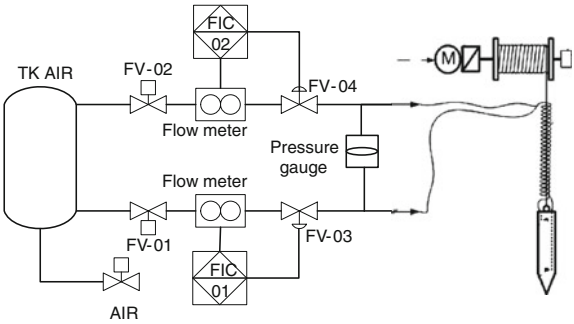

Fig. 8.62 Schematic view of the SMC (SediTest on-line)

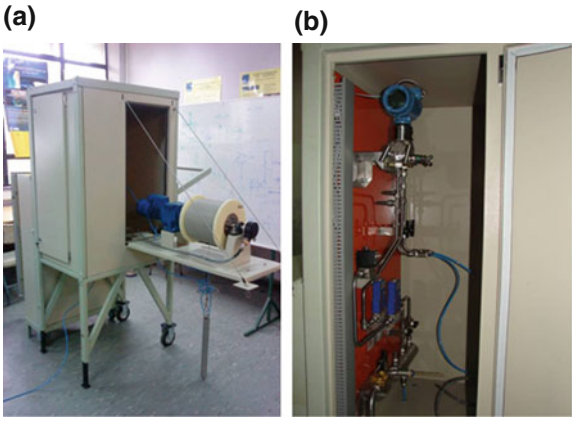

Fig. 8.63 Prototype of SMC instrument. **a** General view of prototype. **b** Sensor and instrumentation

- Descent detention.
- Differential pressure measurement.
- Washing the cable and detector.
- Data processing.

The instrument measures the pulp concentration as solid volume fraction in the thickener on the basis of differential pressure measurements following the equation:

$$\varphi_{pulp} = \frac{\Delta P}{(\rho_{solid} - \rho_{Liquid}) \cdot g \cdot \Delta h} - \frac{\rho_{Liquid}}{(\rho_{solid} - \rho_{Liquid})} \tag{8.107}$$

Figure 8.64 shows concentration profiles measured in an industrial thickener of a Chilean copper concentrator. The horizontal axis represents the solid concentration and the vertical axis represents the height of the thickener.

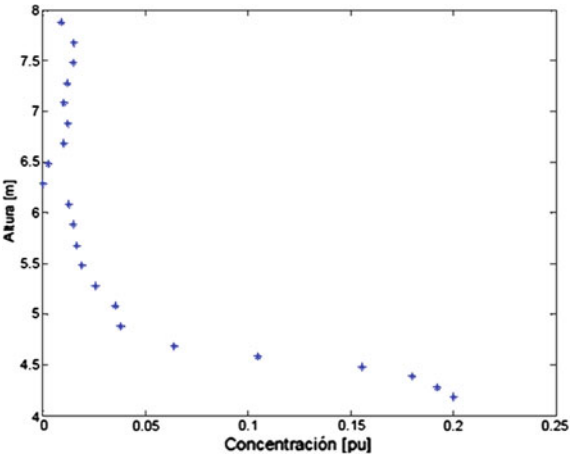

Fig. 8.64 Concentration profile in an industrial copper tailing thickener obtained by the SMC

8.6 Thickener Design

The design of a new thickener or the determination of the capacity of an existing thickener requires calculations at steady state. Since 1912, several methods have been proposed for thickener design. They can be classified based on their physical foundation as: *macroscopic balances, batch Kynch kinematical process, continuous Kynch kinematic process and dynamic sedimentation process* (Concha and Barrientos 1993). In this section, we discuss their advantages and limitations.

8.6.1 Methods Based on Macroscopic Balances

Mishler (1912) and Coe and Clevenger (1916) proposed the first methods of thickener design based on macroscopic balances.

(a) **Mishler's method**

Consider a thickener at steady state, with a solid mass feed flow of F (MT^{-1}), a concentration $\mathfrak{D}_F$ [−], expressed as a *dilution*, defined as the ratio of liquid to solid mass, an underflow mass rate and concentration D (MT^{-1}) and $\mathfrak{D}_D$ [−] respectively and a mass flow rate of water in the overflow of O (MT^{-1}). A solid and water mass balances gives:

$$\text{Solid}: \quad F = D \tag{8.108}$$

$$\text{Water}: \quad F\mathfrak{D}_F = D\mathfrak{D}_D + O \tag{8.109}$$

If ρ_f is the water density, the volume overflow rate of water is $Q_O = O/\rho_f$, then:

$$Q_O = \frac{F(\mathfrak{D}_F - \mathfrak{D}_D)}{\rho_f} \tag{8.110}$$

According to Mishler (1912) the overflow rate of water Q_O within the thickener is equal to the volume flow rate of water formed in a settling column during sedimentation for a suspension of the same concentration as that of the feed (Fig. 8.65).

Since the rate of water appearance, $R > 0$ in the batch test is equal to the rate of descent of the water suspension interface, the water volume flow rate is $Q_O = S \times R$, and from Eq. (8.110):

$$S = \frac{F(\mathfrak{D}_F - \mathfrak{D}_D)}{\rho_f R} \tag{8.111}$$

Mishler used the units of (short tons/day) for F, (feet/min) for R and (pounds/cubic feet) for ρ_f, so that the area in square feet is:

$$S = 0.0222S = \frac{F(\mathfrak{D}_F - \mathfrak{D}_D)}{\rho_f R(\mathfrak{D}_F)} \text{ in } (\text{ft}^2) \tag{8.112}$$

The method consists of measuring the settling velocity $R(\mathfrak{D}_F)$ of the water-suspension interface in a settling column, with the dilutions of the feed to the thickener, and using Eq. (8.112). This balance has the implicit assumption that the concentration in zone II in a thickener is that of the feed to the thickener.

The unit area, defined as $UA = S/F$, is given by:

$$UA = 0.0222S = \frac{(\mathfrak{D}_F - \mathfrak{D}_D)}{\rho_f R(\mathfrak{D}_F)} \text{ in } (\text{ft}^2/\text{stpd}) \tag{8.113}$$

Problem 8.6 Use Mishler's method to calculate the area of a thickener to treat 1,200 (tpd) of calcium carbonate with a density of 3.6 t/m^3 and feed concentration of $w_F = 35\,\%$ solids by weight. The settling velocity of a sample of feed is $R = 8.24 \times 10^{-6}$ m/s and the density of the water is 1.0 t/m^3. An underflow concentration of 52.4 % solid by weight is needed.

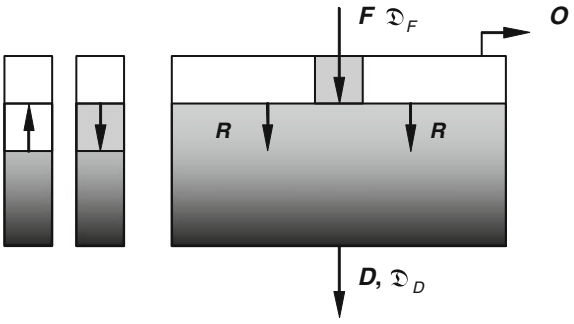

Fig. 8.65 Macroscopic mass balance in a continuous thickener according to Mishler (1912)

The relationship between dilution and % solid by weight is:

$$\mathfrak{D}_F = \frac{100 - w_F}{w_F} = \frac{100 - 35.0}{35.0} = 1.857$$

$$\mathfrak{D}_D = \frac{100 - w_D}{w_D} = \frac{100 - 52.4}{52.4} = 0.908$$

$$UA_M = \frac{\mathfrak{D}_F - \mathfrak{D}_D}{\rho_f R} = \frac{1.857 - 0.9084}{1.0 \times 8.24 \times 10^{-6} \times 24 \times 3600} = 1.33 \ (\mathrm{m^2/tpd})$$

$$S = UA_M \times F = 1.3326 \times 1.200 = 1599 \ (\mathrm{m^2})$$

$$D = (4 \times S/\pi)^{1/2} = 45.1 \ (\mathrm{m})$$

The following table shows the results.

w_F % solid weight	$\mathfrak{D}_F$	$\mathfrak{D}_D$	R m/s	UA m^2/tpd	F tpd	S m^2	D m
35	1.8570	0.9080	8.24E−06	1.333	1,200	1,599	45

(b) Coe and Clevenger's method

Coe and Clevenger (1916) used the same mass balance as Mishler, but indicating that in a thickener a range of pulp concentrations, each with a specific settling velocity, will appear from the feed to the discharge the concentration. See Fig. 8.66.

The feed with pulp dilution $\mathfrak{D}_F$ passes through several dilutions $\mathfrak{D}_k$ before leaving the thickener with dilution $\mathfrak{D}_D$. The pulp with the lowest settling velocity predominates in the settling zone. A mass balance at the level of dilution $\mathfrak{D}_k$ gives:

$$\text{Solid}: \quad F = D \tag{8.114}$$

$$\text{Water}: \quad F\mathfrak{D}_k = D\mathfrak{D}_D + O \tag{8.115}$$

Calculating the mass flow rate of water O and the volume flow rate Q_O results in:

$$Q_o = \frac{F(\mathfrak{D}_\mathfrak{f} - \mathfrak{D}_\mathfrak{D})}{\rho_f}$$

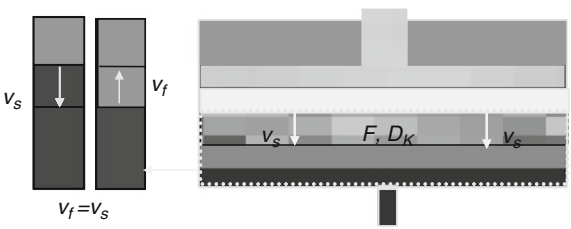

Fig. 8.66 Macroscopic mass balance in a continuous thickener according to Coe and Clevenger (1916)

With the same argument given by Mishler, the unit area UA is given by:

$$UA_{CC} = \frac{(\mathfrak{D}_k - \mathfrak{D}_D)}{\rho_f R(\mathfrak{D}_k)} \tag{8.116}$$

Since settling velocities at different dilutions give different UAs, several settling experiments should be made with dilutions ranging from the feed to the discharge dilution, calculating the respective unit area. The maximum unit area should be chosen. Coe and Clevenger used the following units: liquid density $\rho_f = 62.4\,(\mathrm{lb/ft^3})$, settling velocity R in (ft/h) and thickener capacity F in (lb/h/ft^2), with the result that the unit area is given in (ft^2/lb/h) per pounds:

$$UA_{CC} = \max_{\mathfrak{D}_F \geq \mathfrak{D}_k \geq \mathfrak{D}_D} \left(0.01604 \frac{\mathfrak{D}_k - \mathfrak{D}_D}{R(\mathfrak{D}_k)} \right) (\mathrm{ft^2/lb/h}) \tag{8.117}$$

Taggart (1927) and Dalstrohm and Fitch (1985) used $\rho_f = 62.4\,(\mathrm{lb/ft^3})$ and the settling velocity R_k in (ft/h), giving the Unit Area in (ft^2/stpd):

$$UA_{TDF} = \max_{\mathfrak{D}_F \geq \mathfrak{D}_k \geq \mathfrak{D}_D} \left(1.33 \frac{\mathfrak{D}_k - \mathfrak{D}_D}{R(\mathfrak{D}_k)} \right) (\mathrm{ft^2/stpd}) \tag{8.118}$$

Expressing the densities ρ in [kg/m^3], the concentrations in volume fraction of solids $\varphi = \rho_f / \left(\rho_f + \rho_s \mathfrak{D} \right)$ and the solid flux density $f_{bk}(\varphi) = -\varphi R(\varphi) < 0$ in (m/s), equation can be written in the form:

$$UA_{CC} = \max_{\varphi_F \leq \varphi_k \leq \varphi_D} \left(1.1574 \times 10^{-2} \times \frac{1}{\rho_s f_{bk}(\varphi_k)} \left(\frac{\varphi_k}{\varphi_D} - 1 \right) \right) \ (\mathrm{m^2/tpd}) \tag{8.119}$$

Problem 8.7 Use Coe and Clevenger's method to calculate the area of a thickener to treat 1,200 tpd of calcium carbonate with a density if 2.53 t/m^3 and feed concentration of w = 35 % solids by weight. The density of the water is 1 t/m^3. The settling velocity of pulps ranging from the feed to the underflow concentration is given in the next table. An underflow concentration of 52.4 % solid by weight is needed.

Experiments at different concentrations gave the following settling velocities:

Concentration as % solids by weight	Concentration as dilution	Settling velocity R in m/s
35.0	1.857	8.24×10^{-6}
40.0	1.500	4.27×10^{-6}
45.0	1.222	2.06×10^{-6}
50.0	1.000	8.9×10^{-7}
52.4	0.908	5.76×10^{-7}

Using equation in metric units, we have for $\mathfrak{D}_k = 1.857$:

$$UA(1.857) = \frac{1.857 - 0.908}{8.24 \times 10^{-6} \times 24 \times 3600} = 1.333 \ \text{m}^2/\text{tpd}$$

Calculating all concentrations of the table above, the following results were obtained:

W_k % sol	φ_k	D_k	D_D	R m/s	AU m^2/tpd	F tpd	S m^2	D m
35.0	0.177	1.8570	0.9080	8.24E−06	1.3330	1,200.00	1,599.6	45
40.0	0.211	1.5000	0.9080	4.27E−06	1.6046	1,200.00	1,925.6	50
45.0	*0.247*	*1.2220*	0.9080	*2.06E−06*	*1.7642*	*1,200.00*	*2,117.0*	*52*
50.0	0.286	1.0000	0.9080	8.90E−07	1.1964	1,200.00	1,435.7	43
52.4	0.306	0.9080	0.9080	5.70E−07	0.0000	1,200.00	0.0	0

The area of the thickener is $S = 2117\,(\text{m}^2)$ and $D = 52\,(\text{m})$.

Coe and Clevenger argued that the height of the thickener is important only if the underflow concentration is greater than the critical concentration. In that case, space should be provided for the sediment to have a sufficient residence time to reach the underflow concentration.

Call t^* the time to reach the required underflow concentration in a batch test. Divide the time interval $[0, t^*]$ in n intervals $\Delta t_i = t_{i-1} - t_i$. The height z_i of each interval is calculated as $z_i = V_i/S$ with $i = 1,2,\ldots n$, where V_i is the volume of the sediment with average pulp density $\bar{\rho}_i$ and S is the column cross-section area. The volume V_i is $V_i = F\Delta t_i/\varphi_i\bar{\rho}_i$, where F is the mass flow rate to the thickener. Then:

$$\begin{aligned} z_i &= \frac{F\Delta t_i}{\varphi_i \bar{\rho}_i S}\ , \quad i = 1, 2, \ldots, n \\ &= \frac{1}{UA}\frac{\Delta t_i}{\bar{\varphi}_i\left(\Delta\rho\bar{\varphi}_i + \rho_f\right)} \end{aligned}$$

and the total height is:

$$\begin{aligned} z_c &= \sum_i z_i \\ &= \frac{1}{UA_{CC}}\sum_i \frac{\Delta t_i}{\bar{\varphi}_i\left(\Delta\rho\bar{\varphi}_i + \rho_f\right)}, \quad i = 1, 2, \ldots, n \end{aligned} \tag{8.120}$$

In these expressions, $\bar{\varphi}_i = \varphi_{i-1} - \varphi_i$. For a height z_c, Coe and Clevenger recommended the addition of 0.50–1.00 m for clear water.

Problem 8.8 For the data of Problem 8.7, calculate the height of the thickener.

The unit area in problem 8.7 was $UA_0 = 1.76\ \text{m}^2/\text{tpd}$ for an underflow concentration of $w_D = 52.4\,[\%]$ solids by weight. In terms of solid volume fraction, the underflow concentration is $\varphi_D = 0.306$ (Figs. 8.67, 8.68).

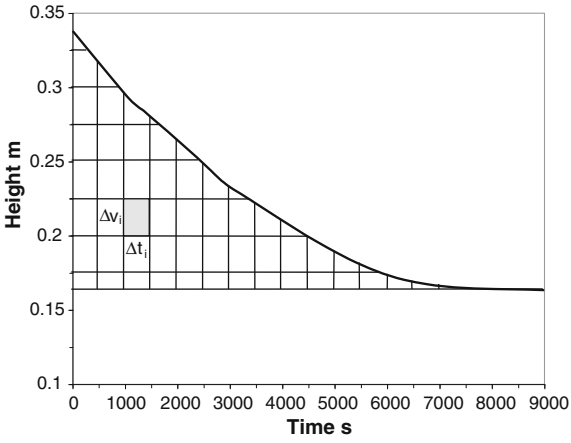

Fig. 8.67 Calculation of the height of a thickener according to Coe and Clevenger (1916) (Concha and Barrientos 1993)

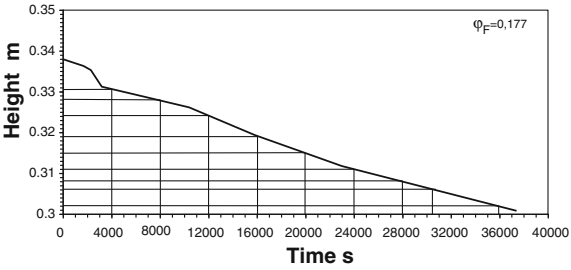

Fig. 8.68 Settling plot to calculate the thickener's height according to Coe and Clevenger (1916)

Applying Eq. (8.120) the sediment height should be 0.813 m. Adding 1.0 m for the clear water zone, the total height of the thickener must be more than 1.813 m. See the following table.

Z_i cm	φ_i	Δt_i s	ΔZ_i m
0.338	0.177	0	0
0.331	0.181	10	0.000
0.328	0.182	8,000	0.221
0.324	0.185	12,000	0.109
0.319	0.188	16,000	0.107
0.315	0.190	20,000	0.105
0.311	0.192	24,000	0.104
0.308	0.194	28,000	0.103
0.306	0.196	30,500	0.064
			H_c (m) = 0.813

8.6.2 Methods Based on Kynch Sedimentation Processes

Kynch's theory led several researchers, including Talmage and Fitch (1955), Wilhelm and Naide (1979), Oltmann (), Hassett (1958, 1961, 1964a, b, 1968) and Yoshioka et al. (1957) to use this theory as the basis for thickener design. The method used universally until then was that of Coe and Clevenger (1916) but it was felt that it required too many laboratory tests. Researchers looked for a methodology that required less effort in the laboratory and Kynch's theory was the answer.

To describe the different methods developed by this group of researchers, divide them into those based on the *Kynch Batch Sedimentation Processes* and on the *Kynch Continuous Sedimentation Process*. To review Kynch's theory see Chap. 5.

(a) **Methods based on Batch Kynch Sedimentation Processes**

Consider an ideal suspension subjected to batch sedimentation. Kynch's theory shows that the suspension concentration $\varphi(z,t)$ can be obtained from a hyperbolic conservation law for regions where the variables are continuous, by the theory of characteristics:

$$\frac{\partial \varphi}{\partial t} + \frac{\partial f}{\partial z} = 0 \tag{8.121}$$

For discontinuities, jump conditions replace Eq. (8.121):

$$\sigma(\varphi^+, \varphi^-) = \frac{[f]}{[\varphi]}, \text{ with } [\circ] = (\circ)^+ - (\circ)^- \tag{8.122}$$

The necessary conditions to obtain a solution to Eq. (8.122) are: to have a constitutive equation for the flux density function $f = f(\varphi)$ and initial and boundary conditions.

In a settling curve $z = z(t)$, as in Fig. 8.69, tangents such as Z/T to the settling curve are the rate of displacement of the discontinuity of a given concentration in the water/suspension, and represents the sedimentation velocity of suspensions of concentration $Z/T = v_s(\varphi_k)$:

$$\sigma_I(\varphi) = \sigma(0,\varphi) = \frac{f_{bk}(\varphi) - f_{bk}(0)}{\varphi - 0} = \frac{f_{bk}(\varphi)}{\varphi} = v_s\varphi \equiv \frac{Z}{T} \tag{8.123}$$

The straight lines starting at $(0,0)$ and ending at (z_k, t_k), for several values of k, are characteristics with constant concentration φ_k and slope $f'_{bk}(\varphi)$.

The volume of solids per unit cross sectional area in the settling column is $\varphi_0 L$. While traveling from $(0,0)$ to (z_k, t_k) the wave of concentration φ_k crosses the total volume of solids, then:

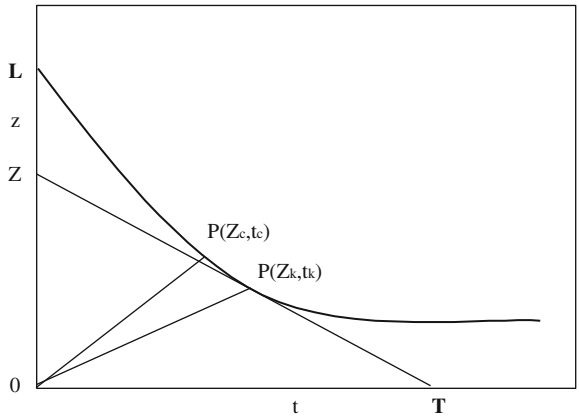

Fig. 8.69 Settling curve

$$\varphi_0 L = \int_0^{t_k} \varphi_k \left(v_s(\varphi_k) + f'_{bk}(\varphi)\right) dt$$
$$= \varphi_k \left(\frac{Z}{T} + \frac{z_k}{t_k}\right) t_k$$

From Fig. 8.69, we see that $Z/T = (Z - z_k)/t_k$, therefore

$$\varphi_0 L = \varphi_k Z \tag{8.124}$$

Therefore, the value of the concentration φ_k can be found as:

$$\varphi_k = \varphi_0 \frac{L}{Z} \tag{8.125}$$

From Kynch's theory, many pars $(\varphi_k, v_s(\varphi_k))$ can be obtained from a settling curve by drawing tangents as shown in Fig. 8.70.

Since $\varphi_k = \varphi_0 L/Z$ and $v_s(\varphi_k) = -Z/T$, then $f_{bk}(\varphi) = \varphi_k v_s(\varphi_k) = -\varphi_0 L/T$. The unit area can be calculated from Coe and Clevenger's equation:

$$UA_{CC} = \max_{\varphi_F \le \varphi_k \le \varphi_D} \left(1.1574 \times 10^{-2} \times \frac{1}{\rho_s f_{bk}(\varphi_k)} \left(\frac{\varphi_k}{\varphi_D} - 1\right)\right) \text{m}^2/\text{tpd}$$

From (8.125) $\varphi_k/\varphi_D = Z_D/Z$ and $f_{bk}(\varphi_k)$ from yields the unit area determined from Kynch'e equation:

$$UA_K = \max_{\varphi_F \le \varphi_k \le \varphi_D} \left(1.1574 \times 10^{-2} \times \frac{T}{\rho_s \varphi_0 L} \left(1 - \frac{Z_D}{Z}\right)\right) \text{m}^2/\text{tpd} \tag{8.126}$$

Problem 8.9 Use Kynch's theory for batch sedimentation to calculate the area of a thickener to treat 1,200 tpd of calcium carbonate with a density if 2.5 t/m^3 and feed concentration of w = 35.0 % solids by weight. The density of the water is

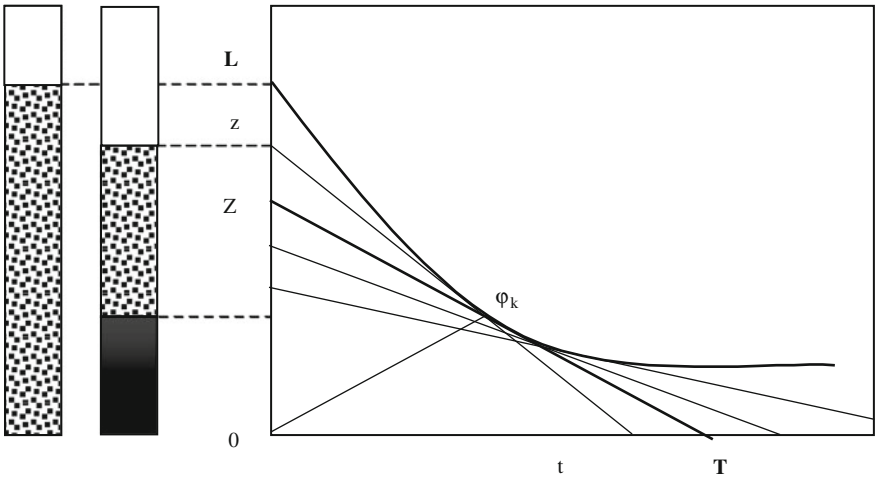

Fig. 8.70 Determination of the concentration and settling velocity of a suspension according to Kynch's method of batch sedimentation

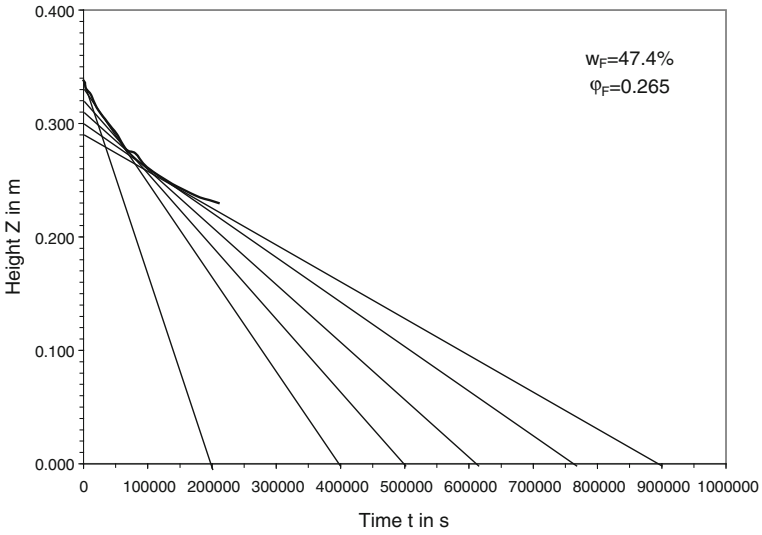

Fig. 8.71 Tangents in the settling curve from Kynch's theory

1 t/m^3. A settling curve is given for a suspension with 10.3 % solid by weight. An underflow concentration of 52.4 % solid by weight is needed.

The table below and Fig. 8.71 show the values of T and Z obtained from the tangents and the tangent drawn to the curve.

Z_k cm	T_k s	L cm	φ_0	φ_k	$f_{bk}(\varphi)$ m/s	AU_0 m$_2$/tpd	F tpd	S m^2	D m
0.338	20,0000	0.338	0.265	0.265	4.4785E−07	1.3762797	1,200	1,652	46
0.330	*395,000*	*0.338*	*0.265*	*0.271*	*2.2676E−07*	*2.2891053*	*1,200*	*2,747*	*59*
0.320	500,000	0.338	0.265	0.280	1.7914E−07	2.1805432	1,200	2,617	58
0.310	610,000	0.338	0.265	0.289	1.4684E−07	1.7290118	1,200	2,075	51
0.300	760,000	0.338	0.265	0.299	1.1786E−07	0.9165819	1,200	1,100	37
0.293	850,000	0.338	0.265	0.306	1.0538E−07	0	1,200	0	0

According to this method, the area of the thickener is $S = 2{,}747\,\text{m}^2$ and the diameter is $D = 59\,\text{m}$.

Talmage and Fitch method

Talmage and Fitch (1955) wrote from Fig. 8.72:

$$\frac{Z}{T} = \frac{Z - Z_D}{t_u}$$

where Z_D is the tangent to the settling curve for the underflow concentration φ_D, and t_u is the intersection of the tangent Z-T with the horizontal drawn from Z_D. The coordinate Z_D is obtained from $Z_D = \varphi_0 L/\varphi_D$.

Replacing into (8.126), and observing that the maximum of t_u is t_U, the following simple equation is obtained:

$$AU = \underbrace{\max}_{Z}\left(\frac{t_u}{\rho_s \varphi_0 L}\right) \equiv \frac{t_U}{\rho_s \varphi_0 L} \tag{8.127}$$

$$AU_{TF} = 1.1574 \times 10^{-2}\frac{t_U}{\rho_s \varphi_0 L},\ (\text{m}^2\text{tpd}) \tag{8.128}$$

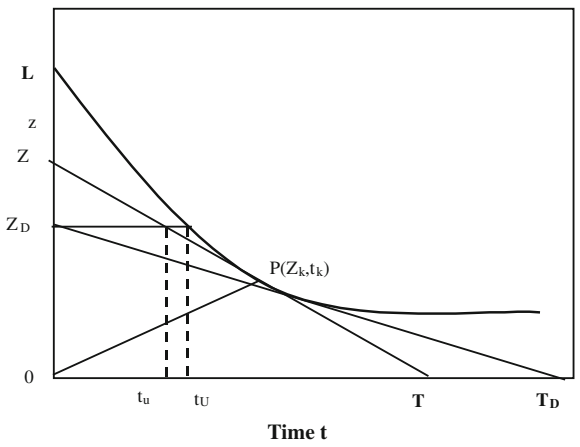

Fig. 8.72 Talmage and Fitch construction (1955)

Time (s)	Height (m)
0	0.338
1692	0.336
2304	0.335
3204	0.331
6804	0.329
10404	0.326
15804	0.319
23004	0.312
37404	0.301
51804	0.291
66204	0.277
80604	0.274
95004	0.264
109404	0.257
123804	0.252
138204	0.247
152604	0.243
167004	0.238
181404	0.235
195804	0.232
210204	0.230

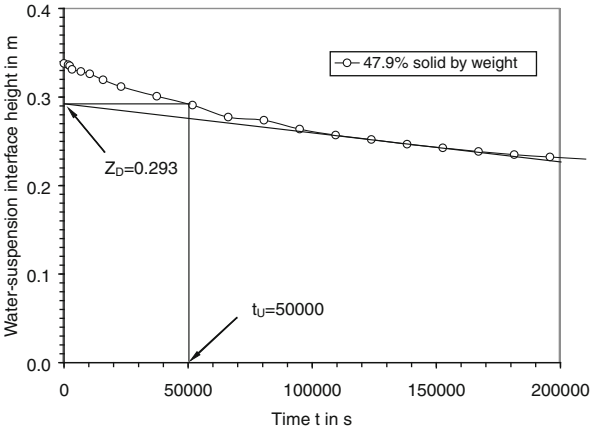

Fig. 8.73 Talmage and Fitch construction (1955)

Talmage and Fitch method consist of:

1. Performing a settling test with an "intermediate "concentration. (we will discuss this further on).
2. Drawing the settling curve.
3. Determining the height Z_D from $Z_D = \varphi_0 L/\varphi_D$.
4. Drawing a horizontal line from Z_D to the settling curve. The intersection defines t_U.
5. If metric units are used, using Eq. (8.128) to calculate the unit area.

Problem 8.10 Use Talmage and Fitch's method to calculate the area of a thickener to treat 1,200 tpd of calcium carbonate with a density if $\rho_s = 2.5\,\mathrm{t/m^3}$ and feed concentration of $w_F = 35\,\%$ solids by weight. The density of the water is $\rho_f = 1\ \mathrm{t/m^3}$. A settling curve is given for a suspension with $w_0 = 47.9\,\%$ solid by weight. The underflow concentration is $w_D = 52.4\,\%$ solid by weight. The critical concentration is $w_c = 42.7\,\%$ by weight.

According to Kynch's theory $Z_D = \varphi_0 \times L/\varphi_D = 0.265 \times 0.338/0.303 = 0.293$. Figure 8.73 should be constructed.

Applying Eq. (8.128), the unit area UA_{TF} can be calculated. The results can be summarized in the following table:

t_U	50,000
AU_0	2.251
S	2,702
D	59

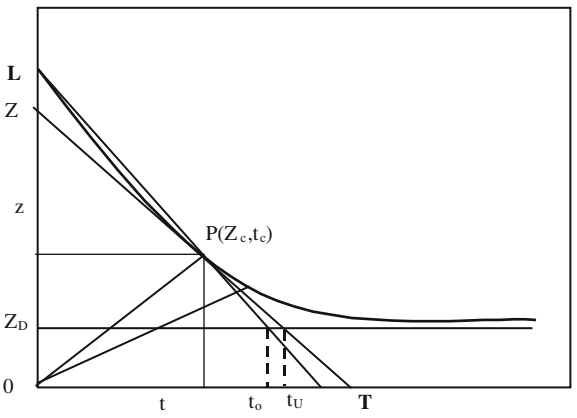

Fig. 8.74 Talmage and Fitch II (1955) and Oltman's construction (Fitch and Stevenson 1976)

Since Talmage and Fitch's method is used for all types of pulps, compressible and incompressible, in some cases the horizontal line drawn from Z_D does not cut the settling curve. In these cases, Talmage and Fitch recommend drawing the tangent *Z-T* for the critical concentration φ_c and obtaining t_U as the intersection of this line with the horizontal line. See Fig. 8.74.

Oltman method

From experience, Fitch and Stevenson (1976) found that thickener area obtained from the critical concentration was too great and adopted an empirical modification proposed by Oltman, an engineer at Dorr Oliver. Without justification, Oltman proposed substituting the tangent to the settling curve by the straight line drawn from point $(L, 0)$ passing through the point (z_c, t_c). See Fig. 8.74.

Talmage and Fitch and Oltman's method are based on the knowledge of the critical concentration and on the assumption (erroneously) that a compressible pulp at the underflow concentration follows Kynch's theory.

8.6.3 Methods Based on Continuous Kynch Sedimentation Processes

In Chap. 5 Sect. 5.2.3 Kynch's theory for a continuous process was studied. Figure 5.14a and c show that Unit Area of an ideal thickener treating an ideal suspension is given by:

$$UA_0 = \frac{1}{\rho_s f_{bk}(\varphi_M^{**})}\left(\frac{\varphi_M^{**}}{\varphi_M} - 1\right)$$

where φ_M and φ_M^{**} are the concentration of the maximum point in the flux-density curve and the conjugate concentration, respectively. The underflow concentration

is $\varphi_D = \varphi_M$. These methods imply knowledge of the flux-density function. See Fig. 5.14a and c.

Yoshioka and Hassett Method

Yoshioka et al. (1957) proposed a method of thickener design based on the knowledge of the batch flux-density function and its relationship with the continuous flux density and the underflow concentration (see Chap. 5, Sect. 5.2.4). If $f_{bk}(\varphi)$ is the batch fluxdensity and $f_k(\varphi)$ is the continuous flux density, we can write at steady state:

$$f_F = f_k = q\varphi + f_{bk}(\varphi) \tag{8.129}$$

(8.129) is written in the form:

$$f_{bk}(\varphi) = f_F - q\varphi \tag{8.130}$$

In a graph of $f_{bk}(\varphi)$ versus φ, Eq. (8.130) represents a straight-line tangent to $f_{bk}(\varphi)$ at $\varphi = \varphi_M$ with slope $q = f_F/\varphi_D$. Figure 8.75 shows these functions with the ordinate axis as $(-f_k(\varphi))$ and $(-f_{bk}(\varphi))$.

The design method can be summarized as follows:

1. Draw the given batch flux-density function.
2. Select the underflow concentration.
3. For the given batch flux-density function, draw a straight line from the point, $(0, \varphi_D)$ tangent to the batch flux density curve at point $\varphi = \varphi_M$.
4. The line cuts the ordinate at point $(f_F, 0)$.

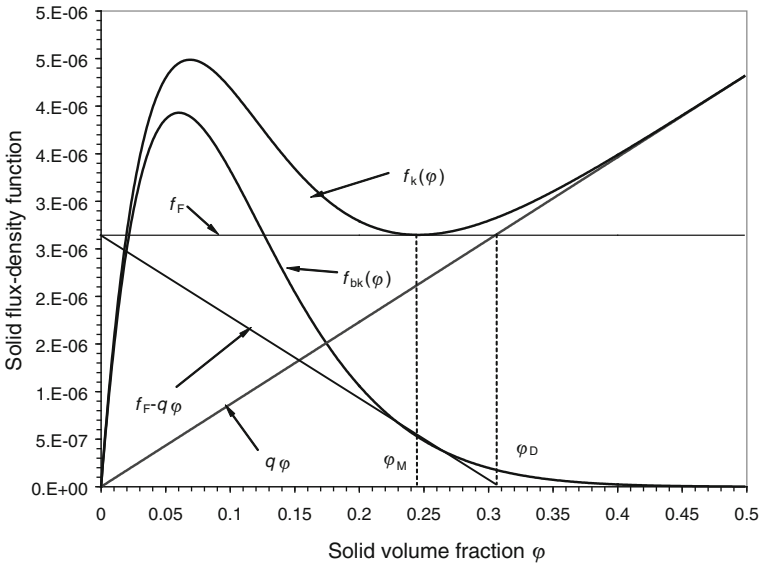

Fig. 8.75 Yoshioka and Hassett design method

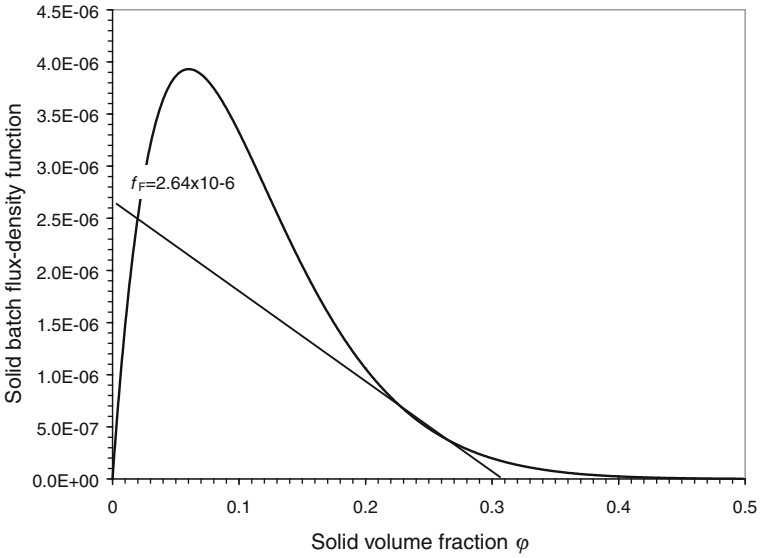

Fig. 8.76 Yoshioka and Hasset construction

Problem 8.11 Using the method of Yoshioka and Hassett, design a thickener to process 1,200 tpd of calcium carbonate with a feed concentration of 35 % solids by weight. The solid density is 2.5 t/m^3 and the desired underflow concentration is 52.4 % solids by weight. The solid batch flux-density function is given in Fig. 8.76.

The feed and underflow concentrations are:

$$\varphi_F = \frac{1 \times 35.0}{2.5 \times (100 - 35.0) + 1 \times 35.0} = 0.177$$

$$\varphi_D = \frac{1 \times 52.1}{2.5 \times (100 - 52.4) + 1 \times 52.4} = 0.306$$

In Fig. 8.76 a straight line starting from and tangent to the curve give a value of $-f_F = 2.64 \times 10^6\,(\mathrm{m/s})$. Then the thickener capacity is given by:

$$S = \frac{F}{-f_F \times \rho_s \times 3600 \times 24} = \frac{1200}{2.64 \times 10^{-6} \times 2.5 \times 3600 \times 24} = 2104\,(\mathrm{m}^2)$$

$$UA_0 = \frac{S}{F} = \frac{2104}{1200} = 1.753\,(\mathrm{m}^2/\mathrm{tpd}); \quad D = 52\ (\mathrm{m})$$

Hassett (1958) noted a problem in the interpretation of the underflow concentration. Figure 8.76 shows that according to Kynch's theory only two concentrations exist in the thickener at steady state, the underflow concentration φ_M and the conjugate concentration φ_M^{**}. Hassett said:

> … In this way the theory predicts the absence of the feed concentration and the underflow concentration in the thickener, which means that an *abrupt growth of concentration* must exist in the underflow….

The theory developed in Chap. 5 shows that Hassett's reasoning is wrong because he tried to apply Kynch's theory to compressible suspensions. The theory is correct for ideal but not for compressible suspensions.

Wilhelm and Naide Method

Wilhelm and Naide (1979) also started from the knowledge of the flux-density function for continuous thickening, like Yoshioka and Hasset, and wrote similar equation at steady state:

$$f_F = q\varphi + f_{bk}(\varphi) = q\varphi_D$$

Differentiating with respect φ results:

$$0 = q + f'_{bk}(\varphi_M)$$

from which:

$$q = -f'_{bk}(\varphi_M) \tag{8.131}$$

Substituting in the previous expression yields:

$$-f'_{bk}(\varphi_M)\varphi + f_{bk}(\varphi) = -f'_{bk}(\varphi_M)\varphi_D$$

This equation should apply for $\varphi = \varphi_M$, then:

$$-f'_{bk}(\varphi_M)\varphi_M + f_{bk}(\varphi_M) = -f'_{bk}(\varphi_M)\varphi_D \tag{8.132}$$

Now, if we assume that the solid settling velocity can be expressed in the form:

$$v_s(\varphi) = -a\varphi^{-b}, \tag{8.133}$$

the solid flux-density function $f_{bk}(\varphi)$ would be $f_{bk}(\varphi) = -a\varphi^{1-b}$ and its derivative at $\varphi = \varphi_M$:

$$f'_{bk}(\varphi) = -a(1-b)\varphi_M^{-b} \tag{8.134}$$

Substituting (8.134) with (8.132), and calculating φ_M results in:

$$\varphi_M = \frac{b-1}{b}\varphi_D \tag{8.135}$$

Relacing φ_M from (8.135) in (8.134) and the result in (8.131) yields:

$$q = -a(1-b)\left(\frac{b-1}{b}\right)^{-b}\varphi_D^{-b} \tag{8.136}$$

Since at steady state $f_F = q\varphi_D$, using (8.136) we reach the result:

$$f_F = -a(1-b)\left(\frac{b-1}{b}\right)^{1-b}\varphi_D^{1-b} \tag{8.137}$$

and the area and unit area AU are:

$$\begin{aligned} S &= \frac{F}{-f_F \times \rho_s \times 3600 \times 24} = \frac{F}{\rho_s \times 3600 \times 24}\frac{\left(\frac{b-1}{b}\right)^{b-1}\varphi_D^{b-1}}{ab(1-b)}\ (\mathrm{m}^2) \\ UA &= \frac{S}{F} = \frac{1}{-f_F \times \rho_s \times 3600 \times 24} = \frac{1}{\rho_s \times 3600 \times 24}\frac{\left(\frac{b-1}{b}\right)^{b-1}\varphi_D^{b-1}}{a(1-b)}\ (\mathrm{m}^2/\mathrm{tpd}) \end{aligned} \tag{8.138}$$

The expression $v_s(\varphi) = -a\varphi^{-b}$ in (8.133) represents the settling velocity solely in a narrow range of concentrations, therefore the complete function $AU(\varphi)$ must be replaced by a series of expressions valid in this narrow range. In this way, expression (8.138) is valid for each region, as shown in Fig. 8.77. Wilhelm and Naide conclude that the maximum value found for $AU(\varphi)$ must be chosen as the correct value for the Unit Area.

Problem 8.12 Using Wilhelm and Nadie's method of thickener design to process 1,200 tpd of calcium carbonate with a feed concentration of 35 % solids by weight. The solid density is 2.5 t/m^3 and the desired underflow concentration is 52.4 % solids by weight. From a table of data, the settling velocity was calculated and plotted in Fig. 8.77. The feed and underflow concentrations are respectively:

$$\begin{aligned} \varphi_F &= \frac{1 \times 35.0}{2.5 \times (100 - 35.0) + 1 \times 35.0} = 0.177 \\ \varphi_D &= \frac{1 \times 52.1}{2.5 \times (100 - 52.4) + 1 \times 52.4} = 0.306 \end{aligned}$$

For each region, these equations can be applied to obtain the following values for the unit area, the highest of which should be chosen. See Fig. 8.78.

Wilhelm and Nadie's design method gives a value of $UA = 1.815\,\mathrm{m}^2/\mathrm{tpd}$ and $S = UA \times F = 1.815 \times 1200 = 2178\ \mathrm{m}^2$; $D = 53\ \mathrm{m}^2$.

8.6.4 Methods Based on the Phenomenological Theory

In Sect. 8.3.6 we demonstrate that, for a steady state to exist in a continuous thickener, it is necessary that the following inequality be obeyed:

$$f_F \geq q\varphi + f_{bk}(\varphi), \quad \text{for } \varphi_L \leq \varphi \leq \varphi_D \tag{8.139}$$

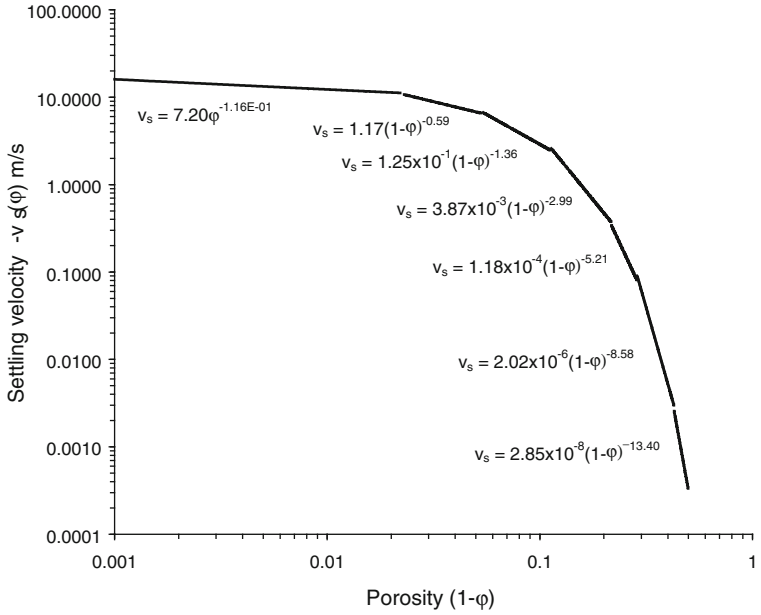

Fig. 8.77 Settling velocity by regions fitting expression

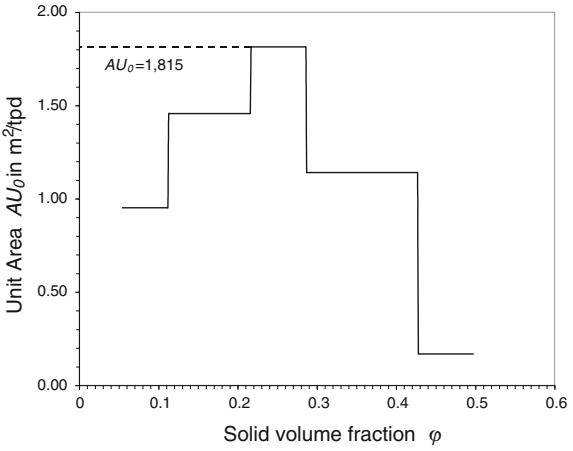

Fig. 8.78 Thickener design according to Wilhelm and Nadie (1979)

where f_F is the feed solid flux-density function, and $f_{bk}(\varphi)$ is Kynch's batch flux density function. Since $q = f_F/\varphi_D$, substituting (8.139), the following is valid for the steady state: $f_F \geq \frac{f_F}{\varphi_D}\varphi + f_{bk}(\varphi)$, for $\varphi_L \leq \varphi \leq \varphi_D$.

Dividing by φ and rearranging yields:

$$f_F \geq \frac{f_{bk}(\varphi)}{1-\frac{\varphi}{\varphi_D}}, \quad \text{for } \varphi_L \leq \varphi \leq \varphi_D \tag{8.140}$$

Flux Density

By definition $F = -\rho_s f_F S$, where F is the thickener capacity measured as solid mass flux, and S is the thickener's cross sectional area. Then, substituting into (8.140) gives:

$$\frac{F}{S} \leq \frac{\rho_s f_{bk}(\varphi)}{1-\frac{\varphi}{\varphi_D}}, \text{ in } \mathrm{ML^{-2}T^{-1}}, \text{ for } \varphi_L \leq \varphi \leq \varphi_D \tag{8.141}$$

Unit Area

Since the unit area is the reciprocal of solid flux density:

$$\frac{S}{F} \geq \frac{1}{\rho_s f_{bk}(\varphi)}\left(1-\frac{\varphi}{\varphi_D}\right), \text{ in } \mathrm{L^{-2}M^{-1}T}, \quad \text{for} \varphi_L \leq \varphi \leq \varphi_D \tag{8.142}$$

Defining the *unit area* function $UA(\varphi)$:

$$UA(\varphi) := \left(-\frac{1}{\rho_s f_{bk}(\varphi)}\right)\left(1-\frac{\varphi}{\varphi_D}\right), \quad \text{for } \varphi_L \leq \varphi \leq \varphi_D \tag{8.143}$$

And the *unit area* is:

$$UA = \max_{\varphi_L \leq \varphi \leq \varphi_D}(UA(\varphi)) \tag{8.144}$$

Height of the Sediment

The height of the sediment is obtained by integrating the equation:

$$z_c = \int_{\varphi_D}^{\varphi_c} \frac{\sigma_e'(\xi) f_{bk}(\xi)}{\Delta\rho\xi g(f_F - q\xi - f_{bk}(\xi))} d\xi \tag{8.145}$$

where φ_D and φ_c are the underflow and the critical concentrations respectively.

To the height of the sediment "z_c" in the thickener, a height "h" for the sedimentation zone and a height "c" for the clear water must be added. The last two zones have arbitrary depth.

$$H = c + h + z_c \tag{8.146}$$

Solid Inventory in the Thickener

Solid inventory is the amount of solid stored as sediment and suspension in the thickener at any time. This material consists of a pulp of the conjugate concentration φ_L and a sediment of variable concentration from φ_c to φ_D. Then, the solid inventory can be expressed as:

$$I = \int_0^L \rho_s \varphi(z) S dz = \rho_s \varphi_L S(L - z_c) + \int_0^{z_c} \rho_s \varphi(z) S dz \tag{8.147}$$

where L is the height of the outlet of the feedwell.

(a) **Adorjand's Method**

Adorjan (1975, 1976) was the first author to utilize Eq. (8.144) for thickener design. Although his deduction differs from the one used here. Adorjan argues that a thickener operated under limiting condition, that is, designed using Eq. (8.143) with the equal sign, requires a considerable pulp depth and therefore it must be operated at only a fraction of the limiting rate. This fraction he called the *loading factor*, and he designed it by $\lambda = F/F_0$, where F is the actual feed rate and F_0 is the limiting feed rate. In terms of unit area $UA = UA_0/\lambda$, with $0 \leq \lambda \leq 1$. Adorjan adopted as criteria to select λ a safety factor in the design, so that a certain deviation from the design would be possible.

Problem 8.13 Using Adorjan's method, design a thickener to process 1,200 (tpd) of calcium carbonate with a feed concentration of 35 % solids by weight. The solid density is 2.5 t/m^3 and the desired underflow concentration is 52.4 % solids by weight. Constitutive equations for the settling velocity and the solid effective stress are available with critical concentration at 42 % solids by weight:

$$f_{bk}(\varphi) = -1.72 \times 10^{-4} \varphi \times (1 - \varphi)^{15.6} \text{ m/s}$$
$$\sigma_e(\varphi) = 2.0 \exp(22\varphi) \text{ Pa}$$

The feed and underflow concentrations are respectively $\varphi_F = 0.177$ and $\varphi_D = 0.306$.

Replacing the corresponding numerical values in Eq. (8.144), the following is obtained:

$$UA_F(\varphi) = -\frac{1}{2.5 \times 3,600 \times 24 \times -1.72 \times 10^{-4} \times \varphi(1 - \varphi)^{15.6}} \left(\frac{\varphi}{0.306} - 1\right)$$

Plotting the unit area function $UA(\varphi)$, gives Fig. 8.79, with a maximum at $\varphi = 0.256$ and a unit area of 1.756 m^2/tpd. Using the safety factor $\lambda = 0.95$,

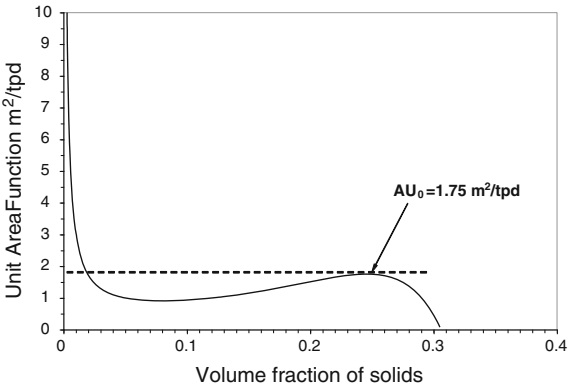

Fig. 8.79 Unit area function versus the concentration with the chosen unit area AU_0

Adorjan's Unit Area becomes: $UA = 1.75/0.95 = 1.84\,\mathrm{m}^2/\mathrm{tpd}$. Finally, the area and diameter of the thickener are: $S = 1.84 \times 1,200 = 2,208\,\mathrm{m}^2$ and $D = 53\,\mathrm{m}$.

(b) **Cettem's Method**

In a recent work, Concha and collaborators (Garrido et al. 2003) developed an algorithm to design and simulate continuous thickeners. Equations (8.143) and (8.144) are also the bases of this method:

$$UA(\varphi, \varphi_D) := \frac{1}{\rho_s f_{bk}(\varphi)} \left(\frac{\varphi}{\varphi_D} - 1 \right), \quad \text{for} \quad \varphi_L \le \varphi \le \varphi_D$$

$$UA = \max_{\varphi_L \le \varphi \le \varphi_D} (UA(\varphi))$$

It is interesting to note that Eq. (8.144) has the same form as Coe and Clevenger's equations. But there is a small but important difference. Coe and Clevenger assumed that the range of concentration where the value of $UA(\varphi, \varphi_D)$ should be maximized was the feed and the underflow concentrations $\varphi_F \le \varphi \le \varphi_D$, while Cettem's method used the known fact that the feed to a thickener is always diluted to the conjugate concentration φ_L when entering the thickener, therefore the range of concentration should be $\varphi_L \le \varphi \le \varphi_D$. Figure 8.80 shows the difference.

In designing a thickener, the desired feed flow rate F and underflow concentration φ_D, together with the thickening parameters $f_{bk}(\varphi)$, $\sigma_e(\varphi)$, φ_c and the solid and liquid densities ρ_s and ρ_f, must be known. With these values, the function $UA(\varphi, \varphi_D)$ can be calculated for any value of $\varphi_L \le \varphi \le \varphi_D$.

The first step in the design procedure makes use of the solution to the phenomenological model at steady state plotting the function $UA(\varphi, \varphi_D)$ in the interval $\varphi_L \le \varphi \le \varphi_D$, see Fig. 8.80.

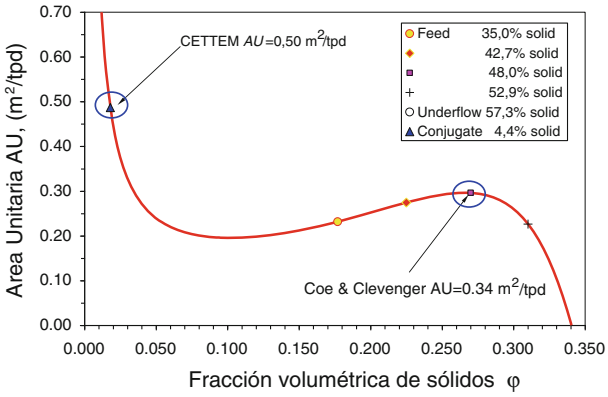

Fig. 8.80 Comparison of CETTEM's and Coe and Clevenger's methods for the determination of the unit area for a copper flotation tailing

The problem to calculate the maximum indicated in the figure is that the conjugate concentration φ_L is unknown until the value of $f_F = -F/\rho_s S$ is calculated, and to do so, we need to know the thickener cross sectional area S, which is the result we are seeking. Therefore, the problem is undetermined and to solve it we must assume a value of φ_L, for example $\varphi_L \approx 0.01$. Once φ_L is chosen, the maximum of $UA(\varphi, \varphi_D)$ is obtained, and the area S and diameter D can be calculated. Now, f_F and q can be obtained and, therefore, the concentration profile in the thickener can be calculated from Eq. (8.145) and the value of the sediment height z_c is obtained.

The next step in the design is to set a target for the value of the sediment height z_c in the thickener. This value is a restriction imposed by the motor of the rakes, which allows a given maximum torque. For example, 20 % of the available height L of the thickener is a reasonable value. Then, an iteration changing the value of D obtains the desired z_c value.

Finally, once the thickener diameter is obtained, it is approximated to the next integer (or to the next commercially available thickener diameter) and the calculation is repeated to obtain: (1) the final thickener diameter, (2) the thickener cross sectional area S, (3) the Unit Area UA, (4) the mass and water balance in the thickener, (5) the solid inventory I, (6) the concentration profile in the thickener, (7) the sediment height z_c and (8) the correct value the conjugate concentration φ_L (Fig. 8.81).

Problem 8.14 Use CETTEMS's method to process 1,200 tpd of calcium carbonate with a feed concentration of 35[%] solids by weight. The solid density is 2.5 (ton/m^3) and the desired underflow concentration is 52.4[%] solids by weight. Constitutive equations for the settling velocity and the solid effective stress are available with critical concentration at 42[%] solids by weight. Consider the design of the thickener with $L = 6$ (m) height and a sediment height of 20 [%] of L, knowing the following properties of the tailings:

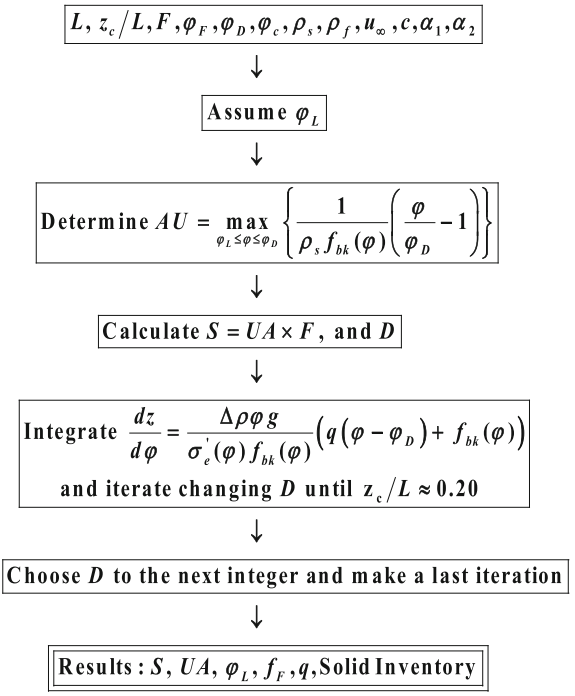

Fig. 8.81 Algorithm for the design of continuous thickeners by CETTEM's method (Concha et al. 2003)

Solid density $\rho_s = 2{,}500\,(\mathrm{kg/m^3})$

Liquid density $\rho_f = 1{,}000\,(\mathrm{kg/m^3})$

Feed concentration $w_F = 35.0\,[\%]$ solid by weight

Critical concentration $w_c = 40.2\,[\%]$ solid by weight

Conjugate concentration $\varphi_L = 0.01$

Underflow concentration $w_D = 52.4\,\%$ solid by weight

Settling parameter $f_{bk}(\varphi) = -1.72 \times 10^{-4} \times \varphi \times (1 - \varphi)^{15.6}\,(\mathrm{m/s})$

Compression parameter $\sigma_e(\varphi) = 2.0 \exp(22\varphi)\,(\mathrm{Pa})$

To perform the calculation we use the software SimEsp developed by Concha and collaborators (Garrido et al. 2003, 2004; Burgos and Concha 2005) (Fig. 8.82).

(a) **Design step**

Choose the *Design Module* and enter: the solid feed rate $F = 50$ (tph), $(1200/24)$, the underflow concentration $w_u = 52.4[\%]$ solid by *weight*, the critical concentration $w_c = 42.8\,[\%] \rightarrow \varphi_c = 0.23$, assume a conjugate concentration $\varphi_L \approx 0.01$ and enter the parameters of the flux density function $u_\infty = -1.72 \times 10^{-4}\,(\mathrm{m/s})$ and c = 15.6. Press the *calculate button* to obtain the

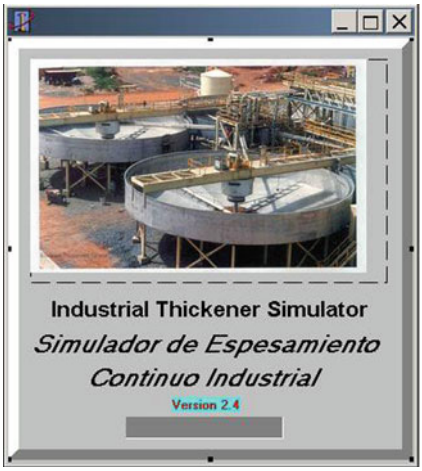

Fig. 8.82 Industrial thickener simulator SimEsp

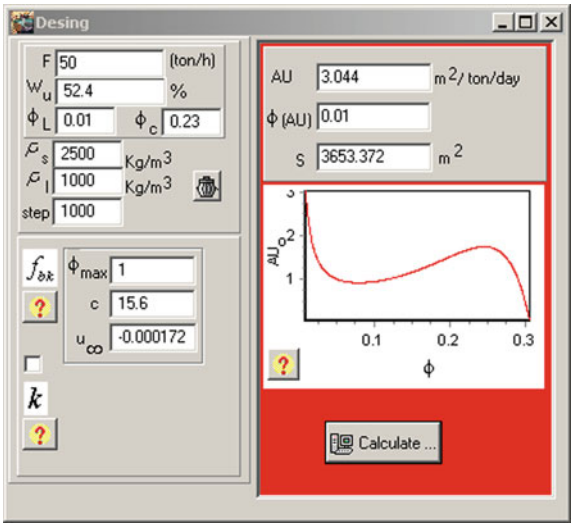

Fig. 8.83 Design module

Unit Area function $UA(\varphi)$ and the unit area $AU(\varphi_L = 0.01) = 3.044\,\mathrm{m}^2/\mathrm{tpd}$ giving a thickener cross sectional area of $S = 3653.4\,\mathrm{m}^2$ for the assumed conjugate concentration. See Fig. 8.83.

- **Simulation step 1**

To continue, press the *Simulation button* to obtain Fig. 8.84. The information from the Design Module is transferred automatically to the Simulation Module. Add the feed concentration $w_F = 35\,\%$, the sediment height in terms of the available thickeners height $z_c = 20\,\%$, the consolidation parameters $\alpha_1 = 2.0\,\mathrm{Pa}$ and $\alpha_2 = 22$. Choose between Case 1, for a flat bottom thickener or

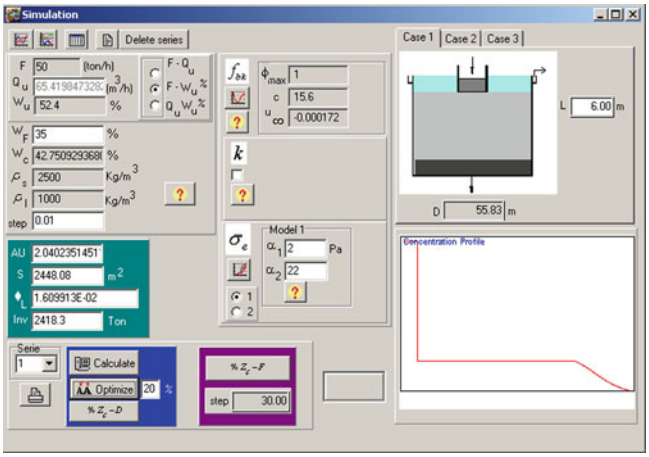

Fig. 8.84 Simulation and optimization module

Case 2 or 3 for conical bottom thickeners. For this problem use Case 1. Now press the *Optimize button* to start the iteration and obtain the thickener diameter: $D = 55.84$ m.

Set the thickener diameter to the next greater integer in meters $D = 56$ m, and press the *Calculate* button to obtain the final result in Fig. 8.85.

$$f_F = -2.256 \times 10^{-6}\,\text{m/s},\ q = -7.378\,\text{m/s},\ z_c = 1.18\,\text{m},\ \varphi_L = 0.016,$$
$$I = 2385.6\,\text{tons},\ AU = 2.05\,\text{m}^2/\text{tpd},\ S = 2,463\,\text{m}^2,\ D = 56\,\text{m},\ \text{Q}_U = 65.42\,\text{m}^3/\text{h}$$

Figure 8.86 gives a material balance around the thickener and Fig. 8.87 shows the concentration profile in the thickener.

Figure 8.88 shows the continuous solid flux density and the feed flux density. The interception of the feed flux density function with the convective flux $q\varphi$ gives the underflow concentration φ_D and with the continuous flux density function gives the conjugate concentration φ_L.

It is possible to design the thickener for 50 tph feed with different values for the sediment height. Press *button* ($\%z_c$-D) and the results are given in Fig. 8.89, which shows that the higher the sediment is allowed, the smaller the thickener diameter required.

- **Simulation step 2**

Once the thickener is designed, it is interesting to study its flexibility to other feed rates. For example, for the designed thickener of $D = 56$ m, choose *button* ($\%z_c$-F) and see the concentration profiles for each the thickener capacity in Fig. 8.90. Figure 8.91 shows the height of the sediment for each thickener capacity.

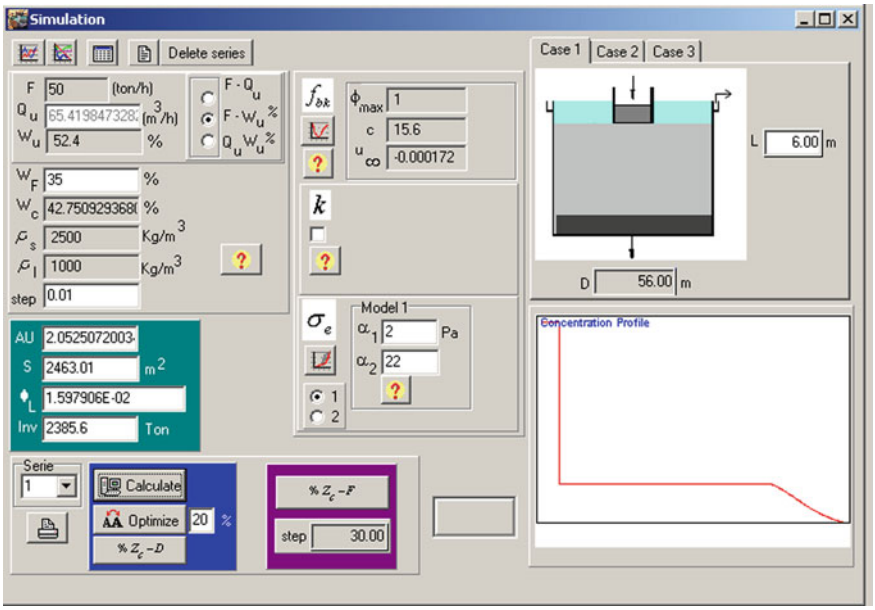

Fig. 8.85 Simulation and optimization module

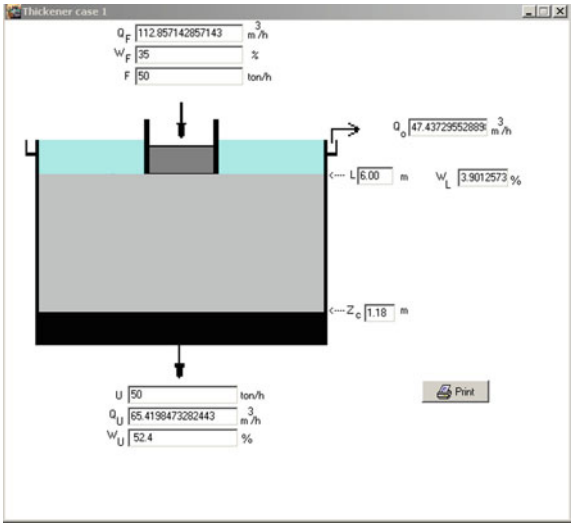

Fig. 8.86 Mass balance in the designed thickener

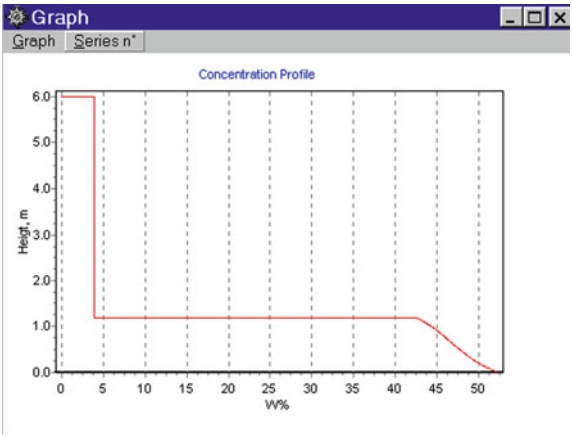

Fig. 8.87 Concentration profile in the designed thickener for sediment with 20 % of the total height

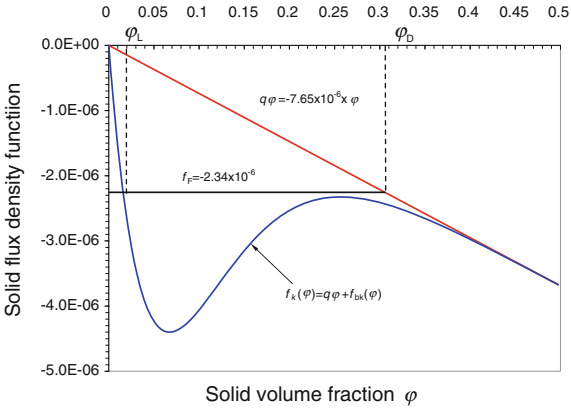

Fig. 8.88 Solid flux density functions

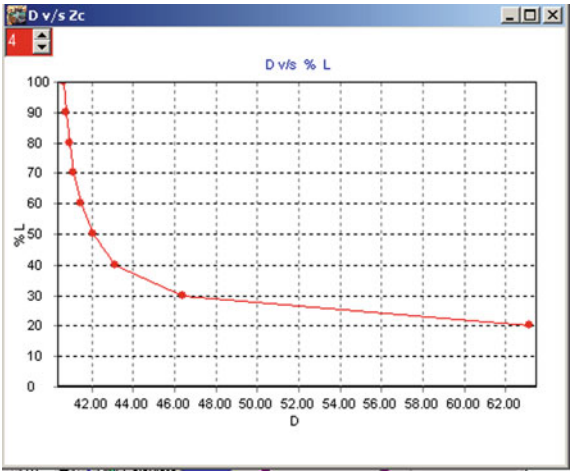

Fig. 8.89 Thickener diameter for several allowed sediment heights

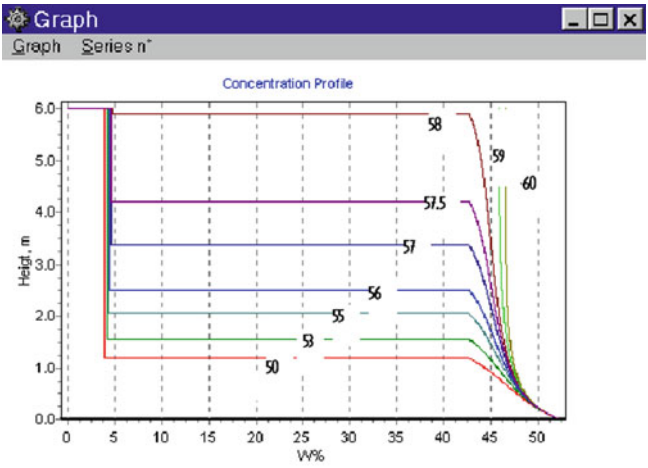

Fig. 8.90 Simulation of the concentration profile for the designed thickener for several thickener feed rates and constant underflow concentration

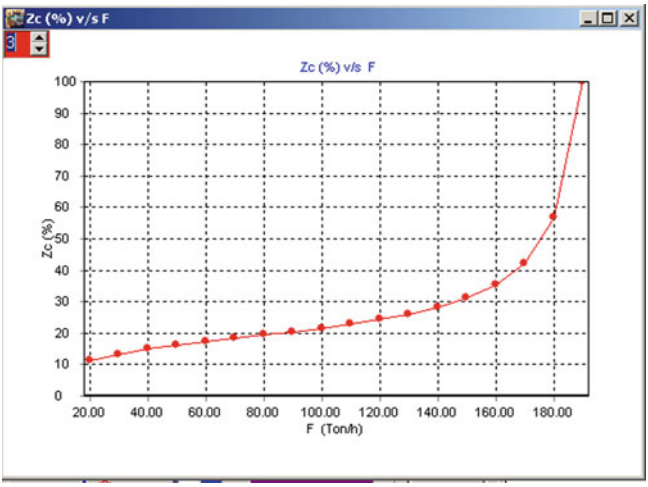

Fig. 8.91 Simulation of the sediment height for several thickener capacities at constant underflow concentration

8.6.5 Comparison of Thickener Design Methods

The following table compares the results of the diverse thickener design methods.

Thickener design	Unit area	Area in m^2	Diameter in m
Mishler	1.333	1,599	45
Coe y Clevenger	1.764	2,117	52
Kynch	2.289	2,747	59
Talmage and Fitch	2.251	2,702	59
Yoshioka and Hasset	1.783	2,104	52
Wilhelm and Naide	1.815	2,178	53
Adorjan	1.840	2,208	53
CETTEM	2.05	2,463	56

The smallest thickener diameter is obtained with Mishler's design and the largest with methods based on Kynch sedimentation processes. The phenomenological methods have the additional advantage that fitting the best equation to the experimental data eliminates experimental errors. Finally, CETTEM's method takes into account the desired height of the sediment in the thickener and provides a plot of thickener capacity versus sediment height.

It is interesting to point out that, although the most recent phenomenological models validated Mishler and Coe and Clevenger's equations for the unit area, these older methods gave the smallest thickener areas. The error in Coe and Clevenger's method is to assume that the concentration in the settling zone of the thickener is that of the feed concentration and, therefore, performing laboratory experiments above this concentration. The phenomenological model gave a value of $\varphi_L = 0.016$ as the limiting concentration for a unit area of $UA = 2.05\,(\mathrm{m}^2/\mathrm{tpd})$. This concentration is far lower than the feed concentration of $\varphi = 0.177$. This is why the laboratory experiments should include smaller concentrations in the range of $\varphi \approx 0.01$.

Figure 8.92 shows the experimental points used by Coe and Clevenger's and the additional point by CETTEM's methods. Figure 8.93 also explains the weakness of Adorjan's method. According to the calculations he obtained $AU = 1.756\,(\mathrm{m}^2/\mathrm{tpd})$, similar to Coe and Clevenger, and with a safety factor of 0.95 he reached $AU = 1.84\,(\mathrm{m}^2/\mathrm{tpd})$. A comparison to Cettem's methods shows the safety factor should have been 0.75.

Problem 8.15 Consider a flocculated suspension of a copper tailing defined by the flux density function $f_{bk}(\varphi) = -6.05 \times 10^{-4}\varphi(1-\varphi)^{12.59}\,(\mathrm{m/s})$ critical concentration of $\varphi_c = 0.23$ and a solid effective stress of $\sigma_e(\varphi) = 5.35\exp(17.9\varphi)\,(\mathrm{Pa})$. Assume feed and underflow concentrations of $w_F = 35.0\,[\%]$ and $w_D = 57.3\,[\%]$ by weight. The solid feed is 178 (tph) and the solid and liquid densities are 2,600 (kg/m^3) and 1,000 (kg/m^3) respectively.

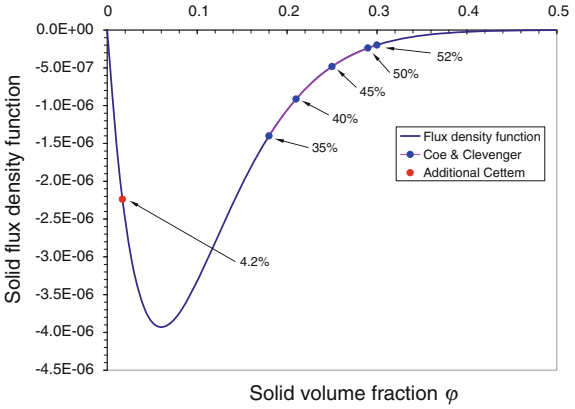

Fig. 8.92 Solid flux density function showing Coe and Clevenger's experimental data and the additional concentration of CETTEM's method

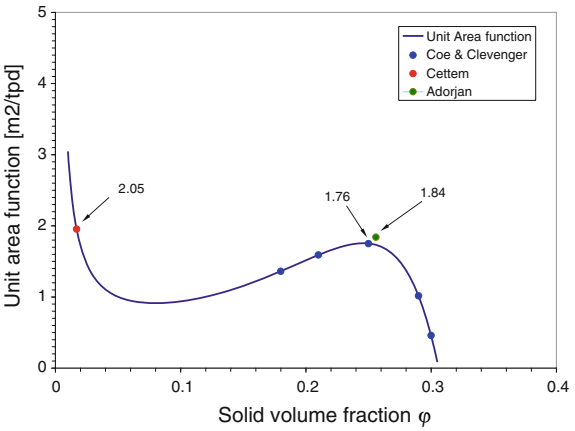

Fig. 8.93 Unit area function showing Coe and Clevenger's results and the unit area by Cettem's and Adorjan's method for a copper flotation tailing

(1) Design a cylindrical thickener with $L = 6$ (m) to handle the feed rate and (2) design a cylindrical-conical thickener to handle the feed rate with 5 (m) and 1 (m) for the cylindrical and conical height respectively. Allow a sediment height of 40 % L.

Using SimEsp we obtain:

Type of thickener	Area m^2	Diameter m	Unit area m^2/tpd	φ_L	Inventory tons
Cylindrical	1,385	42	0.324	3.05×10^{-2}	2,739
Cylindrical-conical	1,521	44	0.417	9.7×10^{-3}	2,993

Figure 8.94 shows the comparison between the concentration profile in the cylindrical and the cylindrical-conical thickeners.

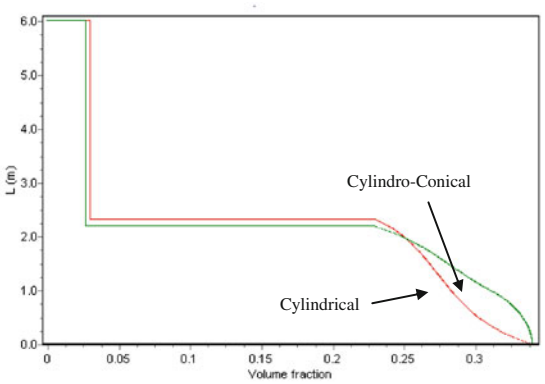

Fig. 8.94 Concentration profile in a flat-bottomed and a conical-bottomed thickener for the same capacity

8.7 Operational Strategies and Metallurgical Control

8.7.1 Steady State

In Sect. 8.3 we showed that the condition for obtaining a steady state in a thickener is that the extended flux density function should lie below the solid feed flux density, in the region of concentration between the conjugate and the underflow concentrations:

$$f_k(\varphi) \leq f_F, \quad \text{for} \quad \varphi_L \leq \varphi \leq \varphi_D$$

At steady state $f_F = q\varphi_D$, where $f_F = -Q_F\varphi_F/S = -F/\rho_s S$, is the solid feed flux density function, $q = -Q_D/S$ is the volume average velocity, Q_F and Q_D are the feed and underflow volume flow rates, F is the solid mass flow rate and S is the thickener cross sectional area.

The sediment height is obtained from (8.145), which can be written in the following form:

$$z_c = -\int_{\varphi_D}^{\varphi_c} \frac{\sigma_e'(\varphi)d\varphi}{\Delta\rho\varphi g\left(\frac{f_F(1-\varphi/\varphi_D)}{f_{bk}(\varphi)} - 1\right)}$$

Varying Feed Rates

If a thickener, provided with an underflow pump with variable speed, is operating at steady state, the solid underflow rate balances the solid feed rate. If the solid feed rate suddenly increases and we do not change the underflow volume flow rate, the excess solid material accumulates in the thickener, increasing the pulp inventory. The increase in sediment height, and weight produces an increase in the

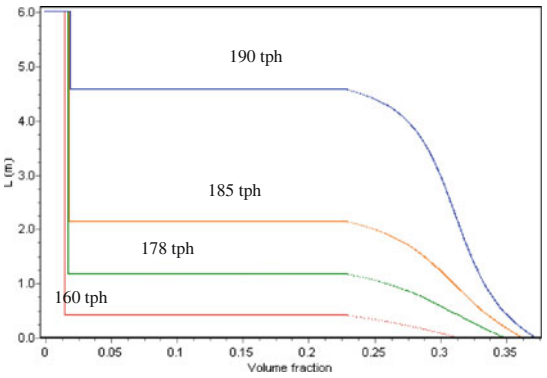

Fig. 8.95 Concentration profile in a copper tailing thickener for increasing feed rate, with a volume underflow rate of $Q_D = 203.9$ m^3/h

underflow concentration so that eventually the solid underflow rate will again balance the solid feed rate. Figure 8.95 shows this effect for copper tailings.

Problem 8.16 Consider a 53 m diameter by 6 m high thickener treating a copper tailing with solid and fluid densities of $\rho_s = 2{,}500$ and $\rho_f = 1{,}000\,(\text{kg/m}^3)$ and several solid feed rates: 160; 178; 185 and 190 tph. The following thickening parameters are given:

$$f_{bk}(\varphi) = -6.05 \times 10^{-4} \times \varphi \times (1-\varphi)^{12.59}$$

$$\sigma_e(\varphi) = \begin{cases} 0 & \text{for } \varphi \le \varphi_c = 0.23 \\ 5.35\exp(17.9\varphi)\ \text{N/m}^2 & \text{for } \varphi \le \varphi_c = 0.23 \end{cases}$$

If the pulp feed is 203.9 m^3/h.

Using the SimEsp simulator, the results shown in Figs. 8.95 and 8.96 and the following table are obtained.

Results of the simulation of Problem 8.16

F tph	f_F m/s	Q_D m^3/h	q m/s	W_D % sol weight	Sediment height m
160	-8.06×10^{-6}	203.4	-2.56×10^{-5}	53.4	0.40
178	-8.97×10^{-6}	203.4	-2.56×10^{-5}	57.4	1.20
185	-9.32×10^{-6}	203.4	-2.56×10^{-5}	58.8	2.20
190	-9.57×10^{-6}	203.4	-2.56×10^{-5}	59.9	4.96

8.7.2 Underflow Concentration Control

During the operation of a thickener, the underflow concentration is expected to remain constant under changes in feed rates. An increase in the solid feed flux F and/or the feed concentration φ_F, is offset by a corresponding increase in the

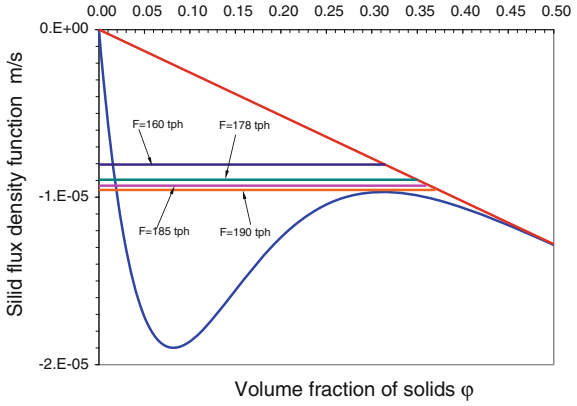

Fig. 8.96 Solid flux density function versus concentration showing the four feed flux density functions expressed as tons per hour

underflow volume rate Q_D to maintain a steady state. In thickeners provided with variable speed underflow pumps, the underflow concentration control is accomplished by changing the pump velocity. If the thickener has gravity discharge, changing underflow discharge rings makes changes in the volume underflow rate.

Usually, the feed rate is not measured in thickeners. In these cases, indirect internal variables must be used. The underflow concentration is the direct effect of the self-weight of the sediment; therefore, the solid pressure at the bottom of the tank or the sediment height can be used as internal variables.

The total pressure P in a suspension of volume fraction φ, is the sum of the solid effective stress $\sigma_e(\varphi)$ and the fluid pore pressure p. Therefore:

$$\sigma_e(\varphi) = P - p \tag{8.148}$$

and depending on the constitutive equation of the solid effective stress, the concentration can be obtained by inverting (8.148). For example, if the solid effective stress is expressed as $\sigma_e(\varphi) = \alpha_1 \exp(\alpha_2 \varphi)$, the concentration is:

$$\varphi = \frac{1}{\alpha_2} \ln\left(\frac{P-p}{\alpha_1}\right) \tag{8.149}$$

or if the solid effective stress is expressed as $\sigma_e(\varphi) = \sigma_0((\varphi/\varphi_c)^n - 1)$, the concentration is:

$$\varphi = \varphi_c \left(\frac{P - p + \sigma_0}{\sigma_0}\right)^{1/n} \tag{8.150}$$

These equations show that the concentration of the sediment can be inferred by measuring the pore pressure and the total pressure. In this case, the measurement is at the bottom of the tank.

As we have already seen, the sediment height z_c can be calculated from equation:

$$z_c = -\int_{\varphi_D}^{\varphi_c} \frac{\sigma'_e(\varphi)d\varphi}{\Delta\rho\varphi g\left(\frac{f_F(1-\varphi/\varphi_U)}{f_{bk}(\varphi)}-1\right)}$$

therefore, z_c can be used to infer the necessary volume underflow rate to maintain a constant underflow concentration under a variable feed rate. For the case of the calcium carbonate, the following relationship exists between the sediment height and the volume underflow rate (Fig. 8.97).

8.7.3 Feed Dilution

The feed enters a thickener, mixes with the upcoming water and dilutes to the *conjugate concentration* φ_L at $z = L$. The conjugate concentration can be obtained by solving the implicit Kynch equation at $z = L$:

$$f_F = q\varphi_L + f_{bk}(\varphi_L) \tag{8.151}$$

The conjugate concentration does not depend directly on the feed concentration φ_F, but only on the solid feed rate f_F, the convective pulp velocity in the thickener q and the pulp nature through the Kynch flux density function $f_{bk}(\varphi)$.

Problem 8.17 Consider a copper tailing with the following settling properties: 2.500 kg/m^3 in density and a solid flux density $f_{bk}(\varphi) = -6.05 \times 10^{-4} \times \varphi \times (1-\varphi)^{12.59}$. For a 53 m diameter thickener with a feed rate of 185 tph, a feed concentration of 21.7 % and underflow concentration of 58.8 % solid by weight, calculate the conjugate concentration.

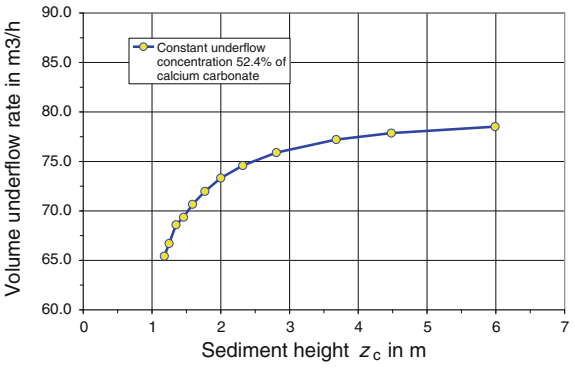

Fig. 8.97 Underflow volume flow rate versus sediment height to obtain a constant underflow concentration of $w_D = 52.4[\%]$ by weight with variable feed rate

From Eq. (8.151):

$$S = \frac{\pi D^2}{4} = \frac{3.14157 \times 53^2}{4} = 2206\,\mathrm{m}^2$$

$$f_F = -\frac{F}{3600 \times \rho_s \times S} = \frac{185}{3600 \times 2.5 \times 2206} = -9.32 \times 10^{-6}\,\mathrm{m/s}$$

$$\varphi_D = \frac{\rho_f \times w_U}{\rho_s \times (100 - w_U) + \rho_f \times w_U} = \frac{1000 \times 58.8}{2500 \times (100 - 58.8) + 1000 \times 58.8} = 0.363$$

$$q = \frac{f_F}{\varphi_D} = \frac{9.32 \times 10^{-6}}{0.363} = -2.57 \times 10^{-5}\,(\mathrm{m/s})$$

$$f_F = q\varphi_L + f_{bk}(\varphi_L)$$

$$-9.32 \times 10^{-6} = -2.57 \times 10^{-5} \times \varphi_L - 6.05 \times 10^{-4} \times \varphi_L \times (1 - \varphi_L)^{12.59}$$

Solving this implicit equation we get: $\varphi_L = 0.0185$, $w_L = 4.5[\%]$ solid by weight

This problem can also be solved graphically as in Fig. 8.98. The value of φ_L is obtained at the intersection of f_F with the continuous solid flux density function $f_k(\varphi)$.

Since the feed to a thickener dilutes naturally, the question arises whether there is any advantage in diluting the pulp before feeding it to the thickener. There are two possible advantages. Firstly, a concentrated pulp entering a more diluted zone behaves like a *density current* that reaches deeper into the tank, requiring more time for its homogeneous distribution. This effect can be minimized if the concentration of the entering feed is similar to that of the receiving zone. Secondly, the flocculant is added to the feed stream and as we will see later, flocculation is more effective for diluted suspensions.

Water is usually very costly around concentrators; therefore mechanisms are introduced into the feed wells to permit *auto-dilution* with the rising overflow water. The most commonly used are; (1) dilution by overflow through ports in the upper part of the feedwell, and (2) dilution by jet-suction.

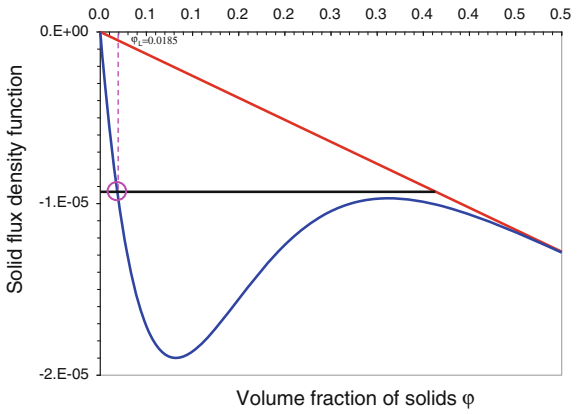

Fig. 8.98 Feed dilution to the conjugate concentration

1. **Dilution ports and overflow**

Consider the feedwell shown in Fig. 8.99. We can make the following mass balance for a feed with density $\rho_F = 1.1\,(\text{ton/m}^3)$ diluted to $\rho_S = 1.05\,(\text{ton/m}^3)$ when entering the thickener, then:

$$\begin{aligned} \rho_F z_F &= \rho_S z_S + \rho_W z_W \\ 1.1 \times z_F &= 1.05 \times z_S + 1.0 \times z_W \\ z_F &= 0.95 \times z_S + 0.91 \times z_W \\ z_F &< z_S + z_W \end{aligned}$$

where ρ_F, ρ_S and ρ_W are the pulp density and z_F, z_S and z_W are the depth of the feed, the suspension and the water respectively.

Because the feed pulp and the conjugate suspension are denser than the water $\rho_W = 1.0$, the water level outside the feedwell is always higher then that of the feed, as shown in Fig. 8.99. This principle can be used for dilution by overflow or through ports in the feedwell. Figure 8.100 shows a feedwell with water ports.

2. **Dilution by jet suction**

When a fluid is injected as a high velocity jet into a tank containing a secondary stationary fluid, the secondary fluid is suctioned into the boundary layer of the first fluid mixing with it. The amount of secondary fluid depends on the jet diameter and velocity. This principle is used to dilute the feed in a thickener, as is shown in Fig. 8.101.

Since the pulp is fed by gravity, the height of the head tank controls the speed of the jet and therefore, the amount of water suctioned. The inner and outer pipes diameters are design variables. Figure 8.102 shows this type of feeding mechanism implemented by a thickener manufacturer.

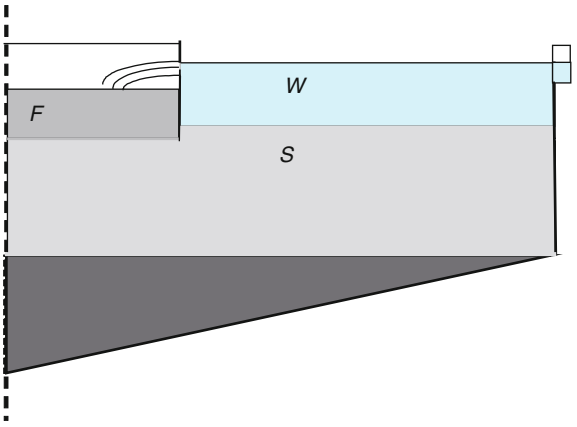

Fig. 8.99 Dilution ports in a feedwell

Fig. 8.100 Feedwell with water ports to dilute the feed (Supaflo technologies)

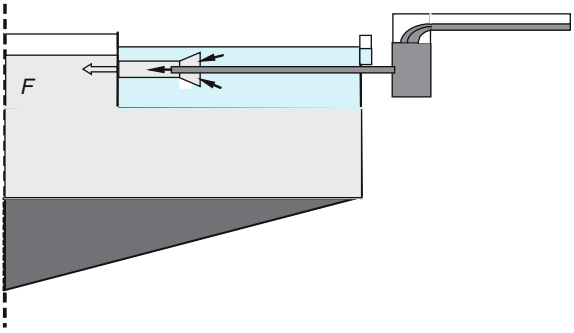

Fig. 8.101 Dilution of the thickener's feed by jet eductor

Figures 8.103 and 8.104 show the velocity magnitude and velocity vectors in a typical E-Duc System and Fig. 8.105 shows the solid concentration distribution in a typical feedwell (Köck and Concha 2003).

Fig. 8.102 E-Duc from EIMCO process equipment

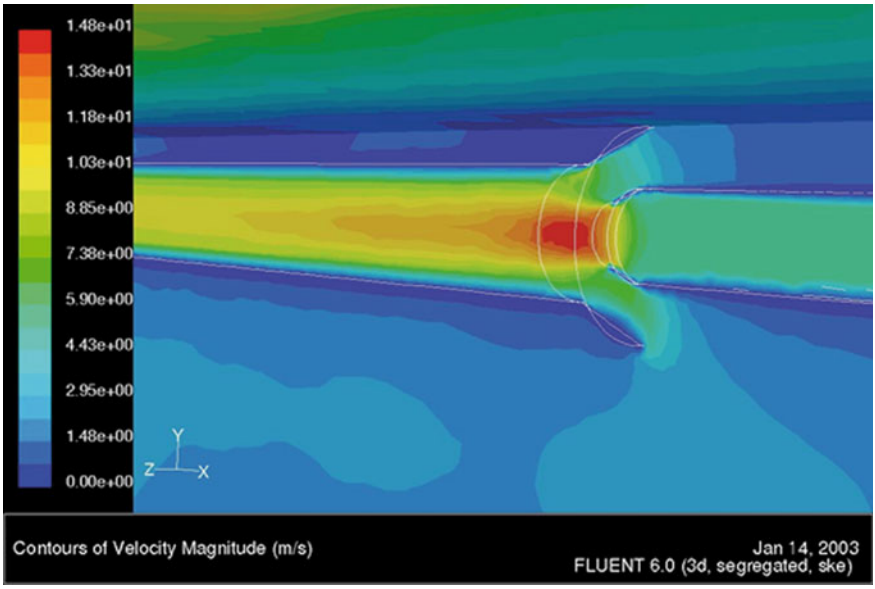

Fig. 8.103 Velocity distribution for the E-Duc dilution system, Köck and Concha 2003

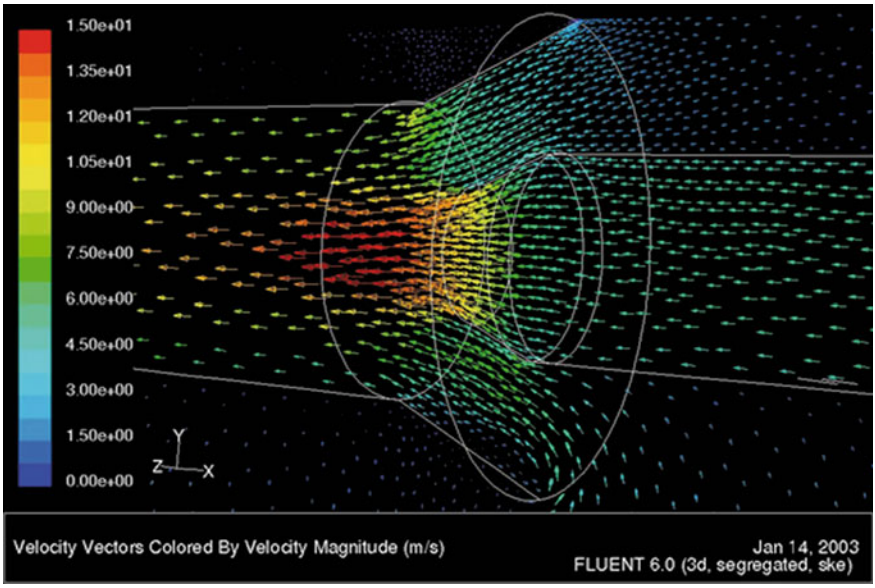

Fig. 8.104 Velocity vector for the E-Duc dilution system, Köck and Concha 2003

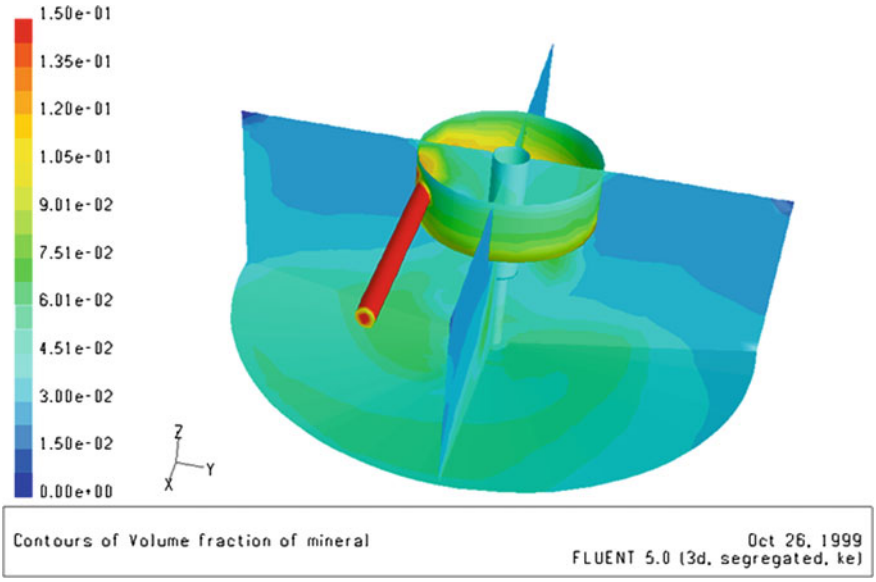

Fig. 8.105 Concentration distribution at the inlet and outlet of a feedwell in a thickener, Köck and Concha 2003

8.7.4 Limiting Concentration

According to Coe and Clevenger, the limiting concentration in a thickener establishes the settling rate and lies between the feed and the underflow concentration. We have seen that the feed is diluted to the conjugate concentration on entering the thickener and therefore the range for the limiting concentration should be extended to include the conjugate concentration.

The limitations are determined by the flux density function and by the values of the conjugate and the underflow concentrations. In most cases, the conjugate concentration is the limiting concentration. See Fig. 8.106 for the cases of copper tailings and calcium carbonate, where the conjugate concentrations are $\varphi_L = 0.0185$ and $\varphi_L = 0.0160$. They are also the limiting concentrations, giving unit areas of $AU = 0.516\,(\mathrm{m}^2/\mathrm{tpd})$ and $AU = 2.05\,(\mathrm{m}^2/\mathrm{tpd})$ respectively.

8.7.5 Effect of the Flocculant Dose on Thickener Capacity and Fines Control

Flocculants are added to a thickener to increase the settling velocity of the particles by forming flocs. A floc is an aggregate of many particles of different sizes having a greater overall size, but a lower density. Flocculated pulps leave clear water and sharp water-suspension interfaces when settling. For more information on this subject see Chap. 7.

The flocculant dose is an important factor from a technical and economic point of view. There is an optimum amount of flocculant that has to be experimentally determined. An excessive dose reduces the settling velocities, and consequently

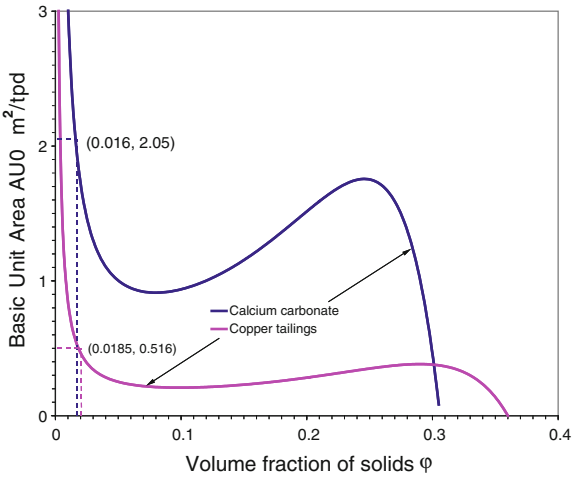

Fig. 8.106 The conjugate concentration is also limiting for the two cases of copper tailings and sodium carbonate

the thickener capacity, and increases the operating cost. There are several ways to optimize the flocculant addition as a thickener, the most commonly used is to perform settling experiments with different pulp dilutions and flocculant dose. There is also the possibility of selecting the dose according to floccules properties such as flocculant molecules size and density.

Problem 8.18 Consider settling tests performed on copper tailings for several flocculant doses. The result shows that the solid flux density function and the solid effective stress can be written in the form: $f_{bk}(\varphi, gpt) = u_{\infty}(gpt) \times \varphi \times (1 - \varphi)^{12.59}$, m/s and $\sigma_e(\varphi) = 5.35 \exp(17.9\varphi)$, Pa.

Calculate the capacity of a 57 m diameter thickener for a solid density of $\rho_s = 2.500\,\mathrm{kg/m^3}$, flocculant dose of 2, 4, 6, 8 and 10 gpt for an underflow concentration of 52 % solid. The feed concentration is 49.3 % solid and the critical concentration is 40.6 [% solid] by weight.

The calculated solid flux density functions and initial settling velocities, for different flocculant dose, are described in Figs. 8.107 and 8.108.

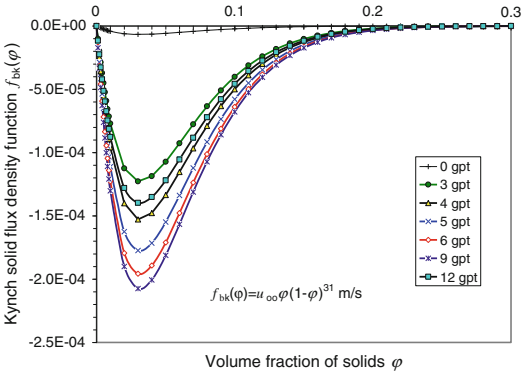

Fig. 8.107 Effect of the flocculant dose on the solid flux density function

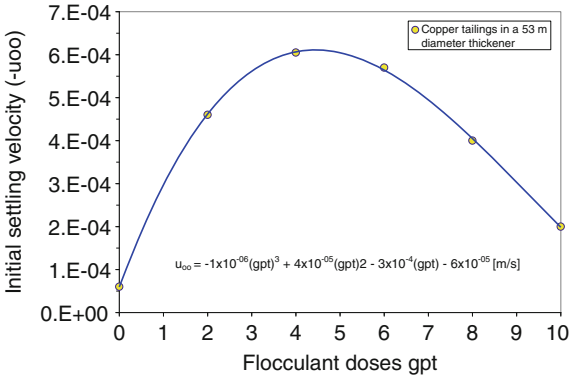

Fig. 8.108 Effect of the flocculant dose on the initial settling velocity

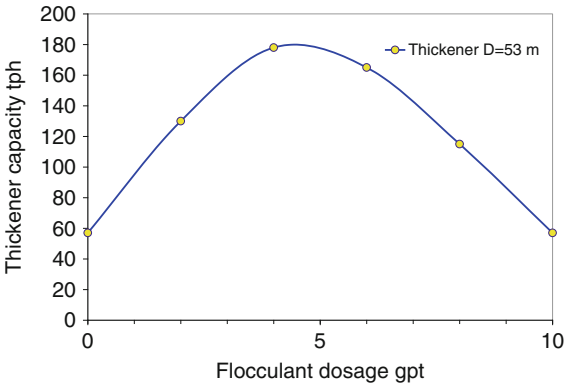

Fig. 8.109 Effect of the flocculant dose on the thickener capacity

With the above information, the capacity of the thickener can be calculated for each flocculant dose, to give the same sediment height, that is, 20 % of the total available thickener height. The result is given in Fig. 8.109.

The fact that a change in the flocculant dose drastically affects the capacity of a thickener shows that the addition of flocculant as a variable to control fines in the overflow water must be taken carefully. In general flocculant is added in proportion of the thickener's solid feed rate. But, when fines are controlled by flocculant addition, an excess of flocculant can be detrimental for the thickener's capacity. This effect was dealt with in Chap. 7.

8.7.6 Effect of the Shear Rate on Flocculation and on Thickener Capacity

The flocculant is injected directly into a thickener in the feedwell or into the pipe feeding the thickener. In both cases the exact position of injection is in the zones of greatest shear. Farrow et al. (2001) presented shear rate distribution in a feedwell calculated with CFD and predicted the favorable positions for flocculant injection. Reports of sampling of industrial thickener by Farrow et al. (1999) confirmed that CFD predictions and modeling resulted in significant improvement in industrial thickener operation in Australia. Kahane et al. (1997) reported on work in a plant in Australia were the relocation of the addition points of flocculant to the lower part of the feedwell, where the natural dilution occurs, doubled the thickening capacity of the plant.

In Chap. 7 Köck and Concha (1999) presented a CFD model of a typical feedwell of a copper tailing flotation thickener, concluding that the average shear rate in the feedwell was very low, on the order of 1 s^{-1}. Köck and Concha (1999)

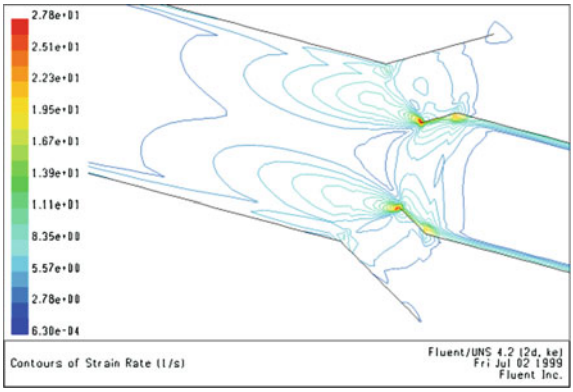

Fig. 8.110 Distribution of shear rate in an E-Duc feeding system to a thickener (Köck and Concha 1999)

also used CFD to establish the properties of an E-Duc system of a copper tailing flotation thickener, Fig. 8.110. It was established that the average shear rate in the tube was $\bar{\dot{\gamma}} \sim 8\,\mathrm{s}^{-1}$ and that in a small region it reached $\dot{\gamma} \sim 27\,\mathrm{s}^{-1}$.

8.7.7 Optimum Flocculation of Thickener Feeds

Farrow et al. (2001) indicated that for a specific solid-flocculant system under high shear conditions, the average size of the flocs increases rapidly from 30 to 130 μm in 15 s before the rupture of flocs occur. Under low shear conditions, flocs slowly increase in size from 30 to 100 (μm) in 50 (s) without any floc rupture. This difference in growth velocity and floc is extremely important in industrial thickeners. The key for a good feedwell design is to provide appropriate hydrodynamic conditions and sufficient residence time for floc growth.

Rulyov (2004) and Concha et al. (2012) showed that optimum flocculation is obtained by a proper combination of feed dilution, high shear rate $\approx 500\,\mathrm{s}^{-1}$ for short periods $\approx 5\,\mathrm{s}$ and a flocculant dose for the collision of particles and flocculant macro-molecules, and low shear floc growth ($\approx 60\,\mathrm{s}$), leading to maximum floc size and density. Unfortunately this combination cannot be obtained within a feedwell. See Chap. 7.

The auto-dilution of a suspension in a feedwell is established once the type of dilution system of the feed has been chosen. The shear rate during flocculation depends on the thickener feeding system or feedwell design, which is determined for a given thickener. Therefore, under a change of mineralogy or particle size distribution, the only control variable available is the flocculant dose so that with operational variables it is not possible to maintain an optimum flocculation in a thickener. The solution to this problem is to flocculate the suspension in a specialized reactor before feeding it to the thickener. This specialized industrial reactor has not yet been developed for copper concentrators.

References

Adorjan, L. A. (1975). *A theory of sediment compression* (pp. 1–22). Calgary: XI IMPC.

Adorjan, L. A. (1976). Determination of thickener dimensions from sediment compression and permeability test results. *Transactions of the Institution of Mining and Metallurgy Section C, 85*, 157–163.

Agricola, G. (1994). 1494–1994, Bergwelten, Edition Glückauf GmbH, Essen.

Ashley, H. E. (1909, June 12). *Theory of the settlement of slimes, mining*. Scientific Press.

Auzerais, F. M., Jackson, R., & Russel, W. B. (1988). The resolution of shocks and the effects of compressible sediments in transient settling. *Journal of Fluid Mechanics, 195*, 437–462.

Barrientos, A. (1978). Parameters determination in the phenomenological model of sedimentation. Engineering Thesis, University of Concepción (in Spanish).

Bascur, O. (1976). Phenomenological model of suspensions in sedimentation. Engineering Thesis, University of Concepción (in Spanish).

Bascur, O. (1989). A unified solid-liquid separation framework. *First Regional Meeting, American Filtration Society, Houston, Texas*, October 30–November 1, 1–11.

Becker, R. (1982). Continuous thickening: Design and simulation of thickeners. Engineering Thesis, University of Concepción (in Spanish).

Beens, K. & Sills, G. C. (1981). Self-weight consolidation of soils: an experimental and theoretical study, Geotechnique 31, 519–535.

Behn, V. C. (1957, October). Settling behavior of waste suspensions. *Proceeding of the ASCE, Journal of the Sanitary Engineering Division*, 1423-5–1423-20.

Betancourt, F. & Concha, F. (2011). Unveiling the myth of high capacity thickeners, 8the International Seminar od Mineral Processing Procemin 20011, Santiago, Chile. (In Spanish).

Betancourt, F., Concha, F., & Sbarbaro, D. (2013). Simple mass balance controllers for continuous sedimentation. *Computers and Chemical Engineering*, 34–43.

Bürger, R., & Concha, F. (1997). Simulation of the transient behavior of flocculated suspensions in a continuous thickener. *Proceedings of the XX International Mineral Processing Congress*, *Achen*, September 4, 21–26 (pp. 91–101).

Bürger, R., & Concha, F. (1998). Mathematical model and numerical simulation of the settling of flocculated suspensions. *International Journal of Multiphase Flow*, *24*(6), 1005–1023.

Bürger, R., & Karlsen, K. H. (2001). On some upwind difference schemes for the phenomenological sedimentation-consolidation model. *Journal of Engineering Mathematics, 41*, 145–166.

Bürger, R., & Tory, E. M. (2000). On upper rarefaction waves in batch settling. *Powder Technology, 108*, 74–87.

Bürger, R., Bustos, M. C., & Concha, F. (1999). Settling velocities of particulate systems: 9. Phenomenological theory of sedimentation processes: Numerical solution of the transient behavior of flocculated suspensions in an ideal batch or continuous thickener. *International Journal of Mineral Processing, 55*(4), 267–282.

Bürger, R., Concha, F., & Tiller, F. M. (2000a). Applications of the phenomenological theory to several published experimental cases of sedimentation process. *Chemical Engineering Journal, 80*(1–3), 105–117.

Bürger, R., Evje, S., Karlsen, K. H., & Lie, K.-A. (2000b). Numerical methods for the simulation of the settling of flocculated suspensions. *Chemical Engineering Journal, 80*, 91–104.

Bürger, R., Evje, S., & Karlsen, K. H. (2000c). On strongly degenerate convection-diffusion problems modeling sedimentation-consolidation processes. *Journal of Mathematical Analysis and Applications, 247*, 517–556.

Bürger, R., Wendland, W., & Concha, F. (2000d). Modelling equations for gravitational sedimentation-consolidation processes. *ZAMM, 80*, 1–18.

Bürger, R., Karlsen, K. H., Klingerberg, C., & Risebro, N. H. (2003). A front tracking approach to a model of continuous sedimentation in ideal clarifier. Thickener units. *Nonlinear Analysis: Real World Applications, 4*, 457–481.

Burgos, R., & Concha, F. (2005). Further development of software for the design and simulation of industrial thickeners. *Chemical Engineering Journal, 111*, 135–144.

Buscall, R., & White, L. R. M. (1987). The consolidation of concentrated suspensions. *Journal of the Chemical Society, Faraday Transactions, 1*(83), 873–891.

Bustos, M. C. (1984). On the existence and determination of discontinuous solutions to hyperbolic conservation laws in the theory of sedimentation. Doctoral Thesis, Mathematical Department, University of Darmstadt.

Bustos, M. C., & Concha, F. (1988a). On the construction of global weak solutions in the Kynch theory of sedimentation. *Mathematical Methods in the Applied Sciences, 10*, 245–264.

Bustos, M. C., & Concha, F. (1988b). Simulation of batch sedimentation with compression. *AIChE Journal, 34*(5), 859–861.

Bustos, M. C., & Concha, F. (1996). Kynch theory of sedimentation. In E. M. Tory (Ed.), *Sedimentation of small particles in a viscous fluid. Advances in fluid mechanics* (Chap. 2, Vol. 7, pp. 7–49). Southampton: Computational Mechanics Publications.

Bustos, M. C., Concha, F., & Wendland, W. (1990a). Global weak solutions to the problem of continuous sedimentation of an Ideal Suspension. *Mathematical Methods in the Applied Sciences, 13*, 1–22.

Bustos, M. C., Paiva, F., & Wendland, W. L. (1990b). Control of continuous sedimentation of ideal suspensions as an initial and boundary value problem. *Mathematical Methods in the Applied Sciences, 12*, 533–548.

Bustos, M. C., Concha, F., Bürger, R., & Tory, E. M. (1999). *Sedimentation and thickening: Phenomenological foundation and mathematical theory*. Dordrecht, The Netherlands: Kluwer Academic Publishers. 285 p.

Clark, A. (1915). A note on the settling of slimes. *Engineering and Mining Journal, 99*(9), 412.

Coe, H. S., & Clevenger, G. H. (1916). Methods for determining the capacity of slime settling tanks. *Transactions, AIME, 55*, 356–385.

Comings, E. W. (1940). Thickening calcium carbonate slurries. *Industrial and Engineering Chemistry, 32*(5), 663–668.

Comings, E. W., Pruiss, C. E., & De Bord, C. (1954). Continuous settling and thickening. *Industrial & Engineering Chemistry Design Processing Development, 46*, 1164–1172.

Concha, F., & Barrientos, A. (1980). Phenomenological theory of thickening. *Engineering Foundation Conference on Particle Science and Technology, New Hampshire, USA*, 7–11 July.

Concha, F., & Barrientos, A. (1993). A critical review of thickener design methods. *Kona, Powder and Particles, 11*, 79–104.

Concha, F., & Bürger, R. (1998). Wave propagation phenomena in the theory of sedimentation. In E. F. Toro & J. F. Clarke (Eds.), *Numerical methods for wave propagation phenomena* (pp. 173–196). Dordrecht, The Netherlands: Kluwer Academic Publishers.

Concha, F., & Bustos, M. C. A. (1991). Settling velocities of particulate systems. Part 6. Kynch sedimentation processes: Batch settling. *International Journal of Mineral Processing, 32*, 193–212.

Concha, F., & Bustos, M. C. A. (1992). Settling velocities of particulate systems. Part 7. Kynch sedimentation processes: Continuous thickening. *International Journal of Mineral Processing, 34*, 33–51.

Concha, F., Burgos, R., & Garrido, P. (2005). Sistema para el diseño y simulación de espesadores industriales, XII Symposium de MolyCop en Procesamiento de Minerales, Termas de Chillán, noviembre 14–18.

Concha, F., Segovia, J. P., Sbarbaro, D., & Ërger, R. (2008). XXIV Int. Mineral Procces. Congress, Beiging 2008.

Concha, F., Sbarbaro, D., Segovia, J. P., & Bürger, R. (2011). *Integrated system of parameter determination, thickener design, simulation and control*. Beijing, China: IMPC. 2008.

Concha, F., Rulyov, N. N., & Laskowski, J. S. (2012). Settling velocities of particulate systems 18: Solid flux density determination by ultra flocculation. *International Journal of Mineral Processes, 104–105*, 53–57.

D'Avila, J. (1976). An analysis of Kynch theory of sedimentation. *Brazilian Journal of Technology, 7*, 447–453. (in Portuguese).
D'Avila, J. (1978). A mathematical model of sedimentation. Ph.D. Thesis, COPPE, Federal University of Río de Janeiro (in Portuguese).
D'Avila, J., & Sampaio, R. (1977). Equations for the solid pressure. *Brazilian Journal of Technology, 8*, 177–191. (in Portuguese).
D'Avila, J., Concha, F., & Telles, A. S. (1978). A phenomenological model for two dimensional continuous sedimentation. *VI Porous Media Seminar, Río Claro, Brazil*, October 11–13, III (pp. 1–19) (in Portuguese).
Davis, K. E., & Russel, W. B. (1989) An asymptotic description of transient settling and ultrafiltration of colloidal suspensions. *Physics of Fluids A*, *1*, 82–100.
De Haas, R. D. (1963). Calculation of the complete batch settling behavior for rigid spheres in a Newtonian liquid. M.Sc Thesis, Purdue University.
De Kretser, R. G., Usher, S. P., Scales, P. J., Bolger, D. V., & Landmann, K. A. (2001). Rapid filtration measurements of dewatering design and optimization parameters. *AIChE Journal, 47*(8), 1758–1769.
Diehl, S. (1995). On scalar conservation laws with point source and discontinuous function modeling continuous sedimentation, *SIAM Journal on Applied Mathematics*, 1425–1451
Diehl, S. (1996). A conservation law with point source and discontinuous flux function modeling continuous sedimentation, *SIAM Journal on Applied Mathematics*, *56* (2), 388–419.
Diehl, S. (1997). Dynamic and steady state behaviour of continuous sedimentation. *SIAM Journal on Applied Mathematics, 57*(4), 991–1018.
Diehl, S. (1999). On boundary conditions and solutions for ideal clarifier-thickener units. *Chemical Engineering Journal, 80*(1–3), 119–133.
Diehl, S. (2000). On boundary conditions and solutions for ideal clarifier-thickener units, *Journal of Chemical Engineering*, *80*, 119–133.
Diehl, S. (2001). Operating charts for continuous sedimentation I: Control steady states, *Journal of Engineering Mathematics*, *41*, 117–144.
Dorr, J. V. N. (1915). The use of hydrometallurgical apparatus in Chemical Engineering. *Journal of Industrial and Engineering Chemistry, 7*, 119–130.
Dorr, J. V. N. (1936). *Cyanidation and concentration of gold and silver ores* (p. 117). New York: McGraw-Hill Book Co. Inc.
Egolf, C. B., & McCabe, W. L. (1937). Rate of sedimentation of flocculated particles. *Transactions AIChE, 33*, 620–640.
Farrow, J. B., Fawell, P. D., Johnston, R. R. M, Nguyen, T. B., Rudman, M., Simic, K., & Swift, J. D. (2001). Técnicas de floculación y metodologías para la optimización de espesadores, in Concha, F., Manual de Filtración y Separación, Cettem, Concepción, Chile, 347–362.
Farrow, J. B., Johnstone, R. R. M, Nguyen, T. B., Rudman, M, Simic, K., Swift, J. D. (2001). Téchniques of flocculation and methodologies to optimize thickners, In Concha, Filtration and Separation, Cettem, Concepción, Chile.
Fitch, B. & Stevenson, D. G. (1977). Gravity Separation Equipment, In Solid Sepazration Equipment Scale up, Ed. D.B. Purchased, Upland Press Inc., Croydon, Englnd.
Fitch, E. B. & Stevenson, D. G. (1997). Gravity Separation Equipment Scale-up, Ed. D.B. Purchas, Uplands Press Ltd., Croydin, England.
Fitch, B. (1983). Kynch theory and compression zones. *AIChE Journal, 29*, 940–947.
Font, R. (1988). Compression zone effect in batch sedimentation. *AIChE Journal, 34*, 229–238.
Forbes, D. L. H. (1912). The settling of mill slimes. *Engineering and Mining Journal, 93*, 411–415.
Free, E. E. (1912). Rate of slime settling. *Engineering and Mining Journal*, *101*, 243, 429, 509, 681.
Garrido, P. (2005). Determinación de los parámetros de espesamiento, Tesis de doctorado, Departamento de Ingeniería Metalúrgica, Universidad de Concepción, Concepción, Chile.

Garrido, P, Bürger, R., & Concha, F. (2000). Settling velocities of particulate systems: 11. Comparison of the phenomenological sedimentation-consolidation model with published experimental results. *International Journal of Mineral Processing*, *60*(3–4), 213–227.

Garrido, P., Burgos, R., Concha, F., & Bürger, R. (2003). Software for the design and simulation of gravity thickeners. *Minerals Engineering, 16*(2), 85–92.

Garrido, P., Burgos, R., Concha, F., & Bürger, R. (2004). Settling velocities of particulate systems: 13. A simulator for batch and continuous sedimentation of flocculated suspensions. *International Journal of Mineral Processing, 73*, 131–144.

Garrido, P. & Concha, F. Dosificzción de Flaculante y su relación a la operación y control de espesadores continuos, III Coloquio Nacional de Filtración y Separación, Santiago, Chile. (In Spanish).

Green, M. D. (1997). Characterization of suspensions in settling and compression (p. 246). PhD Thesis, Particulate Fluids Processing Centre, Department of Chemical Engineering, The University of Melbourne, Melbourne, Australia.

Green, M. D., Landman, K. A., de Kretser, R. G., & Bolger, D. V. (1998). Pressure filtration technique for complete characterization of consolidating suspensions. *Industrial and Engineering Chemistry Research*, *37*(10) 4152–4156.

Hassett, N. J. (1958). Design and operation of continuous thickeners. *The Industrial Chemist*, *34,* 116–120; 169–172; 489–494.

Hassett, N. J. (1961, January). Theories of the operation of continuous thickeners. *The Industrial Chemist*, 25–28.

Hassett, N. J. (1964a). Mechanism of thickening and thickener design. *Transactions Institution of Mining and Metallurgy, 74*, 627–656.

Hassett, N. J. (1964, January). Concentrations in a continuous thickener. *Industrial Chemist*, 29–33.

Hassett, N. J. (1968). Thickening in theory and practice. *Mining Science Engineering, 1*, 24–40.

Holdich, R. G., & Butt, G. (1997). Experimental and numerical analysis of a sedimentation forming compressible compacts. *Separation Science and Technology, 32*, 2149–2171.

Kahane, R. B., Schwarz, P., & Johnston, R. R. M. (1997). *International Conference on Computational Fluid Dynamics in Minerals and Metals Processing and Power Generation* (pp. 109–117), 3–5 July, Melbourne, Australia.

Kammermeyer, K. (1941). Settling and thickening of aqueous suspensions. *Industrial and Engineering Chemistry, 33*, 1481–1491.

Kos, P. (1977). Fundamentals of gravity thickening. *Chemical Engineering Progress, 73*(99–105), 1975.

Kynch, G. J. (1952). A theory of sedimentation. *Transactions of the Faraday Society, 48*, 166–176.

Landmann, K. A., White, L. R., & Buscall, R. (1988). The continuous-flow gravity thickener: Steady state behavior. *AIChE Journal, 34*(2), 239–252.

Mishler, R. T. (1912, October 5). Settling slimes at the Tigre Mill. *Engineering and Mining Journal*, *94*(14), 643–646.

Nichols, H. G. (1908a). A method of settling slimes, as applied to their separation from solution in cyanide treatment. *Transactions Institution of Mining and Metallurgy, London, 17*, 293–329.

Nichols, H. G. (1908, July 11). *Theory of settlement of slimes* (pp. 54–56). Mining and Scientific Press.

Petty, C. A. (1975). Continuous sedimentation of a suspension with a nonconvex flux law. *Chemical Engineering Science, 30*, 1451–1458.

Ralston, O. C. (1916). The control of ore slimes. *Engineering and Mining Journal*, *101*, 763, 890.

Roberts, E. J. (1949, March). Thickening: Art or Science? *Transactions AIME*, 61–64; *Mining Engineering*, *1*, 61.

Rulyov, N. N. (2004). *Ultra-flocculation, theory, experiments and applications* (pp. 197–2014). Hamilton, Canada: CIMM Metallurgical Society.

Scott, K. J. (1968a). Theory of thickening: Factors affecting settling rate of solids in flocculated pulps. *Transactions Institution of Mining and Metallurgy, 77*, C85–C97.
Scott, K. J. (1968b). Experimental study of continuous thickening of flocculated silica slurry. *IEC Fundamentals, 7*, 582–595.
Segovia, J. P., & Concha, F. (2012). AMIRA Final Report, June 2012.
Shannon, P. T., Stroupe, E., & Tory E. M. (1963). Batch and continuous thickening. *Industrial & Engineering Chemistry Fundamentals*, *2*(3), 203–211.
Shannon, P. T., & Tory, E. M. (1965). Settling of slurries. *Industrial and Engineering Chemistry, 57*(2), 18–25.
Shannon, P. T., Tory, E. M. (1966, December). The analysis of continuous thickening. *Transactions SME*, *235*, 375–382.
Shirato, M., Kato, H., Kobayashi, K., & Sakazahi, H. (1970). Analysis of settling of thick slurries due to consolidation. *Journal of Chemical Engineering Japan, 3*, 98–104.
Stewart, R. F., & Roberts, E. J. (1933). The sedimentation of fine particles in liquids. *Transactions. Institute of Chemical Engineers, 11*, 124–141.
Stroupe, E. (1962). Batch sedimentation of rigid spheres in a Newtonian liquid. M.Sc. Thesis, Purdue University, West Lafayette, USA.
Talmage, W. P., & Fitch, E. B. (1955). Determining thickener unit areas. *Industrial and Engineering Chemistry, Engineering Design and Development, 47*(1), 38–41.
Thacker, W. C., & Lavelle, J. W. (1977). Two-phase flow analysis of hindered settling. *The Physics of Fluids, 20*(9), 1577–1579.
Tory, E. M. (1961). Batch and continuous thickening of slurries. Ph.D. Thesis, Purdue University, West Lafayette, USA.
Tory, E. M., & Shannon, P. J. (1965). Reappraisal of the concept of settling in compression. *I&EC Fund, 4*, 194–204.
Usher, S. P. (2002). Suspension dewatering: Characterization and optimization (p. 347). PhD Thesis, Particulate Fluids Processing Centre, Department of Chemical Engineering, The University of Melbourne, Melbourne, Australia.
Usher, S. P., de Kretser, R. G., & Scales, P. J. (2001). Validation of a new filtration technique for dewaterability characterization. *AIChE Journal, 47*(7), 1561–1570.
Wilhelm, J. H., & Naide, Y. (1979). Sizing and operating thickeners. *SME, AIME annual meeting*, Preprint N°79-30, New Orleans, (pp. 18–22).
Wilson, A. J. (1994). *The living rock*. Cambridge: Woodhead Pub. Ltd.
Work, L. T., & Kohler, A. S. (1940). Sedimentation of suspensions. *Industrial and Engineering Chemistry, 32*(10), 1329–1334.
Yoshioka, N., Hotta, Y., Tanaka, S., Naito, S., & Tsugami, S. (1957). Continuous thickening of homogeneous flocculated slurries. *Chemical Engineering Japan, 21*, 66–75.